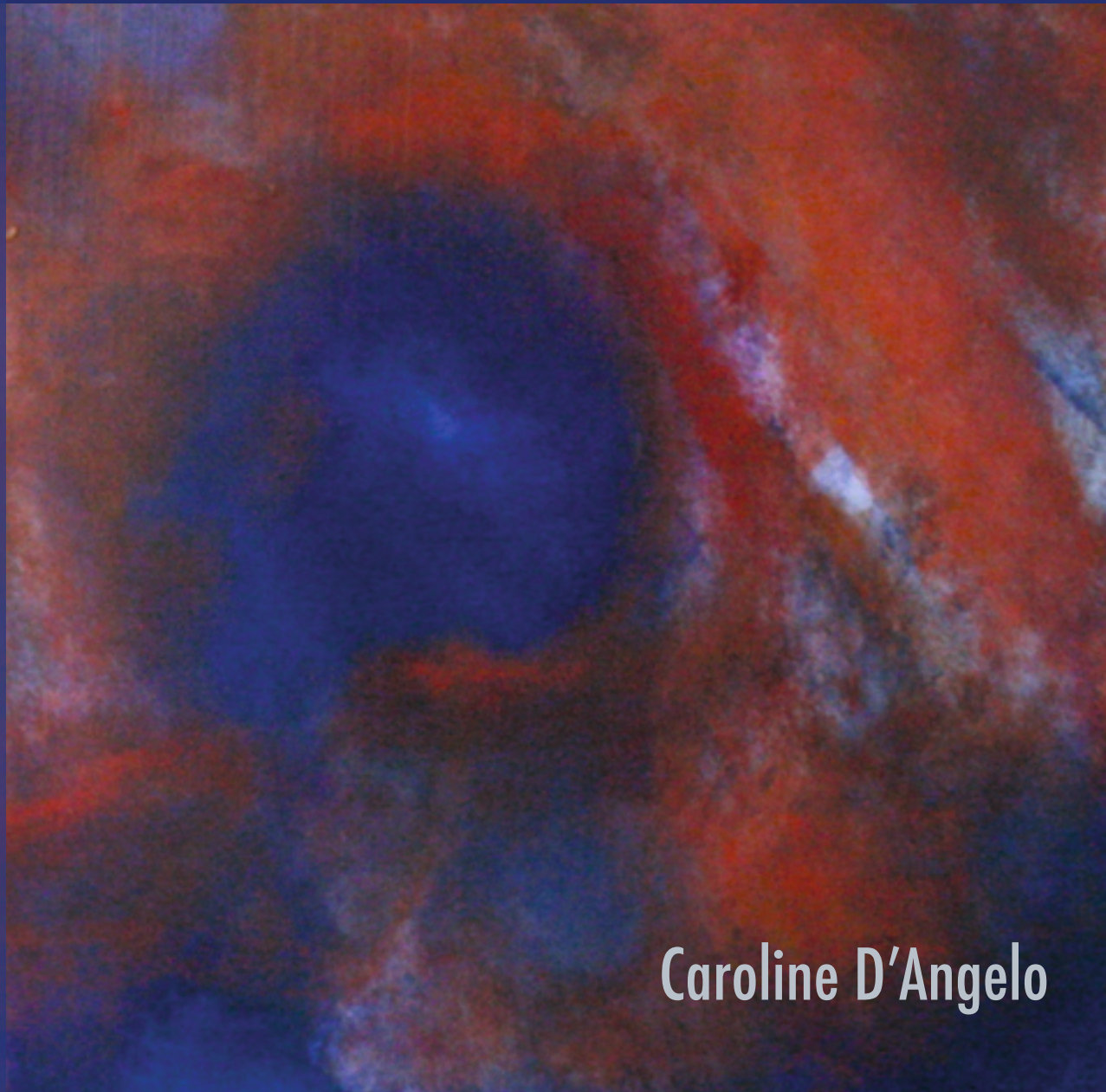
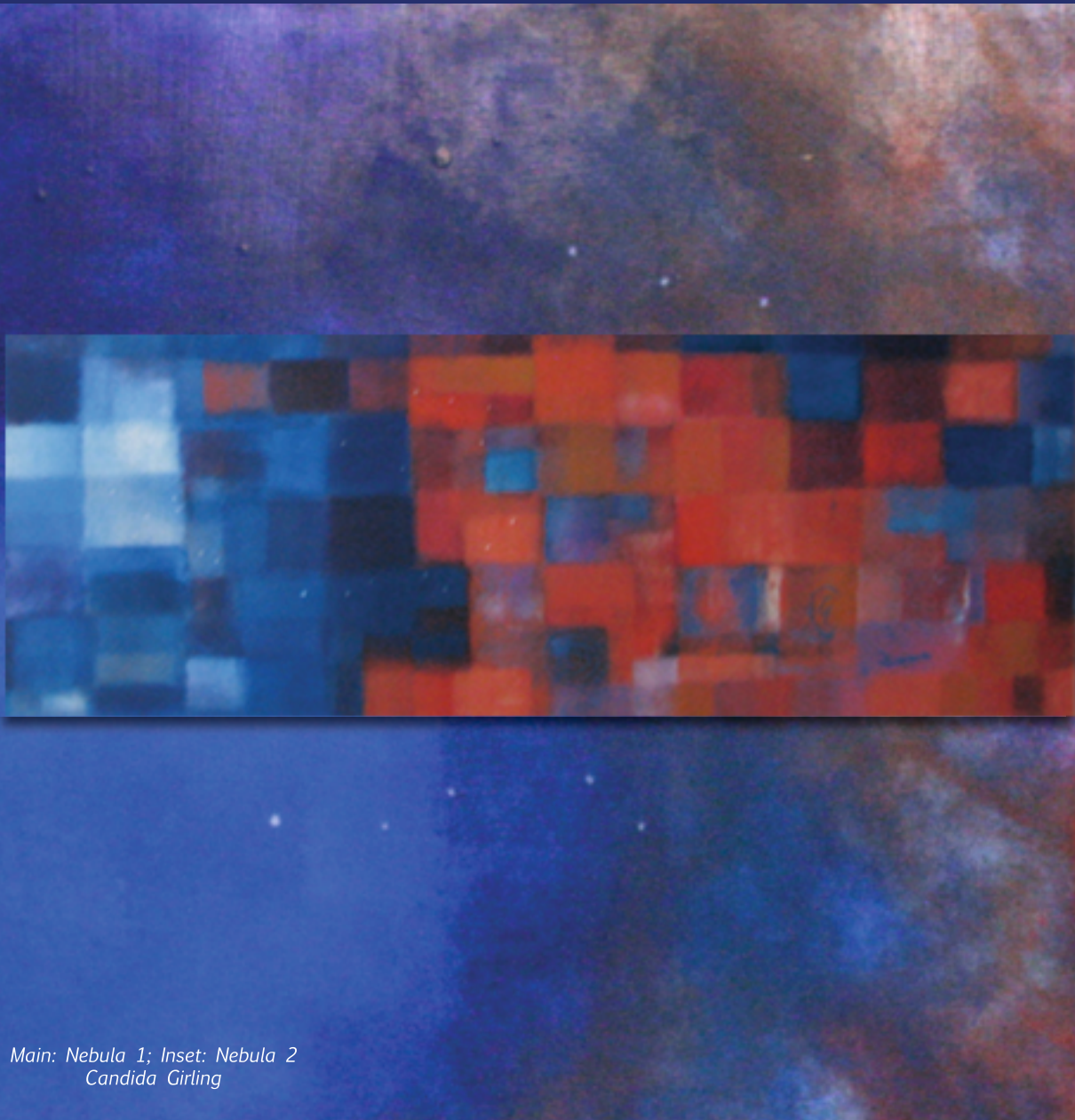


# TRUNCATED ACCRETION DISCS AROUND STELLAR MASS OBJECTS

TRUNCATED ACCRETION DISCS AROUND STELLAR-MASS OBJECTS by Caroline D'Angelo



Caroline D'Angelo

# **TRUNCATED ACCRETION DISCS AROUND STELLAR MASS OBJECTS**

## **ACADEMISCH PROEFSCHRIFT**

ter verkrijging van de grad van doctor  
aan de Universiteit van Amsterdam  
op gezag van de Rector Magnificus  
Prof. Dr. D.C. van den Boom  
ten overstaan van een door het college voor promoties ingestelde  
commissie, in het openbaar te verdedigen in de Agnietenkapel  
op donderdag 3 maart 2011, te 14:00

door

**Caroline Rebecca Mary Xavier D'Angelo Doctoranda**

geboren te North York, Canada

## Promotiecommissie

Promotor:

Prof. Dr. H. C. Spruit

Overige leden:

Prof. Dr. M. B. M. van der Klis

Prof. Dr. R. A. M. J. Wijers

Dr. A. L. Watts

Prof. Dr. H. F. Henrichs

Dr. L. Kaper

Dr. C. P. Dullemond

Faculteit Natuurwetenschappen, Wiskunde en Informatica

*This thesis is dedicated in loving memory to  
my grandmother Zoë Girling (1924-1999)  
and  
my aunt Rosalia Martellacci (1950-2010),  
and to my parents,  
Lucy Girling and Joseph D'Angelo*



*I have come to believe that the whole world is an enigma, a harmless enigma that is made terrible by our own mad attempt to interpret it as though it had an underlying truth.*

- UMBERTO ECO

*Everything passes away - suffering, pain, blood, hunger, pestilence. The sword will pass away too, but the stars will still remain when the shadows of our presence and our deeds have vanished from the earth.*

-MIKHAIL BULGAKOV, THE WHITE GUARD



# Contents

<b>1</b>	<b>Introduction</b>	<b>1</b>
1.1	Overview	1
1.2	Accretion processes around stars	1
1.2.1	Thin accretion discs	3
1.3	Accreting stars with strong magnetic fields	3
1.3.1	Observations of magnetospheric accretion	5
1.4	Magnetic accretion at low $\dot{M}$ : ‘propellers’, outflows and dead discs	6
1.5	Accretion around black holes at low luminosities	8
1.5.1	X-ray spectra of black holes	9
1.5.2	Is the thin disc truncated at low $\dot{M}$ ?	10
1.5.3	Accretion discs bombarded by ions	10
1.5.4	Soft excesses: evidence of an untruncated disc?	11
1.6	Summary of the main results of thesis	11
<b>2</b>	<b>Episodic Accretion on to Strongly Magnetic Stars</b>	<b>15</b>
2.1	Introduction	16
2.2	Magnetosphere-Disc Interactions	17
2.2.1	Interaction region between a disc and magnetic field	17
2.2.2	Accretion and angular momentum transport	20
2.2.3	Evolution of a disc truncated inside the corotation radius	22
2.2.4	Evolution of a disc truncated outside the corotation radius	23
2.3	Cyclic accretion	24
2.3.1	Surface density profile for $r_{\text{in}} > r_{\text{c}}$	25
2.3.2	Transition region	26
2.3.3	Physical constraints on $\Delta r$ and $\Delta r_2$	27
2.4	Numerical Implementation	28
2.4.1	Disc equation and viscosity prescription	28
2.4.2	Steady-State solution	29
2.4.3	Numerical setup	30
2.5	Results	32
2.6	Discussion	38
2.7	Conclusions	40
2.8	Acknowledgments	40

<b>3</b>	<b>Long-term Evolution of Discs Around Magnetic Stars</b>	<b>43</b>
3.1	Introduction . . . . .	44
3.2	Magnetospheric interactions with a thin disc . . . . .	46
3.2.1	Magnetic torque . . . . .	46
3.2.2	Model for disc-magnetosphere interaction . . . . .	47
3.2.3	Numerical method . . . . .	50
3.3	Characteristic Timescales of Disc-Star Evolution . . . . .	52
3.3.1	Representative Model . . . . .	54
3.4	Trapped discs . . . . .	54
3.4.1	Trapped disc evolving from an accreting disc . . . . .	54
3.4.2	Trapped disc evolving from a dead disc . . . . .	55
3.4.3	Analytic estimates for a trapped disc . . . . .	57
3.5	Trapped and untrapped . . . . .	61
3.5.1	Accreting discs evolving to trapped or dead disc states . . . . .	61
3.5.2	Dead discs evolving into trapped discs . . . . .	64
3.5.3	Long-term behaviour of discs of finite size . . . . .	66
3.6	Conclusions . . . . .	68
3.7	Discussion . . . . .	69
3.7.1	‘Propellering’ . . . . .	71
<b>4</b>	<b>Accretion Discs Trapped Near Corotation</b>	<b>75</b>
4.1	Introduction . . . . .	76
4.1.1	Accretion at a centrifugal barrier . . . . .	77
4.1.2	Trapped discs . . . . .	78
4.2	The model for magnetospheric accretion . . . . .	79
4.2.1	Characteristic numbers . . . . .	81
4.3	Spin evolution and physical properties of a trapped disc . . . . .	82
4.3.1	Observability of trapped discs . . . . .	82
4.3.2	Accretion rate and angular momentum exchange with the star . . . . .	83
4.4	Cyclic accretion . . . . .	85
4.4.1	Parameter map of the instability . . . . .	85
4.4.2	Period and Amplitude of Instability . . . . .	88
4.4.3	Interpretation of the instability regions . . . . .	91
4.4.4	The effect of cycles on angular momentum exchange . . . . .	91
4.4.5	Transient instability cycles . . . . .	94
4.5	Relevance for Astrophysical Sources . . . . .	96
4.5.1	Trapped discs and the disc instability in EXors . . . . .	96
4.5.2	NS transients w/ weak recurrent outbursts . . . . .	98
4.5.3	Persistent X-ray pulsars . . . . .	99
4.6	Discussion . . . . .	100
4.7	Conclusions . . . . .	102

---

4.8	Acknowledgments . . . . .	103
<b>5</b>	<b>Soft X-ray Components in the Hard State of Accreting Black Holes</b>	<b>107</b>
5.1	Introduction . . . . .	108
5.2	Physics of interaction region . . . . .	110
5.2.1	Origin of soft excesses . . . . .	110
5.2.2	Definition of the model . . . . .	110
5.2.3	Energy and mass balance . . . . .	112
5.2.4	Reference model . . . . .	113
5.2.5	Results for the reference model . . . . .	119
5.3	Comparison to observations . . . . .	120
5.3.1	SWIFT J1753.5-0127 . . . . .	121
5.3.2	GX 339-4 . . . . .	123
5.4	Discussion . . . . .	124
5.4.1	Mass flux in the hot layer . . . . .	125
5.4.2	Spectrum of the hot ring . . . . .	126
5.4.3	Comparison with other work . . . . .	126
5.5	Conclusions . . . . .	128
<b>6</b>	<b>Samenvatting</b>	<b>131</b>
6.1	Röntgendubbelsterren . . . . .	131
6.2	'Magnetosferische' accretie . . . . .	132
	<b>Acknowledgments</b>	<b>135</b>



---

# Chapter 1

---

## Introduction

### 1.1 OVERVIEW

This thesis explores dynamical and radiative processes that occur in accretion flows around various stellar-mass objects. The work is divided into two separate themes: the interaction between strong stellar magnetic fields and accretion flows (chapters 2, 3, and 4) and radiative processes and accretion flow geometry in black holes at low luminosity (chapter 5).

### 1.2 ACCRETION PROCESSES AROUND STARS

Accretion in astrophysics is defined as the process in which gas falls into a gravitational potential well (such as a star or a black hole), which converts its gravitational energy into kinetic, thermal or radiative energy. Typically a large fraction of the gravitational potential energy is released as radiation, making accretion-powered stars much brighter than their non-accreting counterparts. The amount of energy released will depend on the depth of the accreting object's potential well. This is often expressed as the *compactness* of an object,  $M_*/R_*$ , or the ratio of the object's mass to radius (in a black hole, the radius is given by the event horizon). The more compact a star, the deeper its potential well. Both neutron stars and black holes are so compact that the fraction of energy released (compared to the rest mass energy of the accreted matter) is considerably larger than in nuclear fusion. Unsurprisingly, accretion-powered objects are some of the brightest, highest-energy observable sources in the Universe.

The luminosity of an accreting object is frequently characterized by its *Eddington luminosity*. This is defined as the luminosity at which the radiation pressure from accretion equals the gravitational potential, which then slows accretion (thus decreasing the luminosity, which is derived from accretion energy). The Eddington luminosity thus acts to set a rough upper boundary on the luminosity of a source. If the accretion is spherically symmetric and electron scattering is the dominant form of radiation pressure (assuming the gas is entirely hydrogen), the Eddington luminosity will be given by:

$$L_{\text{Edd}} = 4\pi GM_* m_p c / \sigma_T, \tag{1.1}$$

where  $\sigma_T$  is the Thomson cross-section of the electron, and  $m_p$  is the proton mass (Frank et al. 2002). The Eddington luminosity will have a corresponding accretion rate,  $\dot{M}_{\text{Edd}}$ , which will depend on the efficiency at which gravitational potential energy is converted to radiation, and the depth of the potential well. For comparison, in a solar-mass star,  $L_{\text{Edd}} \sim 10^{38} \text{ ergs}^{-1}$ , or roughly  $25\,000 L_{\odot}$ , while both accreting neutron stars and black holes show maximum luminosities  $\sim L_{\text{Edd}}$ .

A number of objects in our galaxy primarily radiate due to accretion. These generally fall into two categories: binaries and single stars. In the first category, compact stars accrete from a binary companion, which donates mass either via Roche lobe overflow or by a stellar wind. The second process arises in the late stages of star formation, after the protostar has formed out of a collapsed molecular cloud but matter continues to fall inwards. The accretion processes are similar in both, although accreting compact stars radiate at much higher energies and generally evolve on much shorter timescales. Most significantly, the gas accreted in both cases will have a large amount of angular momentum, which the gas must shed in order to move inwards.

The initial angular momentum of the accreting gas slows the rate of accretion onto the star. Unless the accretion time is very short compared with the cooling time of the gas, the gas will rapidly cool as it orbits around the star. Since the accretion flow is pressure-supported, the gas will fall into an axisymmetric disc in orbit around the star, with a pressure scale-height  $H/r < 1$ . Except in unusual cases (such as an ADAF, described in 1.5.2), this condition will generally hold, and accretion will proceed from an *accretion disc*. Gas will thus rotate in the disc in nearly Keplerian orbits, slowly accreting inwards.

In order to accrete onto the star, the angular momentum must be transported outwards in the disc, which requires that gas in adjacent orbits interacts viscously. The magnitude of viscosity needed to power observed accreting sources is much larger than the molecular viscosity of the gas and is generally attributed to some form of turbulence generated by instabilities in the disc, which act over some radial extent and produce an effective viscosity in the disc. Discovering likely instability candidates for viscosity has been a major area of research in accretion physics. Currently the leading viscosity candidate is the Magneto-Rotational Instability (MRI; Balbus & Hawley 1991), which is produced by weak magnetic fields being sheared by the relative rotation in the disc. Questions such as the magnitude of instability (Fromang & Papaloizou 2007), or whether it can account for accretion in weakly ionized young star discs (Gammie 1996) remain unanswered, however.

Even without knowing the exact source of the effective viscosity in an accretion disc, researchers have still been able to make tremendous progress in understanding accretion physics. One of the most fruitful achievements in 20<sup>th</sup>-century astrophysics was an estimate for the effective viscosity in an accretion disc by Shakura & Sunyaev (1973). They speculated that some (unknown) source of turbulence was responsible for the viscosity in the disc, which would then have some characteristic lengthscale and speed. They assumed  $H$ , the pressure scale height in the disc, to be the characteristic length scale for the turbulent eddies, and  $c_s$ , the sound speed in the disc, to be a characteristic speed. This allowed them to write

down a definition for viscosity:

$$\nu \simeq \alpha c_s H, \quad (1.2)$$

in which  $\alpha \leq 1$  is a dimensionless number that parameterizes the uncertainty in the viscosity. The magnitude of  $\alpha$  and its functional dependence on other parameters remains unknown, but this description of the viscosity has allowed for considerable progress.

### 1.2.1 Thin accretion discs

Using (1.2) for the viscosity, and defining an inner boundary condition for the disc (where material deviates from Keplerian orbits to crash onto the star), Shakura & Sunyaev (1973) constructed a solution for the density and temperature structure of a thin, diffusive accretion disc with a fixed accretion rate ( $\dot{M}$ ). Assuming that the disc is optically thick, their results predict a disc radiating thermally with a maximum temperature that depends on the compactness of the accreting object and the accretion rate. In a neutron star or black hole accreting at a moderately high rate, the thermal peak will be in the soft X-ray band, corresponding well with observed luminosities and X-ray spectra. This early accreting disc model has provided the basis for accretion physics.

## 1.3 ACCRETING STARS WITH STRONG MAGNETIC FIELDS

Many accreting stars (X-ray pulsars, Intermediate Polars, T Tauri stars) have large organized magnetic fields that govern the gas dynamics in the inner regions of the accreting flow, disrupting the disc and channelling material along field lines onto the surface of star. The point where the disc will be disrupted is usually called the *magnetospheric radius* or *Alfvén radius*, which we here define as the inner edge of the disc,  $r_{\text{in}}$ . It can be (somewhat crudely) estimated as the location where the magnetic pressure,  $B^2/4\pi$ , is equal to the ram pressure of the infalling gas,  $\dot{M}v_r$  (Pringle & Rees 1972).

We assume for simplicity that the magnetic field is a dipole aligned with the star's spin axis and the disc (so that the problem is axisymmetric). Adopting cylindrical coordinates  $[r, \phi, z]$  with the  $z$ -axis aligned with the star's spin axis, the magnitude of the field in the plane of the disc is  $B_z = B_S \left(\frac{R_*}{r}\right)^3$  (where  $B_S$  is the field at the stellar surface, and  $R_*$  is the star's radius). If the radial velocity of the gas is of order to the Keplerian velocity so that  $v_r \sim (GM_*/r)^{1/2}$ , the magnetospheric radius will be approximately:

$$r_{\text{in}} \sim \left( \frac{B_S^2 r_*^6}{(GM_*)^{1/2} \dot{M}} \right)^{2/7}. \quad (1.3)$$

Material passing through  $r_{\text{in}}$  will be channelled onto a small region near the magnetic pole, and add a considerable amount of angular momentum ( $\sim \dot{M}(GM_* r_{\text{in}})^{1/2}$ ) to the star, causing the star to spin faster.

Since  $r_{\text{in}}$  can be considerably larger than  $R_*$ , a rapidly-spinning star could in principle spin faster than the Keplerian rotation rate at  $r_{\text{in}}$ . In this case, the spinning magnetosphere will create a centrifugal barrier at  $r_{\text{in}}$  that can prevent gas from accreting (Pringle & Rees 1972; Illarionov & Sunyaev 1975). This introduces a second characteristic length scale into the problem, the *corotation radius*, defined as the point where the Keplerian frequency in the disc is equal to  $\Omega_*$ , the star's rotation frequency:

$$r_c \equiv \left( \frac{GM_*}{\Omega_*^2} \right)^{1/3}. \quad (1.4)$$

When  $r_{\text{in}} < r_c$ , accretion can proceed normally, while for  $r_{\text{in}} > r_c$  the centrifugal barrier will likely reduce or even halt accretion onto the star. As we describe in section 1.4, the behaviour of the disc in the latter case is subject to considerable uncertainties.

Beyond  $r_{\text{in}}$  the magnetic field is not strong enough to completely disrupt the disc, but can still strongly influence its behaviour. This is especially true for the region close to  $r_{\text{in}}$  where the magnetic pressure and gas pressure are still of similar order. Exactly how the magnetic field and disc interact in this region remains the subject of considerable controversy and active research. (For an excellent review of the current state of magnetospheric accretion studies, please see Uzdensky 2004). The picture summarized below represents the closest current consensus between analytical and numerical study.

Provided that the disc is somewhat ionized, magnetic field lines will likely become strongly embedded in the disc's surface, so that the field's footpoint rotates with the Keplerian rate of the disc (Lovelace et al. 1995). The other footpoint of the field line is of course attached the star and will rotate at  $\Omega_*$ . Except for at  $r = r_c$ , the relative rotation rate of the star and the disc will distort the field lines and create an additional  $B_\phi$  component. This will generate a magnetic torque which allows additional angular momentum exchange between the star and the disc:

$$\tau = \pm \int_{r_{\text{in}}}^{r_{\text{in}}+\Delta r} 4\pi r^2 \frac{B_p B_\phi}{4\pi} \hat{z}, \quad (1.5)$$

where  $\Delta r$  is the width of the region coupling the disc and the star. The sign of the angular momentum exchange depends on the relative location of the connected field line and  $r_c$ : if  $r < r_c$ , this exchange adds angular momentum to the star, while if  $r > r_c$ , angular momentum is extracted.

Analytic arguments suggest that the region of coupling between the magnetic field lines and the disc (which we call the *interaction region*,  $\Delta r$  in our work) will be small, with  $\Delta r < r_{\text{in}}$  (Lovelace et al. 1995). This is because the induced  $B_\phi$  component can only grow to a maximum of  $\sim B_p$  before the twisted magnetic field line inflates and eventually opens, severing the connection between the star and the disc (Aly 1985; Uzdensky et al. 2002). The opened field lines could then launch an outflow of material from the disc (e.g. Blandford & Payne 1982; Lovelace et al. 1999), or provide a site for reconnection (Uzdensky et al. 2002). In the late 1990's, magnetohydrodynamical simulations of a magnetic field interacting with a disc confirmed this basic picture (Hayashi et al. 1996; Miller & Stone 1997; Goodson et al.

1999). Simulations have typically found that the field adopts a largely open geometry (shown schematically in fig. 2.1 in the next chapter), with only the inner regions of the disc strongly interacting with the star. Both outflows and accretion are also typically seen, as field lines open and then reconnect.

A number of questions remain unresolved within the picture outlined above. Particularly unclear is the relative importance of the interaction with the disc and outflows in regulating the angular momentum of the star. Outflows provide an additional way for the star and disc to shed angular momentum, but the details of how they are powered and how much mass can be lost via outflow is uncertain (Spruit 2010). The star-disc coupling can in principle be very efficient in transporting angular momentum, but this depends on the extent of the connected region (which in turn depends on the rate at which field lines can reconnect above the disc or diffuse through it). Additionally, some authors have suggested that on long timescales the field itself could evolve radially through the disc, either spreading out radially (Agapitou & Papaloizou 2000), or being dragged in by the accreting matter (as in the X-wind model of Shu et al. 1994). All of these factors will influence the efficiency and importance of disc-field coupling on angular momentum transport through the disc.

In our work we construct a parameterized model for the disc-field interaction that incorporates most of the uncertainties listed above, and assume that any variability created by field line opening and reconnection can be time-averaged over the timescales that we are interested in. We explicitly neglect the (unknown) role of outflows in our calculations, in order to focus on the evolution as a result of the coupling between the disc and the field.

### 1.3.1 Observations of magnetospheric accretion

Observations of accreting magnetic stars offer both support and challenges for the basic picture of magnetospheric accretion outlined above. Below we summarize the evidence for magnetospheric accretion in two different types of accreting magnetic stars: T Tauri stars and X-ray pulsars. Both these stars show strong evidence for magnetically-regulated accretion, as well as unexplained observations.

#### **T Tauri Stars**

T Tauri stars are often observed to have strong stellar magnetic fields (up to  $1 - 2$  kG), and show some evidence of spin regulation by the interaction between the disc and magnetic field. They also show a significant amount of X-ray activity, which is attributed to magnetic flares in either the star or the star-disc coupling (Getman et al. 2008). In this thesis we focus particularly on observations of one class of T Tauri stars known as ‘EXors’. EXors, like their prototype, EX Lupi are characterized by repeated large outbursts: changes by up to four magnitudes in luminosity lasting several months, with a characteristic total period of several years (Herbig 2007, 2008). The timescale of the outbursts suggests variations in the

disc structure in the inner region of the disc, which could arise as a result of the interaction between a disc and field.

### X-ray pulsars

Accreting X-ray pulsars show direct evidence of magnetospheric accretion, through their pulsations on timescale between  $\sim 10^{-3} - 10^2$  seconds, which is attributed to the magnetic pole sweeping through our line of sight (Davidson & Ostriker 1973). In some pulsars, this probe of the star's rotational period shows an evolution in time (e.g. Bildsten et al. 1997), and variations in the derivative of the period that correlate (or anticorrelate) with luminosity changes in the star.

X-ray pulsars also show more indirect evidence of magnetic field-disc interaction. Two millisecond accreting X-ray pulsars, NGC 6440 X-2 (Patruno et al. 2010; Hartman et al. 2010) and SAX J1808.4-3658 (Patruno et al. 2009) show strong quasi-periodic oscillations on timescales similar to the evolution timescales in the inner disc, which might be powered by the same mechanism as the accretion bursts in EXors. NGC 6440 X-2 also shows short-duration outbursts of accretion with a very short recurrence time, which could be a result of magnetic fields suppressing accretion.

## 1.4 MAGNETIC ACCRETION AT LOW $\dot{M}$ : 'PROPELLERS', OUTFLOWS AND DEAD DISCS

In sec. 1.3 we presented the standard argument for determining the truncation radius of an accretion disc in the presence of a magnetic field. This calculation presupposes that there is some accretion at the inner edge of the disc. However, when  $r_{\text{in}} > r_{\text{c}}$ , the interaction between the disc and the field creates a centrifugal barrier that opposes accretion onto the star, so this reasoning no longer holds. Matter will continue to move inwards from large distances, but will be prevented from accreting onto the star. What then happens in this case?

A common assumption is that once  $r_{\text{in}} > r_{\text{c}}$ , the interaction between the disc and the magnetic field will completely expel the mass at  $r_{\text{in}}$  in an outflow. This is known as the 'propeller' regime, with the behaviour of the spinning magnetosphere likened to a propeller flinging matter out of the system (Illarionov & Sunyaev 1975). The propelling disc 'solves' the problem of (1.3) by assuming that when  $r_{\text{in}} > r_{\text{c}}$  the matter flowing through the disc will be expelled rather than accreted.

It is not clear what the accretion rate (if any) onto the star should be for the propeller regime, although one would assume that it should decrease sharply around  $r_{\text{in}} = r_{\text{c}}$  if most of the mass flowing through the disc is being expelled in an outflow and only a small amount accreted onto the star (and hence render the source observable). Despite this, observational results often refer to sources as being in the 'propeller' regime, meaning only that  $r_{\text{c}}$  [eqn (1.4)] is larger than  $r_{\text{in}}$  (as calculated using (1.3) for the observed accretion rate). This clearly

does not make sense: if the ratio of accreted to outflowing matter were very small, then the total accretion rate through the disc (incorporating the unobserved outflow) could be large enough to make (1.3) smaller than (1.4)!

The problem is caused by what is understood by ‘propeller regime’. The original suggestion referred to systems in which the disc is truncated at a considerable distance outside  $r_c$ , so that  $\Omega_* \gg \Omega_K(r_{in})$ . In this case the rotational energy of the magnetosphere is much larger than that of the disc, so it seems reasonable to expect that the majority of the disc mass will be expelled in the disc-field interaction. However, in order to avoid a logical problem (i.e. what happens if most but not all the mass is expelled at  $r_{in}$ ?), models of the propeller regime are typically *constructed* to ensure that the disc is completely expelled in a magnetic outflow by the time it reaches  $r_{in}$  (e.g. Lovelace et al. 1999). This is in spite of the fact that the physics of powering magnetospheric outflows (e.g. how much energy is required, or how much mass can be expelled) is still uncertain (Spruit 1997). Further adding to the confusion is the tendency (as noted above), to define the ‘propeller’ regime as the one where  $r_{in} > r_c$  as determined by (1.3) and (1.4), despite the fact that the definition of a propeller implies a system in which matter is expelled rather than accreted. The logic is thus: a) the centrifugal barrier at  $r_{in}$  will prevent accretion onto the star, b) there is (probably) enough energy in the rotation of the magnetosphere to expel the disc in an outflow, c) since the accretion rate in the disc is determined far from  $r_{in}$ , the disc *must* be expelled, otherwise, where would the mass go?

This logic fails most obviously for cases where  $r_{in} < 1.26 r_c$ , where the rotation rate of the magnetosphere is less than the escape speed of the gas. As the gas at  $r_{in}$  is brought into corotation with the star, the added rotational energy will not be enough to expel it, but the centrifugal barrier will prevent it from accreting onto the star (Spruit & Taam 1993). The same condition could of course hold for a disc truncated even further from  $r_c$ : having enough energy for the gas to escape is a necessary but not sufficient condition for the disc to be expelled, and some of the gas at  $r_{in}$  could remain confined in the disc.

The solution to this problem is that the standard disc solution that describes accretion onto a star or magnetosphere (Shakura & Sunyaev 1973) does not necessarily apply to discs truncated outside  $r_c$ . This is not such a problem as it initially appears, since there are in fact a whole class of time-independent accretion disc solutions with different boundary conditions at  $r_{in}$ . The most well-known of these is the solution for a disc accreting onto the surface of a non-magnetic star spinning close to break-up. Popham & Narayan (1991) and Paczynski (1991) independently demonstrated that the interaction between the disc and the rapidly spinning star can transfer angular momentum outwards so that accretion can proceed while the star remains spinning at breakup. This changes the inner boundary condition, and alters the surface density profile in the inner regions of the disc so that the angular momentum added at  $r_{in}$  can be transported outward.

A similar disc solution exists for the case where accretion onto the star is completely suppressed but the disc-field interaction adds angular momentum to the inner edge of the disc. This solution (described in more detail in chapter 2) was first proposed by Sunyaev

& Shakura (1977), who dubbed it a ‘dead disc’ since the accretion rate onto the star is close to zero and the temperature of the disc itself is low enough to render the disc nearly undetectable. The inner edge of the disc in a dead disc is determined by the location where the rate of angular momentum being injected into the disc at  $r_{\text{in}}$  balances the rate at which the disc can transport it outwards (which depends on the surface density of the disc). In a dead disc, the inner radius is thus determined by the amount of mass in the disc, rather than the accretion rate through it. More mass in the inner parts of the disc means that the disc can transport more angular momentum outwards, and  $r_{\text{in}}$  will move to  $r_c$ . This disc solution will also be relevant for systems in which there is an outflow near  $r_{\text{in}}$  that is not strong enough to expel gas at the same rate at which it is being accreted from further away.

If the average accretion rate falls enough that accretion onto the star is suppressed, then mass can begin to pile up in the inner regions of the disc. This will last until there is enough mass in the disc to push  $r_{\text{in}}$  inside  $r_c$ , where the excess mass can be accreted. The result will be bursts of accretion onto the star, with the timescale regulated by the viscous diffusion timescale in the inner regions of the disc (Sunyaev & Shakura 1977; Spruit & Taam 1993). A new physical description of this instability (which incorporates the dead disc phase) is presented in chapter 2, where we investigate the nature of the resulting outburst (e.g. its shape, amplitude and duration). In chapter 4 we continue this investigation more quantitatively, and explore how the instability evolves together with the spin evolution of the star.

This picture for magnetospheric accretion has a number of other consequences in addition to accretion bursts. It also predicts that the disc will remain truncated very close to  $r_c$  as long as there is accretion onto the star. As a result, the disc can efficiently spin down the star even when the accretion rate is essentially zero. In chapter 3 we investigate the long-term evolution of dead and marginally accreting discs, following their evolution as the spin-rate of the star also changes.

## 1.5 ACCRETION AROUND BLACK HOLES AT LOW LUMINOSITIES

Observations of accreting black hole binaries offer a unique opportunity to test accretion physics. Since black holes themselves have no detectable intrinsic radiation, virtually all of the detectable radiation comes from accretion processes. As well, the deep potential well of a black hole means that accreted matter will lose a substantial fraction (between 6-40%) of its rest mass energy as it falls into the hole (Frank et al. 2002). Accreting black holes thus also offer the opportunity to probe the physics of matter at very high energies and densities, far above what is accessible to terrestrial laboratories. The early development of the theory of accretion flows and discs (e.g. Pringle & Rees 1972; Shakura & Sunyaev 1973) arose as a consequence of early X-ray observations of black holes, and the field of accretion physics has evolved in tandem with improving spectral and photometric observations. Chapter 5 concerns accretion around black holes at very low accretion rates. As we outline below,

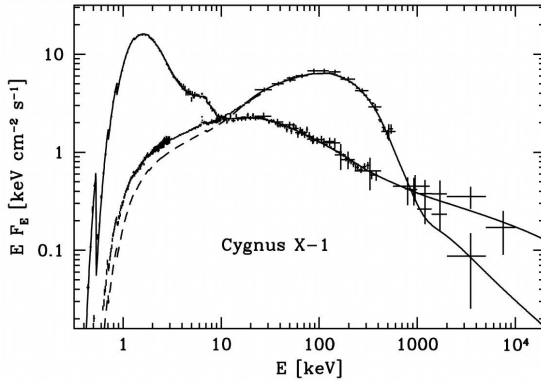


**Figure 1.1:** High  $\dot{M}$  and low  $\dot{M}$  spectral states for Cyg X-1. The high state spectrum peaks at  $\sim 2$  keV, and has a power-law tail that continues up to  $\gamma$ -ray energies. The low state shows much harder power-law emission that peaks at  $\sim 200$  keV then rapidly declines. (Figure taken from McConnell et al. 2002).

much of the physics of accretion at these low accretion rates remains uncertain.

### 1.5.1 X-ray spectra of black holes

The X-ray spectra of accreting black hole binaries change dramatically as a function of the accretion rate. This is illustrated in figure 1.1, which is taken from McConnell et al. (2002). The crosses (with spectral fit models overlaid) shows two observations of X-ray and  $\gamma$ -ray emission for Cyg X-1 (a  $\sim 10 M_{\odot}$  accreting black hole) at different accretion rates. At high accretion rates (above  $\sim 10\%$   $L_{\text{Edd}}$ , the ‘high/soft’ state), the spectrum is typically dominated by a soft X-ray quasi-thermal profile, peaking at  $1 - 2$  keV, with a steep, power law tail extending up to  $\gamma$ -rays. As the X-ray luminosity of the source drops, the X-ray spectrum becomes dominated by hard roughly power-law emission that cuts off in the hard X-rays ( $\sim 200$  keV), and the soft X-ray thermal component disappears (the ‘low/hard’ state). Both spectra show excess emission around  $6 - 7$  keV produced by iron K- $\alpha$  emission and broadened by rotation and relativistic effects (Remillard & McClintock 2006).

The interpretation of black hole X-ray spectra is somewhat controversial. In the high/soft state, the quasi-thermal spectrum is attributed to a standard optically thick accretion disc (Shakura & Sunyaev 1973), and the iron K- $\alpha$  line (and related ‘reflection’ spectrum, Ross & Fabian 2007) is attributed to back-scattering of the high-energy spectral component off the surface of the disc. The power-law component itself is likely generated by inverse Compton scattering, the up-scattering of soft ( $\sim 1$  keV) X-ray photons to much higher energies as they collide with a population of high-energy ( $\sim 100$  keV) electrons (e.g. Rybicki & Lightman 1986) in an optically-thin corona above the disc. In the low/hard state, the power-law emission is usually also attributed to inverse Compton scattering, but both the geometry of the upscattering plasma and the fate of the optically thick disc are unclear.

### 1.5.2 Is the thin disc truncated at low $\dot{M}$ ?

The change in X-ray spectra indicate dramatic changes in the accretion flow as the accretion rate decreases. The thermal disc becomes nearly undetectable, indicating that it does not contribute much to the overall accretion energy budget. The upscattering electrons must be hot enough to produce the hard X-ray spectrum, which means that only a small fraction of the disc can interact with the corona (Haard & Maraschi 1991). This has led some researchers to suggest that the optically thick disc might vanish in the inner regions of the accretion flow when the mean accretion rate drops. Instead, the inner regions of the flow are filled with an optically thin, hot plasma that is the source of upscattering electrons needed to produce Inverse Compton radiation.

The most well-known model of this type is the ‘Advection-Dominated Accretion Flow’ (ADAF) solution proposed by Narayan & Yi (1994). In an ADAF the gas is fully ionized, and the density of the plasma is so low that the collision timescale between protons and electrons becomes comparable to the viscous timescale of the flow (the time it takes material to flow into the black hole). Since the protons can only effectively cool through collisions with electrons (which can then cool via bremsstrahlung or inverse Compton scattering), as viscous turbulence heats up the plasma, the protons will keep heating up while the electrons can cool. The result is a two-temperature plasma, with an electron temperature of about 200 keV and a proton temperature of about 20 MeV. Since the protons carry most of the energy of the flow (due to their much larger mass), the majority of the accretion energy is advected into the hole rather than radiated (hence ‘advection dominated’). The electrons will upscatter seed photons (either from the truncated disc or other processes like synchrotron radiation), which then produce the observed spectra.

The ADAF solution is only one of a large class of radiatively inefficient accretion solutions for the inner disc region. However, for the entire class the picture is very different from a standard optically thick accretion disc. Instead, the inner disc is truncated when the accretion rate is very low, and the inner regions close to the star are optically thin, radiatively inefficient, and much hotter.

### 1.5.3 Accretion discs bombarded by ions

It is not known how the accretion flow transitions from an outer cool disc to a hot inner ADAF, although in order for the ADAF to accrete, it must be able to shed excess angular momentum outward (cf. sec. 1.2). Spruit (1997) considered the interaction between the 20 MeV protons of an ADAF and a cool (1 keV) accretion disc. He suggested that as the protons bombarded the disc, the large energy transfer would evaporate the upper layers of the disc into a hot ( $\sim 100$  keV) surface corona. Deufel & Spruit (2000); Deufel et al. (2001, 2002) further developed this work using Monte Carlo simulations of ions bombarding a cool disc to confirm the presence of a surface corona and determine its temperature and optical depth. Since the surface corona has a much higher temperature than the cool disc, its viscosity will

also be higher (1.2), so that the corona will flow inside the cool disc. In Spruit & Deufel (2002) the authors found that this process would heat up the corona in this inner region until it finally evaporated back into an ADAF, making the cycle self-sustaining. Finally, Dullemond & Spruit (2005) constructed a steady-state model for the accretion flow, incorporating the interaction between the ADAF and the disc. This allowed them to calculate the energetic contribution of each part of the flow. The main conclusion of this work is that some fraction of energy from the ADAF (which would otherwise be advected) can instead be converted somewhat indirectly into detectable radiation. The result emphasizes the importance of energy exchange (either by radiation or matter) between the different components of the accretion flow – particularly at low luminosities when the disc does not directly contribute much to the overall energy budget.

#### 1.5.4 Soft excesses: evidence of an untruncated disc?

Recent observations of two X-ray sources (GX339-4 and SWIFT J1753.5-0127) have challenged the picture of a truncated emission disc at low accretion rates (Miller et al. 2006a,b). These researchers found soft emission below 2 keV in both sources in excess of the power-law component. By fitting their data with thermal disc models, they claimed that the spectra showed direct evidence of very faint thermal accretion discs ( $kT \sim 0.2 - 0.3$  keV), consistent with being untruncated. Their interpretation of the spectra was somewhat simplistic (in particular, they account for reflected emission off the cool disc but not reprocessing), but nonetheless posed a challenge for the truncated disc paradigm.

In Chapter 5 we re-examine this conclusion, considering the energy exchange between different components of the accretion flow. Using the results of Dullemond & Spruit (2005) we construct a model spectrum for the accretion flow, to demonstrate that the soft excesses seen in the low/hard state of black hole binaries can be consistent with a moderately truncated accretion disc.

## 1.6 SUMMARY OF THE MAIN RESULTS OF THESIS

- When an accretion disc is truncated by a strong stellar magnetic field close to the corotation radius ( $r_c$ ; where the spin of the star equals the Keplerian rotation of the disc), the angular momentum transferred from the star to the disc can remain confined in the disc and be transferred outward, preventing the disc from accreting (called a ‘dead disc’). A dead disc is characterized by a very low accretion or outflow rate, but active angular momentum transport outward. Chapter 2
- The dead disc state can result in cyclic accretion bursts, in which mass builds up and is periodically accreted onto the star. The presence, duration, magnitude, and outburst profile of these bursts depend on the time-averaged accretion rate in the disc, and the

radial width of the transition region between accreting ( $r_{\text{in}} < r_c$ ) and non-accreting ( $r_{\text{in}} > r_c$ ) regions. The timescale for the accretion bursts varies by more than five orders of magnitude. Chapter 2

- The instability timescale and burst magnitude agrees with observed variability in several classes of magnetic stars. In particular, low-frequency QPOs observed in accreting Neutron Stars (such as appear in the tail of outbursts in SAX J1808.-3658 and NGC 6440-X2) happen on the order of viscous frequencies in the inner accretion disc, and could be the result of this instability. As well, a class of T Tauri stars known as ‘EX-ors’, show periodic outbursts that could also be caused by this instability. *Chapters 2 and 4.*
- If the accretion rate in the disc falls to zero, a dead disc can persist and spin down the star. The evolution of the system in this case will follow one of two paths. In the first, the disc will move gradually away from  $r_c$  as angular momentum is added, and stellar spin-down will effectively stop. In the second, the dead disc will remain trapped close to  $r_c$  as  $r_c$  moves outwards, and the star can spin down indefinitely. We refer to these as ‘trapped’ discs. This bifurcation could account for observed magnetic white dwarfs and Ap stars, some of which rotate rapidly, and some very slowly. *Chapter 3*
- Accretion in a trapped disc will typically be very low, and can proceed either as steady-state accretion (*Chapter 3*) or accretion bursts (*Chapter 4*). The presence of cycles in a trapped disc can appear transiently as the star’s spin changes. *Chapter 4*
- Whether or not a disc will become trapped will depend on the physical extent of the disc, and whether it has a sink for angular momentum at the outer edge of the disc (for example, a companion). It will also depend on the detailed disc-field coupling, and ratio of the viscous diffusion timescale at  $r_c$  compared to the spindown timescale of the star. *Chapter 3*
- Two forms of accretion instability exist: one at low  $\dot{M}$  with periods of quiescence (as envisioned in previous work), and one at higher  $\dot{M}$  with no periods of quiescence and much higher frequency. The presence of the instability in both cases can modify the rate of angular momentum transfer between the star and the disc (with respect to steadily accreting cases). *Chapter 4*
- In the low-luminosity state around accreting black holes, different components in the accretion flow are responsible for different components in the observed X-ray spectrum. These different components exist in close proximity and likely exchange energy via matter or radiation, so that considering this energetic coupling is critical when modelling the spectrum. *Chapter 5.*
- The energy exchange (by matter and radiation) between a cool truncated accretion disc and a hot ADAF produces a 100 keV corona above the disc and hot ring 200 keV just

inside it. The energy exchange between the corona and the disc will heat the disc and produce an excess of soft X-ray emission even at low luminosities. This excess can reproduce the soft excesses observed in black hole binaries in the low-luminosity state.  
*Chapter 5.*

## REFERENCES

- Agapitou V., Papaloizou J. C. B., 2000, MNRAS, 317, 273
- Aly J. J., 1985, A&A, 143, 19
- Balbus S. A., Hawley J. F., 1991, ApJ, 376, 214
- Bildsten L., Chakrabarty D., Chiu J., Finger M. H., Koh D. T., Nelson R. W., Prince T. A., Rubin B. C., Scott D. M., Stollberg M., Vaughan B. A., Wilson C. A., Wilson R. B., 1997, ApJS, 113, 367
- Blandford R. D., Payne D. G., 1982, MNRAS, 199, 883
- Davidson K., Ostriker J. P., 1973, ApJ, 179, 585
- Deufel B., Dullemond C. P., Spruit H. C., 2001, A&A, 377, 955
- Deufel B., Dullemond C. P., Spruit H. C., 2002, A&A, 387, 907
- Deufel B., Spruit H. C., 2000, A&A, 362, 1
- Dullemond C. P., Spruit H. C., 2005, A&A, 434, 415
- Frank J., King A., Raine D. J., 2002, *Accretion Power in Astrophysics: Third Edition.* Cambridge, UK: Cambridge University Press
- Fromang S., Papaloizou J., 2007, A&A, 476, 1113
- Gammie C. F., 1996, ApJ, 457, 355
- Getman K. V., Feigelson E. D., Micela G., Jardine M. M., Gregory S. G., Garmire G. P., 2008, ApJ, 688, 437
- Goodson A. P., Böhm K.-H., Winglee R. M., 1999, ApJ, 524, 142
- Haard F., Maraschi L., 1991, ApJ, 380, L51
- Hartman J. M., Galloway D. K., Chakrabarty D., 2010, ArXiv e-prints
- Hayashi M. R., Shibata K., Matsumoto R., 1996, ApJ, 468, L37+
- Herbig G. H., 2007, AJ, 133, 2679
- Herbig G. H., 2008, AJ, 135, 637
- Illarionov A. F., Sunyaev R. A., 1975, A&A, 39, 185
- Lovelace R. V. E., Romanova M. M., Bisnovaty-Kogan G. S., 1995, MNRAS, 275, 244
- Lovelace R. V. E., Romanova M. M., Bisnovaty-Kogan G. S., 1999, ApJ, 514, 368

- McConnell M. L., Zdziarski A. A., Bennett K., Bloemen H., Collmar W., Hermsen W., Kuiper L., Paciesas W., Philips B. F., Poutanen J., Ryan J. M., Schönfelder V., Steinle H., Strong A. W., 2002, *ApJ*, 572, 984
- Miller J. M., Homan J., Miniutti G., 2006, *ApJ*, 652, L113
- Miller J. M., Homan J., Steeghs D., Rupen M., Hunstead R. W., Wijnands R., Charles P. A., Fabian A. C., 2006, *ApJ*, 653, 525
- Miller K. A., Stone J. M., 1997, *ApJ*, 489, 890
- Narayan R., Yi I., 1994, *ApJ*, 428, L13
- Paczynski B., 1991, *ApJ*, 370, 597
- Patruno A., Watts A., Klein Wolt M., Wijnands R., van der Klis M., 2009, *ApJ*, 707, 1296
- Patruno A., Yang Y., Altamirano D., Armas-Padilla M., Cavecchi Y., Degenaar N., Kalamkar M., Kaur R., Klis M. V. D., Watts A., Wijnands R., Linares M., Casella P., Rea N., Soleri P., Markwardt C., Strohmayer T., Heinke C., 2010, *The Astronomer's Telegram*, 2672, 1
- Popham R., Narayan R., 1991, *ApJ*, 370, 604
- Pringle J. E., Rees M. J., 1972, *A&A*, 21, 1
- Remillard R. A., McClintock J. E., 2006, *ARA&A*, 44, 49
- Ross R. R., Fabian A. C., 2007, *MNRAS*, 381, 1697
- Rybicki G. B., Lightman A. P., 1986, *Radiative Processes in Astrophysics*
- Shakura N. I., Sunyaev R. A., 1973, *A&A*, 24, 337
- Shu F., Najita J., Ostriker E., Wilkin F., Ruden S., Lizano S., 1994, *ApJ*, 429, 781
- Spruit H. C., 1997, in Meyer-Hofmeister E., Spruit H., eds, *LNP Vol. 487: Accretion Disks - New Aspects X-ray spectrum of a disk illuminated by ions*. pp 67–76
- Spruit H. C., 2010, in T. Belloni ed., *Lecture Notes in Physics, Berlin Springer Verlag Vol. 794 of Lecture Notes in Physics, Berlin Springer Verlag, Theory of Magnetically Powered Jets*. pp 233–
- Spruit H. C., Deufel B., 2002, *A&A*, 387, 918
- Spruit H. C., Taam R. E., 1993, *ApJ*, 402, 593
- Sunyaev R. A., Shakura N. I., 1977, *Pis ma Astronomicheskii Zhurnal*, 3, 262
- Uzdensky D. A., 2004, *Ap&SS*, 292, 573
- Uzdensky D. A., Königl A., Litwin C., 2002, *ApJ*, 565, 1191

---

## Chapter 2

---

# Episodic Accretion on to Strongly Magnetic Stars

Caroline R. D'Angelo and Hendrik C. Spruit

MNRAS 406, 1208, 2010

Some accreting neutron stars and young stars show unexplained episodic flares in the form of quasi-periodic oscillations or recurrent outbursts. In a series of two papers we present new work on an instability that can lead to episodic outbursts when the accretion disc is truncated by the star's strong magnetic field close to the corotation radius (where the Keplerian frequency matches the star's rotational frequency). In this paper we outline the physics of the instability and use a simple parameterization of the disc-field interaction to explore the instability numerically, which we show can lead to repeated bursts of accretion as well as steady-state solutions, as first suggested by Sunyaev and Shakura (1977). The cycle time of these bursts increases with decreasing accretion rate. These solutions show that the usually assumed 'propeller' state, in which mass is ejected from the system, does not need to occur even at very low accretion rates.

## 2.1 INTRODUCTION

The interaction between a strong stellar magnetic field and an accretion disc can affect both the evolution and observational properties of the star. Close to the star the field is strong enough that the accretion disc is truncated, and mass is channelled along field lines to accrete on to the star's surface. At the inner edge of the truncated disc, the field and disc interact directly over some finite region, allowing for angular momentum exchange from the differential rotation between the Keplerian accretion disc and the star.

Angular momentum exchange between the field and the disc leads to two different states that can exist for a disc truncated by a magnetic field. The distinction depends on the position of the truncation radius relative to the corotation radius,  $r_c \equiv (GM_*/\Omega_*^2)^{1/3}$  (where  $M_*$  and  $\Omega_*$  are respectively the mass and spin frequency of the star), the radius at which the Keplerian frequency in the disc equals the star's rotational frequency. If the disc is truncated inside  $r_c$  then the field-disc interaction extracts angular momentum from the disc and accretion can proceed. If on the other hand the disc is truncated outside  $r_c$ , the star-field interaction will create a centrifugal barrier that inhibits accretion. This is usually called the 'propeller regime', under the assumption that most of the mass in the disc is expelled as an outflow (Illarionov & Sunyaev 1975).

Accreting stars with strong magnetic fields such as T Tauri stars, and X-ray millisecond pulsars show a large degree of variability in luminosity (corresponding to changes in accretion rate), which may be ascribable to magnetic activity. For example, the protostar EX Lupi (the prototype of the 'EXor' class), a T Tauri star, increases and decreases in brightness by several magnitudes every 2–3 years (Herbig 2007). At much higher energies, a 1 Hz quasi-periodic oscillation in accreting millisecond pulsar SAX J1808.8-3658 has been observed during the decay phase of several outbursts (Patruno et al. 2009). The time-scale and magnitude of the variability in both sources suggest changes in accretion rate in the inner regions of the accretion disc, where it interacts with the star's magnetic field.

In this paper we revisit a disc instability first suggested in Sunyaev & Shakura (1977) and developed in Spruit & Taam (1993) (hereafter ST93), which can lead to episodic bursts of accretion. The instability arises when the magnetic field truncates the disc near the corotation radius. The magnetic field initially truncates the disc outside but close to the corotation radius, thus transferring angular momentum from the star to the disc and inhibiting gas from accreting on to the star (the propeller state). However, close to  $r_c$ , the energy and angular momentum transferred by the field to the gas will not be enough to unbind much of the disc mass from the system and drive an outflow. Instead, the interaction with the magnetic field will prevent accretion (Sunyaev & Shakura 1977). As gas in the inner regions of the disc piles up, the local gas pressure increases, forcing the inner edge of the disc to move inwards until it crosses  $r_c$ . When the inner region of the disc crosses inside  $r_c$ , the centrifugal barrier preventing accretion disappears (since now the differential rotation between star and disc has changed sign) and the accumulated reservoir of gas is accreted on to the star. Once the reservoir has been accreted, the accretion rate through the disc's inner edge decreases, and

the disc will again move outside  $r_c$ , allowing another cycle to start.

We study this process by following the time evolution of a thin axisymmetric viscous disc, with a parameterization of the interaction between the disc and the magnetic field both inside and outside  $r_c$ . This approach allows us to investigate the behaviour of the disc on time-scales much longer than the rotation period of the star. Long time-scales are important since the instability evolves on viscous rather than dynamical time-scales of the disc. We are able to reduce the uncertainties in the detailed MHD interaction between the field and the disc to two free (but constrained) parameters. Using this description we can then investigate the physical conditions for which the instability develops.

In this paper we describe in detail the physics that can lead to episodic bursts of accretion and give a brief overview of the observed oscillations. In a later paper we will explore the range of outbursts seen in our simulations in more detail, and discuss their prospects for observability in specific stellar systems.

## 2.2 MAGNETOSPHERE-DISC INTERACTIONS

### 2.2.1 Interaction region between a disc and magnetic field

We consider a star with a strong dipolar magnetic field surrounded by a thin Keplerian accretion disc. We assume that the dipole is aligned with both the star's spin axis and the spin axis of the disc, so that the system is axisymmetric. Near the surface of the star the magnetic field will truncate the disc, forcing gas into corotation with the star. This inner region (in which the gas dynamics is regulated by the magnetic field) is called the magnetosphere, and we define the *magnetospheric radius*,  $r_m$  as the radius at which the magnetic field is no longer strong enough to force the disc into corotation (Spruit & Taam 1993). Outside  $r_m$  the magnetic field will penetrate the disc and become strongly coupled over some radial extent, which we call the *interaction region*,  $\Delta r$ . Beyond the interaction region the disc and magnetic field are decoupled, so that the outer parts of the disc are not directly affected by the stellar magnetic field. Figure 2.1 shows a schematic picture for the magnetic field configuration, with a closed magnetosphere close to the star, and a large region of opened field lines further out.

In the interaction region, the differential rotation between the Keplerian disc and star shears the magnetic field, generating an azimuthal component  $B_\phi$  from the initially poloidal field. This in turn creates a magnetic stress which exerts a torque on the disc, transferring angular momentum between the disc and star. The torque per unit area exerted by the field on the disc is given by  $d\tau/dr = rS_{z\phi}\hat{\mathbf{z}}$ , where

$$S_{z\phi} \equiv \pm \frac{B_\phi B_z}{4\pi} \quad (2.1)$$

is the magnetic stress generated by the twisted field lines. The sign of the torque will depend on the location of the coupled disc region relative to the corotation radius,  $r_c \equiv (GM_*/\Omega_*^2)^{1/3}$ .

If the coupling takes place inside  $r_c$  the torque will extract angular momentum from the disc, spinning down the disc (and spinning up the star), while if the coupling is outside  $r_c$  the torque adds angular momentum to the disc, spinning it up (and spinning down the star).

The radial extent of the interaction region has been a point of long-standing controversy in the study of accretion discs. In an early series of influential papers, Ghosh et al. (1977; Ghosh & Lamb 1979a,b) argued that the coupled region is large ( $\Delta r/r \gg 1$ ), so that the magnetic field exerts a torque over a considerable fraction of the disc with a resulting large influence on the spin evolution of the star. However, the original model proposed by Ghosh & Lamb was shown to be inconsistent by Wang (1987), since the magnetic pressure they derived from field winding far from  $r_c$  is high enough to completely disrupt the majority of the disc.

More recent analytical and numerical work has shown that the interaction region is likely much smaller, and much of the disc is disconnected from the star (see Uzdensky 2004 for a recent review). This comes about from the fact that in force-free regions (where the magnetic pressure dominates over the gas pressure) as are likely to exist above an accretion disc, field lines will tend to become open as the twisting increases (Aly 1985; Lynden-Bell & Boily 1994). As the disc and star rotate differentially, the increasing twist  $\Delta\phi$  in the field line will only increase the  $B_\phi$  component to some maximum  $B_\phi \sim B_z$  before the increased magnetic pressure above the disc causes the field lines to become inflated and eventually open, severing the connection between the disc and star. Analytic studies of a sheared force-free magnetic field (Aly 1985; van Ballegoijen 1994; Uzdensky et al. 2002) have shown that the  $B_\phi$  component will grow to a maximum twist angle  $\Delta\phi \sim \pi$  before opening. The twist angle grows on the time-scale of the beat frequency  $\equiv |\Omega_* - \Omega_K|^{-1}$ , which is very short compared to the viscous time-scale in the disc except in a very small region around corotation.

To prevent field lines from opening, they must be able to slip through the disc faster than the field is being wound up. The rate at which the field can move through the disc is set by the effective diffusivity,  $\eta$ , of the disc. Like the effective viscosity,  $\nu$ , that drives the transport of angular momentum, the effective diffusivity is also assumed to be driven by turbulent processes in the disc. Recent numerical studies of MRI turbulence (believed to be responsible for angular momentum transport in at least the inner regions of accretion discs) have tried to measure  $\eta$  directly. In these simulations, an external magnetic field is imposed on a shearing box simulation, and the effective magnetic diffusivity is estimated as the flow becomes unstable. The results suggest that the effective diffusivity and viscosity are of similar size, that is, the effective magnetic Prandtl number,  $Pr \equiv \nu/\eta$  is of order unity (Fromang & Stone 2009). Such a large magnetic Prandtl number implies that for realistic disc parameters the magnetic field will not be able to slip through the majority of the disc fast enough to prevent field lines from opening (Lovelace et al. 1995; Uzdensky et al. 2002). Outside this region there will still be some coupling between the disc and the star (as the disc moves from Keplerian to corotating orbits), but this estimate suggests that the actual extent of coupling is small ( $\Delta r/r < 1$ ) regardless of where the disc is truncated relative to the

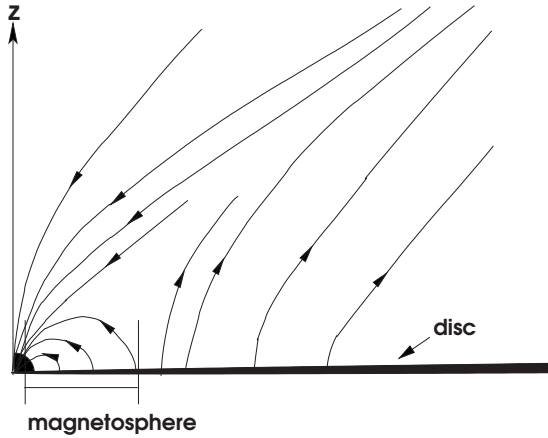


**Figure 2.1:** Global magnetic field configuration for a strongly magnetic star surrounded by an accretion disc. In this picture, the majority of the field exists in an open configuration, and the connected region between the field and the disc is very small. Adapted from Lovelace et al. (1995).

corotation radius.

Once the field lines are opened, there may be some reconnection across the region above the disc between open magnetic field lines (e.g. Aly & Kuijpers 1990; Goodson et al. 1997; Uzdensky et al. 2002). The effective size of the interaction region would then depend on the efficiency of reconnection, and could also then become time-dependent (although likely on time-scales of order the dynamical time, which is much shorter than the viscous evolution time-scale). The opening and reconnection of field lines has also been suggested as a possible launching mechanism for strong disc winds and a jet (e.g. Aly & Kuijpers 1990; Hayashi et al. 1996; Goodson et al. 1997). This picture of a small interaction region with some reconnection was first proposed by Lovelace et al. (1995), and has been supported by 2 and 3D simulations of accretion discs interacting with a magnetic field (e.g. Miller & Stone 1997; Goodson et al. 1997; Hayashi et al. 1996; Romanova et al. 2009).

In summary, although the extent of the interaction region is uncertain (subject to uncertainties in the effective diffusivity of magnetic field in the disc and its possible reconnection in the magnetosphere, as well as the detailed interaction between the disc and field near the magnetosphere), numerical and analytic work suggests that it is small. Except for very special geometries for the magnetic field (such as Agapitou & Papaloizou 2000; Shu et al. 1994), the low effective magnetic diffusivity in the disc will force the magnetic field into a largely open configuration, and the majority of the accretion disc will be decoupled from the star, in strong contrast to the prediction of the Ghosh & Lamb (1979a) model.

The extent of the interaction region as well as the average magnitude of the  $B_\phi$  component generated by the disc-field interaction will depend on the detailed interaction between the disc and the field as it varies from Keplerian orbits to corotation with the star, as well as the frequency and magnitude of possible reconnection events. In the present work we therefore assume that the time-averaged  $B_\phi$  component generated by field-line twisting will be some

constant fraction of  $B_z$ , so that  $B_\phi/B_z \equiv \gamma < 1$ . We also assume that  $\Delta r/r$  is small ( $< 1$ ) but leave it as a free parameter.

### 2.2.2 Accretion and angular momentum transport

In this paper we describe the evolution of an accretion disc in which the conditions at the inner boundary are changing in time. Before doing this, however, we review how the conditions at the inner boundary affect the angular momentum transport and density structure of a thin accretion disc. In the thin-disc limit the evolution equation for the surface density  $\Sigma$  can be written:

$$\frac{\partial \Sigma}{\partial t} = \frac{3}{r} \frac{\partial}{\partial r} \left[ r^{1/2} \frac{\partial}{\partial r} (r^{1/2} v \Sigma) \right], \quad (2.2)$$

where  $v$  is the effective viscosity in the disc that enables angular momentum transport. In a steady state (in which the accretion rate is constant throughout the disc), the general solution for  $v \Sigma$  is given by:

$$v \Sigma = \frac{\dot{m}}{3\pi} \left( 1 - \beta \left( \frac{r_i}{r} \right)^{1/2} \right), \quad (2.3)$$

where  $r_i$  is the inner edge of the disc,  $\dot{m}$  is the accretion rate and  $\beta$  is a dimensionless measure of the angular momentum flux through the disc per unit mass accreted (Popham & Narayan 1991; Paczynski 1991).

All accretion discs have a boundary layer at their inner edge that connects the disc with either the surface of the star or the star's magnetosphere. In the boundary layer the gas must transition from Keplerian orbits to orbits corotating with the star in order to accrete. The structure of this boundary layer will determine the value of  $\beta$  in (2.3). In the standard accretion scenario, that is, for accretion on to a slowly-rotating star or on to the star's magnetosphere inside the corotation radius, the gas in the boundary layer will be decelerated, meaning that there will be a maximum in the rotation profile,  $\Omega(r)$ . At the maximum in  $\Omega(r)$ , there is no longer an outward transfer of angular momentum from viscous torques, which in the thin-disc approximation will cause the surface density to decrease sharply, so that  $\beta = 1$  in (2.3) (Pringle & Rees 1972; Shakura & Sunyaev 1973). The maximum in  $\Omega(r)$  effectively corresponds to the inner radius of the disc, since inside this radius gas is viscously decoupled from the rest of disc. The gas falling through the inner boundary of the disc will add its specific angular momentum ( $\dot{m} r_{\text{in}}^2 \Omega$ ) to the star, spinning it up.

However, there are in fact a wide range of solutions for the surface density profile of an accretion disc depending on the conditions imposed by the boundary layer, which in turn set the rate of angular momentum transport across the inner boundary of the disc. In a nonmagnetic star spinning close to breakup (Paczynski 1991; Popham & Narayan 1991), the angular momentum flux can be inward or outward, depending on the accretion history of the star. The dimensionless angular momentum flux  $\beta$  can in principle have any value less than

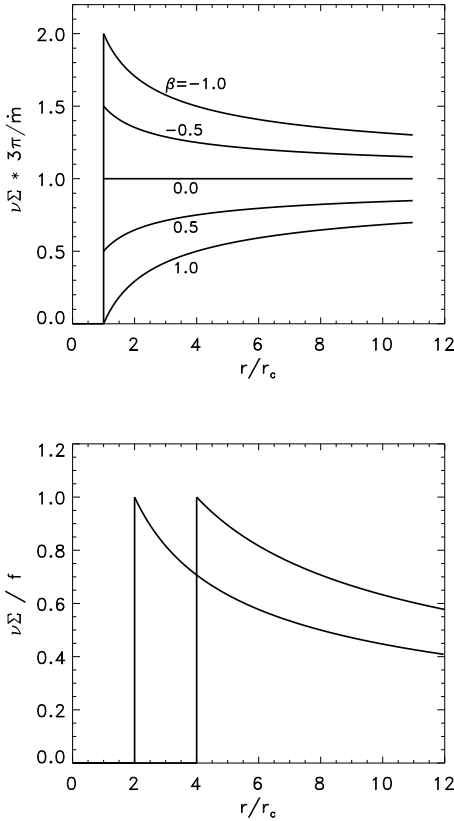


**Figure 2.2:** Surface density  $\nu\Sigma$  of a thin disc as a function of distance from the corotation radius  $r_c$ , for a steady, thin viscous disc. Top: steady accretion at a fixed accretion rate  $\dot{m}$ , for inner edge of the disc at corotation.  $\beta$  measures the angular momentum flux,  $\beta = 1$  corresponding to the standard case of accretion on to a slowly rotation object. For  $\beta < 0$  the angular momentum flux is outward (spindown of the star). Bottom: ‘quiescent disc’ solutions with  $\dot{m} = 0$  and a steady outward angular momentum flux due to a torque  $f$  applied at the inner edge. The two curves show solutions for  $r_{in}/r_c = 2$  and 4.

1 in this case. The top panel of Fig. 2.2 shows the steady-state surface density profile for a range of different values of  $\beta$  from -1 to 1.

Sunyaev & Shakura (1977) studied a similar situation in which there is outward angular momentum transport in an accretion disc, and showed adding angular momentum at the inner edge of the accretion can in fact halt accretion altogether. The evolution of the disc in this case depends on the rate at which angular momentum is being injected at the inner edge of the disc compared to the rate at which it is carried outwards via viscous coupling. If angular momentum is injected into the inner boundary of the disc at exactly the same rate as viscous transport carries it outwards, then all accretion on to the star will cease. For a steady state like this to exist, the outward angular momentum flux due to the magnetic torque at the inner

edge of the disc has to be taken up at some larger distance. In a binary system, this sink of angular momentum can be the orbit of the companion star. If the disc is sufficiently large, the angular momentum can also be taken up by the outer parts of the disc, while the inner parts of the disc are close to a steady state. The inner edge of the disc then slowly moves outward under the influence of the angular momentum flux. The surface density distribution in this case can be found from (2.3) by taking the limit  $\dot{m} \rightarrow 0$ , while letting  $\beta \rightarrow -\infty$  (noting that it measures the angular flux per unit accreted mass). This yields:

$$v\Sigma = f(r_i) \left(\frac{r_i}{r}\right)^{1/2}, \quad (2.4)$$

where  $f(r_i)$  is a measure of the torque exerted at the inner edge of the disc. The bottom panel of Fig. 2 shows the surface density, scaled to the value of  $f(r_i)$ , for two instances of (2.4) with different values of  $r_{\text{in}}$ .

Sunyaev & Shakura (1977) refer to this solution as a ‘dead disc’, since there is no accretion on to the star. In this paper we call non-accreting discs without large outflows ‘quiescent discs’, to avoid confusion with ‘dead zones’ thought to be present in proto-stellar discs (regions in which there is insufficient ionization to drive angular momentum transport via MRI but are too hot for efficient angular momentum transport via gravitational instabilities; e.g. Gammie 1996). These quiescent discs play a role in the cyclic solutions discussed in Section 2.3. In these solutions accreting phases are separated by long intervals in which the inner disc is close to the quiescent state described by (2.4).

### 2.2.3 Evolution of a disc truncated inside the corotation radius

When the accretion disc is truncated by a magnetic field inside the corotation radius, the standard  $\beta = 1$  case applies for a steady-state solution. The location of the inner edge of the disc  $r_{\text{in}}$  will be determined by the interaction between the disc and magnetic field, and change with changing conditions at the inner edge (such as the accretion rate on to the star). Here we estimate the location of  $r_{\text{in}}$ , and use it to show how the inner boundary of the disc will change in a non-steady disc.

We define the inner edge of the disc as the point at which material in the disc is forced into corotation with the star. We use the azimuthal equation of motion for gas at the magnetospheric radius to obtain an estimate for  $r_{\text{in}}$  in a disc (see, e.g. ST93):

$$2\pi\Sigma \frac{\partial}{\partial t}(rv_\phi) - \frac{\dot{m}_{\text{in}}}{r} \frac{\partial}{\partial r}(rv_\phi) + 2\pi r S_{z\phi} = 0, \quad (2.5)$$

where  $\dot{m}_{\text{in}} = -2\pi r \Sigma v_r$  is the accretion rate through the inner edge of the disc. (2.5) neglects viscous angular momentum transport through the inner regions of the disc, under the assumption that it will be much smaller than angular momentum transport from the magnetic field. Using  $v_\phi = \Omega_* r$  (since at  $r_{\text{in}}$  the gas corotates with the star), and assuming a steady-state solution ( $\partial/\partial t = 0$ ), (2.5) becomes:

$$\frac{\dot{m}\Omega_*}{\pi} = r_{\text{in}}S_{z\phi} = \frac{r_{\text{in}}B_\phi B_z}{4\pi}, \quad (2.6)$$

where  $S_{z\phi}$  is the magnetic stress from the coupling between the disc and star (introduced in Section 2.2.1). As long as the wind-up time for the field is shorter than the rate at which  $r_{\text{in}}$  is changing,  $B_\phi/B_z$  will be roughly constant, so we make the assumption that  $B_\phi = \eta B_z$ , where  $\eta < 1$  and is constant.

For a dipole field aligned with the star's axis of rotation ( $B_z = \mu/r^3$ , where  $\mu = B_S R_*^3$  is the star's magnetic dipole moment), (2.6) can be re-written:

$$r_{\text{in}} = \left( \frac{\eta\mu^2}{4\Omega_*\dot{m}_{\text{in}}} \right)^{1/5}. \quad (2.7)$$

For  $\eta = 0.1$ , this estimate gives a value for  $r_{\text{in}}$  about 40% smaller than the simple estimate found by equating the magnetic pressure from the field ( $B^2/8\pi$ ) to the ram pressure from spherically-symmetric gas in free-fall on to the star (e.g. Pringle & Rees (1972)).

The derivation for  $r_{\text{in}}$  above holds for steady accretion. For the problem studied here the position of the inner edge (set by the location of the magnetosphere) will change in time, which requires a minor reinterpretation of (2.7). If  $r_{\text{in}}$  is moving in time, the mass flux  $\dot{m}_{\text{co}}$  in the reference frame comoving with  $r_{\text{in}}$  differs from the mass flux,  $\dot{m}$ , measured in a fixed frame:

$$\dot{m}_{\text{co}} = \dot{m} + 2\pi r \Sigma \dot{r}_{\text{in}}, \quad (2.8)$$

where  $\dot{r}_{\text{in}}$  is the time derivative of  $r_{\text{in}}$ .

Since the torque between the magnetosphere and the disc acts at the inner edge, the mass flux entering the magnetosphere (used in (2.7)) is given by  $\dot{m}_{\text{co}}$ , not  $\dot{m}$ . As before,  $\dot{m}$  itself is given in terms of the surface density by the usual thin disc expression:

$$\dot{m} = 3r_{\text{in}}^{1/2} \frac{\partial}{\partial r} \left( r^{1/2} v \Sigma \right) \Big|_{r_{\text{in}}}. \quad (2.9)$$

## 2.2.4 Evolution of a disc truncated outside the corotation radius

If the star is spinning fast enough, the magnetic field can truncate the disc *outside*  $r_c$ . In this case the interaction with the magnetic field will *add* angular momentum to the disc, creating a centrifugal barrier that inhibits accretion. This scenario was first described by Illarionov & Sunyaev (1975) and is often termed the 'propeller' regime, under the assumption that the interaction with the magnetic field will expel the disc at  $r_{\text{in}}$  as an outflow via the 'magnetic slingshot' mechanism (Blandford & Payne 1982).

However, in order for the gas to be ejected from the system, it must be accelerated to at least the escape speed ( $v_{\text{esc}} = \sqrt{GM_*/2r}$ ). At the inner edge of the interaction region the gas is brought into corotation with the star, where  $v_c = \Omega_* r$ . If this is less than the

escape speed, the majority of the gas will not be accelerated enough to be expelled. Setting  $v_{esc} = v_c = \sqrt{GM_*/r_c^3}r$  implies that for  $r_{in} < 1.26r_c$  most of the gas will not be expelled.

Part of the disc could still be expelled in an outflow, but while the majority of the gas remains confined in the disc, the disc can act as an efficient sink for angular momentum from the star and accretion can effectively be halted. The open field lines at larger radii could launch a disc wind which would provide an additional sink for angular momentum and somewhat change the structure of the disc (e.g. Matt & Pudritz 2005). As well, numerical studies of the field-disc interaction find that reconnection across field lines can lead to intermittent accretion (e.g. Goodson et al. 1997, see also Section 2.6). However, models of disc winds typically include mass loss rate as a parameter of the problem, so that the amount of mass actually lost to the wind is uncertain. In this paper we make the assumption that the disc becomes quiescent, that is, for  $r_{in} > r_c$  no accretion or outflows occur. The steady-state disc solution is then given by (2.4).

In the next section we will derive  $f(r_{in})$ , the boundary condition for the surface density at the inner edge of a quiescent disc. Like for cases when  $r_{in} < r_c$ , we want to study non-steady-state solutions in which  $r_{in}$  moves in time. As in the steady-state case, to derive  $\dot{r}_{in}$  we consider the difference in accretion rate at  $r_{in}$  in a fixed frame and in a frame comoving with  $r_{in}$ . Since for a quiescent disc no matter is being accreted on to the star,  $\dot{m}_{co} = 0$ , so that (2.8) can be written:

$$2\pi r \Sigma \dot{r}_{in} = -3r_{in}^{1/2} \frac{\partial}{\partial r} \left( r^{1/2} v \Sigma \right) \Big|_{r_{in}}. \quad (2.10)$$

Together with (2.2), a viscosity prescription and condition for the outer boundary, we can use the results from this section and the previous one to study the time-dependent behaviour of an accretion disc.

## 2.3 CYCLIC ACCRETION

The existence of quiescent disc solutions can naturally lead to bursts of accretion. Since there is very little accretion on to the star or outflow, if mass continues to accrete from larger radii it will pile up in the inner regions in the disc until the gas pressure is high enough to overcome the centrifugal barrier from the magnetic field-disc interaction and accretion can proceed. Once the reservoir has been emptied the inner edge of the disc will move back outside the corotation radius and the reservoir will start to build up again.

In Sections 2.2.3 and 2.2.4 we showed how the inner radius of a thin viscous accretion disc will evolve inside and outside corotation. To study the time-dependent evolution of a disc, we must connect these two states as the inner edge of the disc passes through the corotation radius. We also require a description for  $f(r_{in})$ , the inner boundary condition for the disc truncated outside  $r_c$ .

### 2.3.1 Surface density profile for $r_{\text{in}} > r_c$

When the interaction region is outside  $r_c$ , the star is rotating faster than the Keplerian disc and the magnetic field lines lead the disc, adding angular momentum to the material in the inner regions. As discussed in Section 2.2.1, the torque per unit area exerted on the disc will be  $\langle S_{\phi z} \rangle r$ , so that the torque exerted across the entire interaction region (assuming it is small) is approximately:

$$\tau \simeq 4\pi \langle S_{\phi z} \rangle r_{\text{in}} \Delta r \hat{z}, \quad (2.11)$$

where the extra factor 2 comes from coupling to both sides of the disc.

As argued in the previous section, if the disc is truncated close to but outside  $r_c$ , the majority of the gas in the interaction region will not be expelled in an outflow. Instead, the angular momentum from the magnetic field is transferred outwards to the rest of the disc. We can derive a relationship between the position of and surface density at the inner edge of non-interacting disc from the conservation of angular momentum across the interaction region.

Since the interaction region is small we do not consider its density profile explicitly, focusing instead on its influence on the non-interacting disc. We therefore define  $r_{\text{in}}$  as the point in the disc just outside the interaction region, where there is no magnetic coupling between the disc and the star. Across the interaction region the density in the disc decreases sharply (since the gas is forced into nearly corotating orbits with the star). We make the simplifying assumption that none of the mass in the disc escapes, either into an outflow or through the magnetosphere on to the star. The inner edge of the interaction region,  $r_{\text{in}} - \Delta r$ , is therefore defined as the point at which the surface density drops to zero.

To determine  $\Sigma$  at  $r_{\text{in}}$  we consider the angular momentum flux across  $\Delta r$  when  $r_{\text{in}} > r_c$ . The flux of angular momentum must be continuous across  $\Delta r$ , meaning that the viscous angular momentum transport outside  $\Delta r$  must balance the angular momentum flux added by the magnetic field across the interaction region. This balance is written:

$$\begin{aligned} \dot{m} r^2 \Omega - 2\pi r (\nu \Sigma)^+ r^2 \Omega' = \\ \dot{m} r^2 \Omega - 2\pi r (\nu \Sigma)^- r^2 \Omega' + \int_{r_{\text{in}}}^{r_{\text{in}} + \Delta r} 4\pi r^2 S_{z\phi} dr. \end{aligned} \quad (2.12)$$

In this equation,  $\nu^\pm$  and  $\Sigma^\pm$  are the viscosity and surface density inside ( $-$ ) and outside ( $+$ )  $\Delta r$ ,  $\dot{m} = 2\pi r (\Sigma \nu_r)^\pm$  is the mass flux through  $\Delta r$  (where  $\nu_r$  is the radial velocity of the gas) and  $\Omega$  is the orbital frequency at  $r_{\text{in}}$ . The first term on either side of the equation denotes the advection of angular momentum across  $r_{\text{in}}$ , while the second is the angular momentum transported by viscous stresses. The final term on the right hand side is the angular momentum added by the magnetic field to the coupled region of the disc. The first term on both sides cancel (to enforce conservation of mass across  $\Delta r$ ), and we make the further assumption

that in the interaction region most of the angular momentum is transported through external magnetic torques rather than viscous stress, so that  $(v\Sigma)^- \ll (v\Sigma)^+$ . For a small interaction region, the last term in (2.12) can be re-written:

$$\int_{r_{\text{in}}-\Delta r}^{r_{\text{in}}} 4\pi r S_{z\phi} dr \approx 4\pi \Delta r r_{\text{in}} \langle S_{z\phi} \rangle. \quad (2.13)$$

(2.12) can then be re-written to yield the surface density at  $r_{\text{in}}$  for  $r > r_c$ :

$$(v\Sigma)^+ = -\frac{2\langle S_{z\phi} \rangle \Delta r}{\pi r_{\text{in}} \Omega'}. \quad (2.14)$$

As predicted in Section 2.2.4, (2.14) shows that the surface density at  $r_{\text{in}}$  will be large, a consequence of the torque being applied by the disc-magnetic field coupling (Sunyaev & Shakura 1977; Popham & Narayan 1991; Paczynski 1991). (2.14) corresponds to the function  $f(r_{\text{in}})$  introduced in Section 2.2.2 for  $r_{\text{in}} > r_c$ , that is, the boundary condition at the inner edge of the disc. In a time-dependent system, as gas accretes from larger radii (via viscous torques) it will pile up near  $r_{\text{in}}$  and the increased gas pressure will push the inner edge of the disc further inwards towards  $r_c$ .

### 2.3.2 Transition region

When the inner edge  $r_{\text{in}}$  is well inside  $r_c$ , conditions at the inner edge are the standard ones for accretion of a thin disc on a slowly rotating object:

$$\Sigma(r_{\text{in}}) = 0, \quad (2.15)$$

while the time-dependent position of the inner edge is determined by (2.7):

$$r_{\text{in}} = \left( \frac{\eta \mu^2}{4\Omega_* \dot{m}_{\text{co}}} \right)^{1/5}, \quad (2.16)$$

where  $\dot{m}_{\text{co}}$  is the mass flux in a frame comoving with  $r_{\text{in}}$  as discussed above.

When the inner edge is outside the corotation radius, the magnetosphere does not accrete:

$$\dot{m}_{\text{co}} = 0, \quad (2.17)$$

while the surface density at  $r_{\text{in}}$  is determined by a magnetic torque, as discussed above. With the Keplerian value for  $\Omega(r_{\text{in}})$  and assuming a dipolar magnetic field, the results of Section 2.3.1 can be re-written:

$$(v\Sigma)^+ = \frac{\eta \mu^2}{3\pi (GM_*)^{1/2}} \frac{\Delta r}{r_{\text{in}}^{9/2}}. \quad (2.18)$$

To connect these two limiting cases, we assume that the effect of the interaction processes is equivalent to a smooth transition in the conditions. This is valid since the time-scales we are interested in are much longer than the orbital time-scale on which the conditions of the transition region between disc and magnetosphere vary. The assumption is thus that the effect of the fast processes in the transition region can be represented by averages. The mass flux on to the magnetosphere is therefore taken to vary smoothly from 0 for  $r_{\text{in}}$  well outside corotation to the value in (2.16) valid well inside:

$$\dot{m}_{\text{co}} = y_m \dot{m}^+, \quad (2.19)$$

where  $\dot{m}^+$  is given by (2.16). For the connecting function  $y_m$  we take a simple function that varies from 0 to 1 across the transition:

$$y_m = \frac{1}{2} \left[ 1 - \tanh \left( \frac{r_{\text{in}} - r_c}{\Delta r_2} \right) \right] \quad (2.20)$$

where  $\Delta r_2$  is the nominal width of the disc-magnetosphere transition and a parameter of the problem.

Similarly the surface density at the inner edge makes a smooth transition from its value in (2.18) to 0:

$$\Sigma_{\text{in}} = y_\Sigma \Sigma^+, \quad (2.21)$$

where the connecting function  $y_\Sigma$  is:

$$y_\Sigma = \frac{1}{2} \left[ 1 + \tanh \left( \frac{r_{\text{in}} - r_c}{\Delta r} \right) \right]. \quad (2.22)$$

All the uncertainties in the transition region are thus subsumed in the parameters  $\Delta r$  and  $\Delta r_2$ . In Section 2.5 we study the effect of these uncertainties with a parameter survey. The effective widths of the transition of magnetospheric accretion rate and inner-edge surface density need not be the same, and we in fact find that the difference between  $\Delta r$  and  $\Delta r_2$  is important for the form of the resulting accretion cycles.

### 2.3.3 Physical constraints on $\Delta r$ and $\Delta r_2$

In this paper we treat  $\Delta r$  and  $\Delta r_2$  as free parameters. However, a lower limit on both parameters can be set by considering the stability of the inner regions of the disc to the interchange instability. In the quiescent disc, the low-density magnetosphere must support the high-density disc against infall. This configuration will be unstable to interchange instability (the analog of the Kelvin-Helmholz instability), unless the surface density gradient in the interaction region is shallow enough to suppress it. This sets a limit on the minimum width of the interaction region,  $\Delta r$ , where the density gradient falls from its maximum (at  $r_{\text{in}}$ ) to close to zero in the magnetosphere.

This instability also sets a limit on the minimum width of  $\Delta r_2$ , the transition length over which the disc moves from a non-accreting quiescent disc to one in which there is accretion through the inner boundary. As  $r_{\text{in}}$  moves closer to  $r_c$  the width of the interaction region preventing accretion (i.e. where the field lines are adding angular momentum to the disc) decreases. When the width of the interaction region outside  $r_c$  becomes smaller than is stable against the interchange instability, accretion through the magnetosphere will begin.  $\Delta r_2$  must therefore be larger or equal to this value, that is, at this minimum distance from  $r_c$  accretion onto the star will take place.

Spruit et al. (1995) studied the stability of a disc interacting with a magnetic field to interchange instabilities, and derived the following linear stability criterion:

$$\frac{B_r B_z}{2\pi\Sigma} \frac{d}{dr} \ln \left| \frac{\Sigma}{B_z} \right| > 2 \left( r \frac{d\Omega}{dr} \right)^2. \quad (2.23)$$

Assuming that  $B_r \sim B_\phi$ , in our formulation this inequality becomes:

$$\frac{3\alpha}{1 + \tanh\left(\frac{\Delta r_2}{\Delta r}\right)} \left(\frac{H}{r}\right)^2 > 2 \left(1 - \left(\frac{r_{\text{in}}}{r_c}\right)^{3/2}\right)^2. \quad (2.24)$$

For  $\alpha = 0.1$  and assuming  $H/r$  is in the range 0.07–0.1, the range of  $\Delta r/r = [0.05, 0.1]$  will satisfy this inequality for  $\Delta r_2/r = [0.01, 0.02]$ . In this inequality larger values of  $\Delta r$  correspond to smaller possible values for  $\Delta r_2$ , since larger  $\Delta r$  correspond to smaller maximum  $\Sigma(r_{\text{in}})$  and hence shallower gradients. This instability has recently been studied using 3D numerical simulations (Kulkarni & Romanova 2008), who find numerically approximately the same criterion for stability as Spruit et al. (1995). The shaded regions of Figs. 2.7 and 2.8 show the values for  $\Delta r_2$  and  $\Delta r$  that are unstable to the instability studied in this paper. The simple analysis of this section suggests that at least part of the shaded sections in Figs. 2.7 and 2.8 will be stable against the interchange instability, so that the larger magnetosphere-disc instability could occur.

## 2.4 NUMERICAL IMPLEMENTATION

### 2.4.1 Disc equation and viscosity prescription

To study the surface density evolution of an accretion disc interacting with a magnetic field as outlined in the previous section, we use a time-dependent numerical simulation of a diffusive accretion disc. Our assumption that the interaction region is small ( $\Delta r/r < 1$ ) means that rather than calculate the disc behaviour in the interaction region explicitly we can instead use the physics of the interaction region to derive boundary conditions for the inner edge of the non-interacting disc.

We assume that the accretion disc (outside the interaction region) can be treated in the thin-disc limit, so that the evolution equation for the surface density  $\Sigma$  is given by (2.2). We assume that the viscosity in the disc follows a power-law dependence, so that:

$$v = v_0 r^\gamma, \quad (2.25)$$

where  $v_0 = \alpha(GM_*)^{1/2}(H/R)^2$  and  $\gamma = 0.5$  following the standard  $\alpha$ -viscosity prescription (Shakura & Sunyaev 1973). To evolve (2.2) in time, we require boundary conditions at  $r_{\text{in}}$  and  $r_{\text{out}}$ , plus an additional equation to describe the movement of the inner edge of the disc,  $\dot{r}_{\text{in}}$ . We set the outer boundary by defining the mass accretion rate through the outer edge of the disc ( $\dot{m}$ ), which we vary as a parameter of the problem. This defines the time-averaged mass accretion rate in the disc. The surface density at the inner edge of the disc is given by (2.21):

$$\Sigma(r_{\text{in}}) = \frac{\eta\mu^2}{6\pi(GM_*)^{1/2}v_0 r_{\text{in}}^{9/2+\gamma}} \left[ \tanh\left(\frac{r_{\text{in}} - r_{\text{c}}}{\Delta r}\right) + 1 \right]. \quad (2.26)$$

We calculate the displacement of the inner boundary using the results of Sections 2.2.3 and 2.2.4, by considering the difference between the total mass flux at  $r_{\text{in}}$  in a fixed and comoving frame of reference:

$$\dot{m}_{\text{co}} = \dot{m} + 2\pi r \Sigma \dot{r}_{\text{in}}, \quad (2.27)$$

where  $\dot{m}_{\text{co}}$  is given by (2.19). This expression can be re-written:

$$6\pi r_{\text{in}}^{1/2} \partial_r (v \Sigma r_{\text{in}}) = -2\pi r_{\text{in}} \Sigma(r_{\text{in}}) \dot{r}_{\text{in}} + \left[ 1 - \tanh\left(\frac{r_{\text{in}} - r_{\text{c}}}{\Delta r_2}\right) \right] \frac{\eta\mu^2}{8\Omega_* r_{\text{in}}^5}. \quad (2.28)$$

Taken together, (2.2), (2.25), (2.26), (2.28) and an outer boundary condition describe the time-dependent evolution of an accretion disc.

## 2.4.2 Steady-State solution

From the results of the previous sections, we can calculate the steady-state solutions for a given  $\dot{m}$ , the average mass accretion rate. For certain values of  $\dot{m}$ ,  $\Delta r$  and  $\Delta r_2$ , this equilibrium is unstable, leading to oscillations in  $r_{\text{in}}$  and corresponding accretion bursts.

In a steady-state, the accretion rate is constant throughout the disc, i.e.  $\dot{m}_{\text{co}} = \dot{m}$ :

$$\dot{m} = \frac{1}{2} \left[ 1 - \tanh\left(\frac{r_{\text{in}} - r_{\text{c}}}{\Delta r_2}\right) \right] \frac{\eta\mu^2}{4\Omega_* r_{\text{in}}^5}. \quad (2.29)$$

Implicitly solving (2.29) for  $r_{\text{in}}$  yields the inner radius of the disc in a steady-state solution.

The general steady-state surface density profile was calculated in Section 2.2.2, and is given by (2.4) with an additional term since  $\dot{m} \neq 0$  in the disc. The function  $f(r_{\text{in}})$  is given by equation (2.18). The steady-state surface density profile will thus be:

$$\begin{aligned} v\Sigma = & \frac{\dot{m}}{3\pi} \left[ 1 - \left( \frac{r_{\text{in}}}{r} \right)^{1/2} \right] \\ & + \frac{\eta\mu^2\Delta r}{6\pi r_{\text{in}}^4 (GMr)^{1/2}} \left[ 1 + \tanh \left( \frac{r_{\text{in}} - r_c}{\Delta r} \right) \right] \end{aligned} \quad (2.30)$$

The numerical simulations described in the following sections of the evolution of a viscous accretion disc show that the equilibrium solution given by (2.29) and (2.30) can become unstable to episodic bursts of accretion by the process outlined in Section 2.3.

### 2.4.3 Numerical setup

To follow the time-dependent evolution of a viscous accretion disc interacting with a magnetic field we use a 1D numerical simulation, first making a series of mathematical transformations.

The power-law prescription for the viscosity, (2.25), allows us to define a new function,  $u$ , for convenience:

$$u \equiv \Sigma r^{1/2+\gamma} \quad (2.31)$$

To make our results more readily applicable to different magnetic stars (e.g. neutron stars, magnetic white dwarves and protostars), we adopt scale-free coordinates. The instability studied in this paper varies on viscous time-scales of the inner disc, which are in general much shorter than the time-scale over which the transfer of angular momentum between the star and the disc can substantially change the star's rotation period. A constant rotation period implies that a constant corotation radius, making it a natural choice for scaling our variables. We thus scale the radial coordinate to the corotation radius, and the time in terms of the viscous time-scale ( $r^2/\nu$ ) at the corotation radius. Further, since we are most interested in the behaviour of inner regions of the disc, we adopt a coordinate system comoving with  $r_{\text{in}}$ :

$$r' \equiv \frac{r - r_{\text{in}}}{r_c}; t' \equiv t \frac{v_0}{r_c^{2-\gamma}}. \quad (2.32)$$

Dropping the prime notation, the surface density evolution equation in the new coordinate system then becomes:

$$\frac{\partial u}{\partial t} = 3r^{\gamma-1/2} \frac{\partial}{\partial r} \left[ r^{1/2} \frac{\partial u}{\partial r} \right] + \dot{r}_{\text{in}} \frac{\partial u}{\partial r}, \quad (2.33)$$

with the boundary condition at  $r_{\text{in}}$  given by:

$$u(r_{\text{in}}) = \frac{\eta\mu^2}{4\pi(GM_*)^{1/2}v_0r_c^4} \frac{\Delta r}{r_{\text{in}}} r_{\text{in}}^{-3} \left[ \tanh\left(\frac{r_{\text{in}}-1}{\Delta r}\right) + 1 \right]. \quad (2.34)$$

The evolution of the inner edge of the disc is given by:

$$\dot{r}_{\text{in}} = \left[ 1 - \tanh\left(\frac{r_{\text{in}}-1}{\Delta r_2}\right) \right] \frac{\eta\mu^2}{16\pi\Omega_*v_0^2r_c^{\gamma-3/2}} \frac{r_{\text{in}}^{-11/2+\gamma}}{u(r_{\text{in}})} - \frac{3r_{\text{in}}^\gamma}{u(r_{\text{in}})} \frac{\partial u}{\partial r} \Big|_{r_{\text{in}}}. \quad (2.35)$$

Finally, to increase the resolution at the inner edge of the disc we make a further coordinate transformation to an exponentially scaled grid:

$$x \equiv \frac{1}{a} \left[ \ln\left(\frac{r-r_{\text{in}}}{r_{\text{out}}-r_{\text{in}}}\right) + 1 \right], \quad (2.36)$$

where  $a$  is a scaling factor to set the clustering of grid points around  $r_{\text{in}}$ .

We calculate the second-order discretization of the spatial derivatives on an equally-spaced grid in  $x$ . To evolve the resulting system of equations in time requires an algorithm suitable for stiff equations. This is necessary to follow the evolution of the inner boundary, (2.28). When  $r_{\text{in}} \gg r_c$ , (2.28) reduces to a differential equation that is first order in time. However, for  $r_{\text{in}} \ll r_c$ ,  $\Sigma(r_{\text{in}})$  becomes very small, and the equation essentially becomes time-independent. We have formulated the problem so that  $\Sigma(r_{\text{in}})$  stays small but non-zero for all values of  $r_{\text{in}}$  (so that the solutions is continuous at all values of  $r_{\text{in}}$ ), but its small value inside  $r_c$  means that the differential equation is stiff (since the evolution equation for  $r_{\text{in}}$  in (2.28) contains terms of very different sizes). To perform the time evolution, we therefore use the semi-implicit extrapolation method (Press et al. (1992), p. 724), which is second-order accurate in time and suitable for stiff equations.

Since the grid comoves with the inner radius, the outer boundary of our disc also moves. We set the accretion rate at the outer boundary to be fixed in the moving coordinate system, so that it changes slightly as the outer boundary moves. The effect is negligible as long as the disc is large enough that the outer parts of the disc are unaffected by the changing inner boundary condition, which we confirm by varying the position of the outer boundary of the disc.

The solutions are sensitive to the changing conditions at the inner boundary of the disc. To confirm that our results are robust for the grid we have chosen, we varied the various numerical parameters of the problem: grid resolution, the exponential stretch parameter  $a$  at the inner boundary (see (2.36)) and the fractional accuracy of the solution computed by the semi-implicit extrapolation method (which sets the maximum possible timestep).

## 2.5 RESULTS

Our primary goal in this paper is to study the conditions for which the disc is unstable to episodic outbursts. To do this we follow the evolution of an accretion disc in which the mean mass accretion rate,  $\dot{m}$  is a parameter of the problem by setting  $\dot{m}$  as the accretion rate through the disc's outer boundary. The other system parameters of the problem are the stellar mass,  $M_*$ , frequency,  $\Omega_*$ , and magnetic moment,  $\mu$ . The interaction between the magnetic field and the disc introduces three additional parameters:  $\eta \equiv B_\phi/B_z$ , the fractional width of the interaction region  $\Delta r/r$ , and  $\Delta r_2/r$ , the length scale over which the inner edge of the disc moves from a non-accreting to accreting state. Finally, our description of the viscosity, (2.25), introduces three additional parameters:  $\alpha$ , the aspect ratio of the disc,  $H/R$  (assumed constant), and  $\gamma$ , the radial power-law dependence of the viscosity.

The problem has two scale invariances, which reduces the number of free parameters. As seen in (2.25),  $\alpha$  and  $H/R$  are degenerate. Additionally, the system parameters  $\mu$ ,  $M_*$ ,  $\Omega_*$  and  $\dot{m}$  can be re-written as the ratio  $\dot{m}/\dot{m}_c$ , where  $\dot{m}_c$  is the accretion rate in (2.7) that puts the magnetospheric radius at  $r_c$ . This ratio is equivalent to the 'fastness parameter',  $\Omega_{\text{in}}/\Omega_*$  (where  $\Omega_{\text{in}}$  is the Keplerian frequency at  $r_{\text{in}}$ ) which is sometimes used to describe disc-magnetosphere interactions.

For reference, our dimensionless parameter  $\dot{m}/\dot{m}_c$  can be expressed in terms of physical parameters appropriate for protostellar systems:

$$\frac{\dot{m}}{\dot{m}_c} = \left( \frac{\dot{m}}{2.3 \times 10^{-7} M_\odot \text{yr}^{-1}} \right) \left( \frac{M_*}{0.6 M_\odot} \right)^{5/3} \left( \frac{B_s}{2000 \text{G}} \right)^{-2} \left( \frac{R_*}{2.1 R_\odot} \right)^{-6} \left( \frac{P_*}{1 \text{ day}} \right)^{7/3}. \quad (2.37)$$

We assume that the time-averaged  $B_\phi$  component will be constant with radius in the coupled region, and set the parameter  $\eta = 0.1$ . For the viscosity,  $\nu = \alpha(GM_*)^{1/2}(H/R)^2 r^{-\gamma}$ , we take  $\alpha = 0.1$  and  $H/R = 0.1$  to calculate the magnitude of  $\nu_0$ , and assume  $\gamma = 0.5$  everywhere in the disc. Varying  $\alpha$ ,  $H/R$  and  $\gamma$  will change the time-scale over which outbursts occur, but will not change the general character of our outburst solutions.

This leaves three scale-free parameters in the problem:  $\dot{m}/\dot{m}_c$ ,  $\Delta r/r$  and  $\Delta r_2/r$ . We vary each of these parameters to explore the range of unstable solutions. For small values of  $\Delta r/r$  ( $\sim 0.1$ ) and  $\Delta r_2/r$  ( $\sim 0.01$ ), and  $\dot{m}/\dot{m}_c < 1$ , the position of the inner boundary quickly becomes unstable and begins oscillating. Since the position of  $r_{\text{in}}$  determines the mass accretion rate on to the star, (2.19), the change in  $r_{\text{in}}$  leads to an accretion outburst. We use the steady-state solution (given by (2.29) and (2.30)) as an initial condition for all our simulations.

Fig. 2.3 shows the growth of the instability for  $\dot{m}/\dot{m}_c = 1$ ,  $\Delta r/r = 0.05$  and  $\Delta r_2/r = 0.014$ . The solid line shows the evolution in  $r_{\text{in}}$ , scaled to the corotation radius. The horizontal

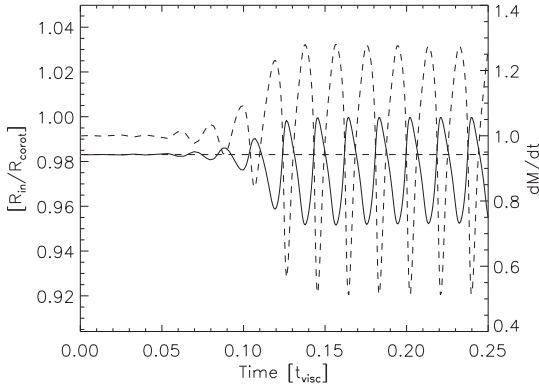


**Figure 2.3:** Growth of instability from steady-state solution, (2.29) and (2.30), for  $\dot{m}/\dot{m}_c = 1$ ,  $\Delta r/r = 0.05$ , and  $\Delta r_2/r = 0.014$ . The inner radius (solid line) evolves around its steady-state value (dashed horizontal line), causing the net accretion rate on to the star to change as well (dashed line).

dotted line shows the steady-state value for  $r_{\text{in}}$ . The right-hand axis plots the accretion rate on to the star as a function of time (the dashed line). The accretion rate is scaled to units of the steady-state accretion rate,  $\dot{m}$ . The instability quickly grows out of the equilibrium solution, and saturates into steady oscillations.

We observe a wide range of oscillatory solutions that span three orders of magnitude in frequency, depending on the values of  $\dot{m}/\dot{m}_c$ ,  $\Delta r/r$  and  $\Delta r_2/r$ . The shape of the accretion burst itself also changes dramatically depending on the system parameters. At large  $\dot{m}/\dot{m}_c$  the bursts are quasi-sinusoidal oscillations, as in Fig. 2.3 and the bottom panel of Fig. 2.4. As the mean accretion rate is decreased, the bursts take the shape of a relaxation oscillator, where the bursts are characterized by an initial sharp spike of accretion which then relaxes to a quasi-steady accretion rate for the duration of the burst, before abruptly turning off as the reservoir is emptied and  $r_{\text{in}}$  quickly moves well outside  $r_c$ . During the outburst phase, higher frequency sub-oscillations are also sometimes seen with varying intensity.

Figs. 2.4 and 2.5 show the evolution of  $r_{\text{in}}$  and accretion rate as we vary  $\dot{m}/\dot{m}_c$  but the other parameters stay fixed. From bottom to top, the panels of Fig. 2.4 show the instability for  $\dot{m}/\dot{m}_c = [0.095, 0.052, 0.031]$  ( $\dot{m} = [2.2, 1.2, 0.73] \times 10^{-8} M_{\odot} \text{yr}^{-1}$  for the parameters in (2.37)). At the highest mean accretion rate,  $r_{\text{in}}$  (the solid line) oscillates with a high frequency around its steady-state value (dotted line), with corresponding bursts of accretion on to the star (dashed line). As  $\dot{m}/\dot{m}_c$  is decreased, the accretion profile changes to much lower frequency outbursts, with long periods of quiescence as  $r_{\text{in}}$  moves away from  $r_c$  and accretion ceases completely. The high-frequency oscillation that dominates for  $\dot{m}/\dot{m}_c = 0.095$  is superimposed over the low-frequency accretion bursts for lower  $\dot{m}/\dot{m}_c$ . Fig. 2.5 shows the continuation of Fig. 2.4 for  $\dot{m}/\dot{m}_c = [0.019, 0.0084, 0.003, 0.0022]$  ( $\dot{m} = [4.5, 1.9, 0.95, 0.38] \times 10^{-9} M_{\odot} \text{yr}^{-1}$ ). The characteristic accretion burst profile essentially stays the same as  $\dot{m}/\dot{m}_c$  is decreased, with sharp spikes at the beginning and end of

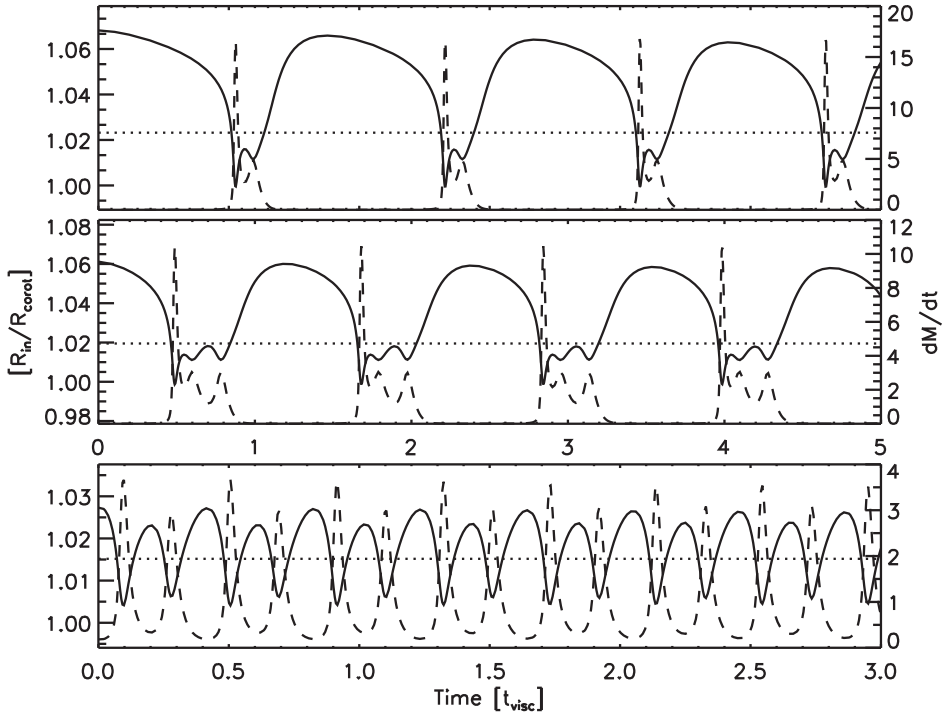


**Figure 2.4:** Outburst profiles of  $r_{\text{in}}$  and  $\dot{m}$  for moderate values of  $\dot{m}/\dot{m}_c$ . From bottom to top,  $\dot{m}/\dot{m}_c = [0.095, 0.052, 0.031]$ . For adopted protostellar parameters this corresponds to  $\dot{m} = [2.2, 1.2, 0.73] \times 10^{-8} M_{\odot} \text{yr}^{-1}$ . The lines are the same as in Fig. 2.3.

an accretion outburst. The overall amplitude of the outburst decreases only slightly with decreasing mean accretion rate. The initial spike decreases by about 20% as the mean accretion rate drops from  $\dot{m}/\dot{m}_c = 0.052$  to  $\dot{m}/\dot{m}_c = 0.0022$ . The more significant effect is that the length of time between outbursts increases with decreasing  $\dot{m}/\dot{m}_c$ , since at low average accretion rates it takes longer to build enough mass to drive another outburst. The overall shape of the outburst is relatively insensitive to changing  $\dot{m}/\dot{m}_c$ , becoming shorter as  $\dot{m}/\dot{m}_c$  decreases. At the lowest accretion rate ( $3.8 \times 10^{-10} M_{\odot} \text{yr}^{-1}$ ; the top panel of Fig. 2.5), the burst consists of only one sharp spike. As we have formulated the problem, the instability will persist down to arbitrarily low accretion rates.

Changing the other parameters,  $\Delta r/r$  and  $\Delta r_2/r$ , has a much stronger effect on the shape of the outburst than changing the mean accretion rate. Fig. 2.6 shows the outburst profiles

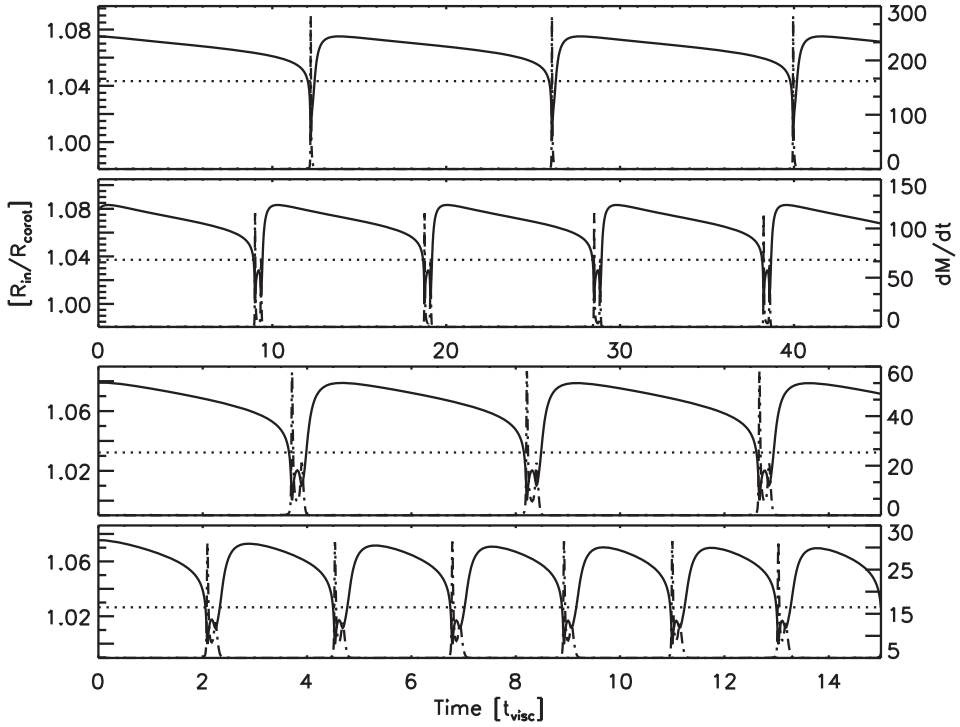


**Figure 2.5:** Outburst profiles of  $r_{\text{in}}$  and  $\dot{m}$  for small values of  $\dot{m}/\dot{m}_c$ . From bottom to top,  $\dot{m}/\dot{m}_c = [0.019, 0.0084, 0.003, 0.0022]$ . For adopted protostellar parameters this corresponds to  $\dot{m} = [4.5, 1.9, 0.95, 0.38] \times 10^{-9} M_{\odot} \text{yr}^{-1}$ . The lines are the same as in Fig. 2.3.

for different values for  $\Delta r/r$ , setting  $\dot{m}/\dot{m}_c = 0.04$  and  $\Delta r_2/r = 0.014$ . From the bottom to top,  $\Delta r/r = [0.03, 0.05, 0.07, 0.09]$ , which spans the unstable region of  $\Delta r/r$  for the adopted  $\dot{m}/\dot{m}_c$ . For small  $\Delta r/r$  the instability manifests itself as repeating short bursts of accretion, with comparatively long quiescent phases. As  $\Delta r/r$  increases, the frequency of the outburst decreases, and the duty cycle increases dramatically. For very large  $\Delta r/r$  the outburst lasts about 200 times as long as for the minimum  $\Delta r/r$  but at lower accretion rate after the initial spike. The burst profile of the instability is thus sensitive to small changes in  $\Delta r/r$ , but the range in  $\Delta r/r$  over which the instability exists is quite small. We find a similar range of outburst profiles by changing  $\Delta r_2/r$  and keeping  $\Delta r/r$  fixed, except with the opposite trend: for large  $\Delta r_2/r$  the instability manifests as a series of short spiky bursts, becoming longer as  $\Delta r_2/r$  decreases.

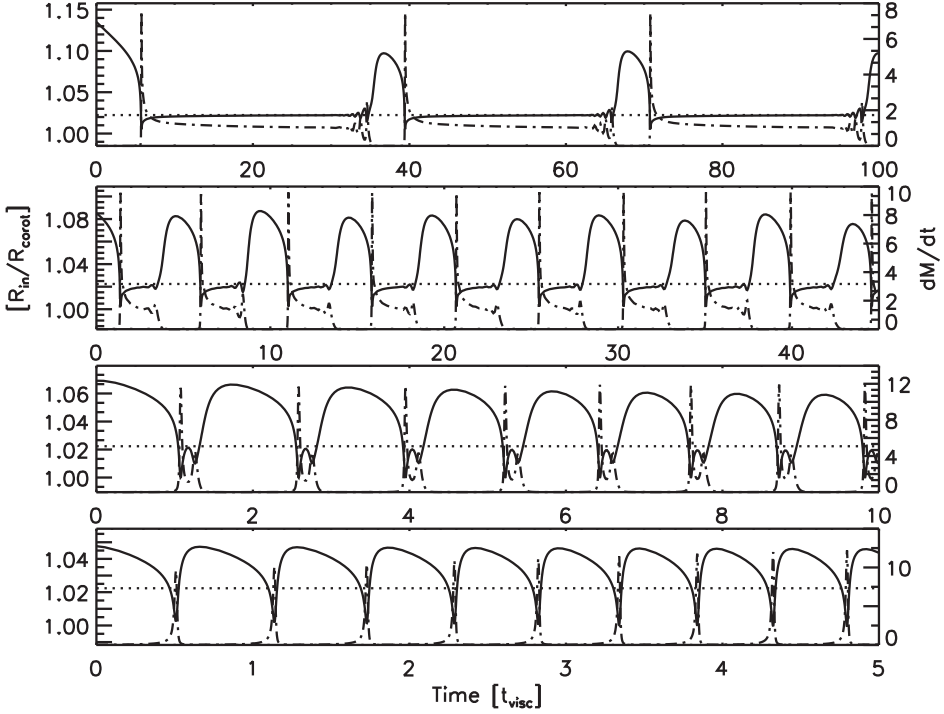
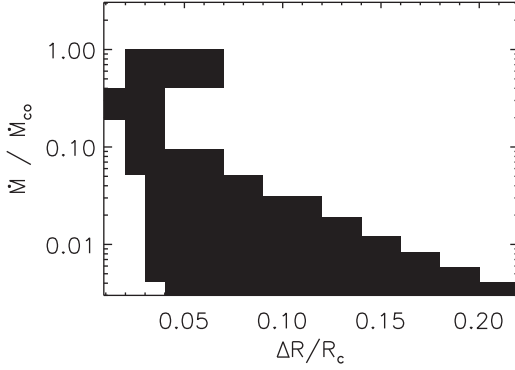


**Figure 2.6:** Outburst profiles of  $r_{\text{in}}$  and  $\dot{m}$  for changing  $\Delta r/r$ , with  $\Delta r_2/r = 0.014$  and  $\dot{m}/\dot{m}_c = 0.04$ . From bottom to top,  $\Delta r/r = [0.03, 0.05, 0.07, 0.09]$ . The lines are the same as in Fig. 2.3.

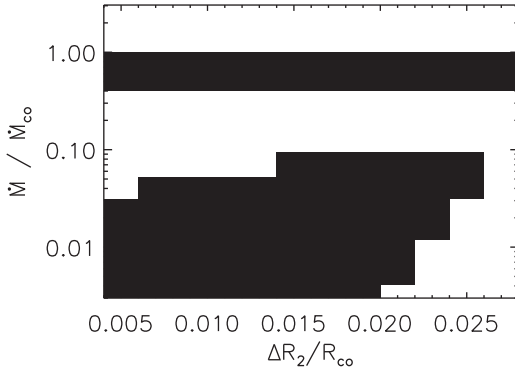
We next considered the parameter space in  $\dot{m}/\dot{m}_c$ ,  $\Delta r/r$  and  $\Delta r_2/r$  over which the instability occurs. We have briefly explored the effect of varying both  $\Delta r/r$  and  $\Delta r_2/r$  over a small range in  $\dot{m}/\dot{m}_c$  and found that although the outburst profile changes somewhat, the range over which  $\Delta r/r$  and  $\Delta r_2/r$  produce unstable solutions are independent of each other. We therefore assume that  $\Delta r/r$  and  $\Delta r_2/r$  vary independently of each other for all  $\dot{m}/\dot{m}_c$ , and consider the range of the instability over the  $[\dot{m}/\dot{m}_c, \Delta r/r]$  and  $[\dot{m}/\dot{m}_c, \Delta r_2/r]$  spaces separately.

Fig. 2.7 shows the range of unstable solutions (shown as shaded regions) changing  $\dot{m}/\dot{m}_c$  and  $\Delta r/r$ , but keeping  $\Delta r_2/r$  fixed at 0.014. Although there is a small unstable branch around  $\dot{m}/\dot{m}_c = 1$ , in general as  $\Delta r/r$  increases, a lower  $\dot{m}/\dot{m}_c$  is required before the instability sets in.

Fig. 2.8 shows the unstable solutions changing  $\dot{m}/\dot{m}_c$  and  $\Delta r_2/r$  but keeping  $\Delta r/r$  fixed



**Figure 2.7:** Parameter map of instability as a function of  $\dot{m}/\dot{m}_c$  and width of interaction region  $\Delta r/r$ , with constant  $\Delta r_2 = 0.014$ . The shaded regions denote unstable parameters.



**Figure 2.8:** Parameter map of instability as a function of  $\dot{m}/\dot{m}_c$  and accretion transition length  $\Delta r_2/r$ , with constant  $\Delta r_2 = 0.014$ . The shaded regions denote unstable parameters.

at 0.05. The opposite trend from Fig. 2.7 is seen, with a larger range of unstable accretion rates. There is again a range of unstable solutions around  $\dot{m}/\dot{m}_c = 1$ , although in this case the unstable region extends over the entire  $\Delta r_2/r$  parameter space. The instability likely extends to smaller  $\Delta r_2/r$ , but we do not explore the region smaller than  $\Delta r_2 = 0.005$  on physical grounds, since such a small transition length will likely be unstable to other instabilities like the interchange instability (see Section 2.3.3). As with changing  $\Delta r/r$ , the outburst profile changes substantially over the small range of  $\Delta r_2/r$  in which the instability occurs.

## 2.6 DISCUSSION

In this paper we studied a disc instability first explored by Sunyaev & Shakura (1977) and ST93, with a more physically motivated and general formulation of the problem than was used in ST93. In particular, we have improved the description of the disc-field interaction when the disc is truncated outside corotation by deriving conditions for a ‘quiescent’ state, in which the angular momentum transferred from the star into the disc halts accretion altogether. In agreement with ST93, we observe a wide range of oscillatory behaviour, and the frequency range of individual outbursts spans three orders of magnitude.

The period of the cycle seen in Figs. 2.3–2.5 varies from 0.02 to  $20t_c$ , where  $t_c$  is the nominal viscous time-scale at the corotation radius  $t_c = r_c^2/\nu(r_c)$ . Though cycle times scale with  $t_c$ , this is evidently not the only factor. As discussed in ST93, the viscous time-scale relevant for the cycle period depends on the size of the disc region involved. This depends itself on the cycle period, hence the period must be determined by additional factors. One of these is the mean accretion rate, but the physical conditions in the magnetosphere-disc interaction region have an equally important effect.

From Figs. 2.7 and 2.8 it appears that there are two different kinds of instability. One of these operates in a narrow range of accretion rates, around the value where steady accretion would put the inner edge at corotation. The instability in this case is of the type shown in Fig. 2.3: an approximately sinusoidal modulation, characteristic for a weak form of instability. The inner edge of the disc oscillates about a mean value, but stays inside the width of the transition region. The longer cycles in the upper parts of Figs. 2.7 and 2.8 are a strongly non-linear, relaxation type of oscillation. The inner edge is somewhat outside the transition region for much of the cycle with no accretion taking place (the ‘quiescent’ phase), and dips in for a brief episode of accretion before moving back out again. This is the kind of cycle envisaged by Sunyaev & Shakura (1977). During the quiescent phase, the disc (Sunyaev & Shakura (1977) call it a ‘dead disc’) extracts angular momentum from the star by the magnetic interaction at its inner edge. These two forms of instability are merged into a continuum in ST93, as a result of the different (and less realistic) assumptions made there about the interaction between disc and magnetosphere outside corotation. This difference also affects the dependence on the mean accretion rate. Whereas in ST93 cyclic behavior was found only in a limited range of accretion rates, our results show that cycles can occur in principle at arbitrarily low accretion rates, with steadily increasing cycle period and decreasing duty cycle of the accretion phase.

Figs. 2.4 and 2.5 show that the radius of the inner edge of the disc does not move by more than 10% around corotation, even at the lowest mean accretion rates. For example in the case  $\dot{m}/\dot{m}_c = 9.5 \times 10^{-2}$  of Fig. 2.4, the standard ‘ram pressure’ estimate would yield a much larger magnetosphere radius, about  $r_m = 3.6r_c$ . The difference arises because in our cyclic accretion states the conditions in the inner disc are very different from those assumed in conventional estimates of  $r_m$ ; the density in the inner disc, for example, is much higher.

At  $r_{in} \leq 1.1r_c$ , the velocity difference between the magnetosphere and the disc is only

5%, much less than the 40% which mass would need in order to escape from the system. ‘Propellering’ of mass out of the system is thus unlikely to be effective. This does not exclude that some mass loss powered by a magnetic wind from the disc or the interaction region around the inner edge of the disc may also take place, but our results show that this is not a necessary consequence for a disc in what is traditionally called ‘propeller’ regime.

At sufficiently low accretion rates one would expect, however, that propellering would also be a possible outcome: if the rotation rate of the star is high enough, matter could be ejected before it has the time to form a dense disc. The existence of a cyclic form of accretion at low accretion rates thus suggests that two different accretion states are possible, and that there would be a second parameter determining which of the two is realised. This might simply be the history of the system.

If a disc is initially absent and accretion is started, the density will initially be low enough that ejection by propellering can prevent accretion altogether. The cataclysmic variable AE Aqr (e.g. Wynn et al. 1997) is likely to be such a case. On the other hand, if a disc is initially in a high accretion state such that the inner edge is inside corotation, a subsequent decline to low accretion rates could lead to the cyclic accretion described here. Such a situation could be at work in the T Tauri star EX Lupi (where the initial high accretion phase has ended). It could also be appropriate for the X-ray millisecond pulsar, SAX J1808.8-3658, which has shown a 1-Hz QPO in the decline phase of several outbursts Patruno et al. (2009). The pile-up of mass at the magnetosphere will maintain the disc this state, and prevent propellering even when the mean accretion rate drops to very low values.

The instability studied in this work has not yet been observed in numerical simulations, partly because most numerical simulations do not run for long enough to observe it, but also because most simulations have focused on either accreting or strong propeller cases. However, in virtually all numerical simulations outflows and variability in the disc are observed, with an intensity that varies between different simulations. Gas pile-up at the inner edge of the disc is also observed, with the amount of pile-up tied to the effective diffusivity of magnetic field at the inner edge of the disc (e.g. Romanova et al. (2004)). The process of closing and opening field lines provides a source of mass to launch both a weakly-collimated outflow (the disc wind) and a well-collimated jet (e.g Hayashi et al. 1996; Goodson et al. 1997; Romanova et al. 2009). The whole cycle takes place on time-scales that can vary between the dynamical and viscous time-scales at the inner edge of the disc, but are generally higher frequency than the disc instability studied in this paper. The inner edge of the disc also oscillates significantly (although it remains on average outside corotation), from between a few stellar radii (Romanova et al. 2009) up to 30 stellar radii (Goodson et al. 1997). Even if such variability is present, the instability studied in this paper can still occur provided the outflows/accretion bursts generated by field lines opening are not strong enough to fully empty the reservoir of matter accumulating just outside  $r_c$ .

## 2.7 CONCLUSIONS

We have studied the accretion of a thin viscous disc on to a magnetosphere of a magnetic star, under the influence of the magnetic torque it exerts on the disc. We focused in particular on cases with low accretion rates. For high accretion rates such that the inner edge  $r_{\text{in}}$  of the disc is inside the corotation radius, standard steady thin viscous disc solutions are recovered. However, when the inner edge is near corotation we find that the accretion becomes time-dependent, and takes the form of cycles consisting of alternating accreting and non-accreting ('quiescent') states. The period of this cycle varies from a small fraction of the characteristic viscous time scale in the inner disc,  $r_{\text{in}}^2/\nu$ , to a large multiple of it, depending on the mean accretion rate as well as on the precise conditions assumed at the magnetosphere.

These cyclic accretion solutions continue to exist indefinitely with decreasing accretion rate. The cycle period increases, while the duty cycle of the accreting phase decreases with decreasing accretion rate. In the quiescent phase after a burst of accretion, the inner edge of the disc moves outward, and mass starts piling up in the inner regions of the disc. In response, the inner edge eventually starts moving back in again and accretion picks up as  $r_{\text{in}}$  crosses the corotation radius. This empties the inner regions of the disc, causing the inner edge to move outward again. The cycle thus has the properties of a relaxation oscillator, as found before in ST93. The reservoir involved is the mass in the inner region of the disc. These results (as well as those of Sunyaev & Shakura (1977) and ST93) show that accretion without mass ejection can occur at accretion rates well inside what is usually called the 'propeller' regime. Instead of the mass being ejected, the accreting mass can stay piled up at high surface density in the inner disc, just outside corotation. We have suggested that systems with very low accretion rates can be in either of these states. Propellering would occur when a disc is initially absent and mass transfer is first initiated (the case of AE Aqr for example), while a system with an accretion rate that drops from an initially high value would end in the cyclic accretion state described in this paper. This would apply to most CVs and X-ray binaries, as well as some T Tauri stars.

## 2.8 ACKNOWLEDGMENTS

CD'A would like to thank Stuart Sim for useful scientific discussion, and acknowledges financial support from the National Science and Engineering Research Council of Canada.

### REFERENCES

- Agapitou V., Papaloizou J. C. B., 2000, MNRAS, 317, 273  
Aly J. J., 1985, A&A, 143, 19  
Aly J. J., Kuijpers J., 1990, A&A, 227, 473

- Blandford R. D., Payne D. G., 1982, MNRAS, 199, 883
- Fromang S., Stone J. M., 2009, A&A, 507, 19
- Gammie C. F., 1996, ApJ, 457, 355
- Ghosh P., Lamb F. K., 1979a, ApJ, 232, 259
- Ghosh P., Lamb F. K., 1979b, ApJ, 234, 296
- Goodson A. P., Winglee R. M., Boehm K., 1997, ApJ, 489, 199
- Hayashi M. R., Shibata K., Matsumoto R., 1996, ApJ, 468, L37+
- Herbig G. H., 2007, AJ, 133, 2679
- Illarionov A. F., Sunyaev R. A., 1975, A&A, 39, 185
- Kulkarni A. K., Romanova M. M., 2008, MNRAS, 386, 673
- Lovelace R. V. E., Romanova M. M., Bisnovaty-Kogan G. S., 1995, MNRAS, 275, 244
- Lynden-Bell D., Boily C., 1994, MNRAS, 267, 146
- Matt S., Pudritz R. E., 2005, ApJ, 632, L135
- Miller K. A., Stone J. M., 1997, ApJ, 489, 890
- Paczynski B., 1991, ApJ, 370, 597
- Patruno A., Watts A., Klein Wolt M., Wijnands R., van der Klis M., 2009, ApJ, 707, 1296
- Popham R., Narayan R., 1991, ApJ, 370, 604
- Press W. H., Teukolsky S. A., Vetterling W. T., Flannery B. P., 1992, Numerical recipes in C. The art of scientific computing. Cambridge: University Press 2nd ed.
- Pringle J. E., Rees M. J., 1972, A&A, 21, 1
- Romanova M. M., Ustyugova G. V., Koldoba A. V., Lovelace R. V. E., 2004, ApJ, 616, L151
- Romanova M. M., Ustyugova G. V., Koldoba A. V., Lovelace R. V. E., 2009, ArXiv e-prints
- Shakura N. I., Sunyaev R. A., 1973, A&A, 24, 337
- Shu F., Najita J., Ostriker E., Wilkin F., Ruden S., Lizano S., 1994, ApJ, 429, 781
- Spruit H. C., Stehle R., Papaloizou J. C. B., 1995, MNRAS, 275, 1223
- Spruit H. C., Taam R. E., 1993, ApJ, 402, 593
- Sunyaev R. A., Shakura N. I., 1977, Pis ma Astronomicheskii Zhurnal, 3, 262
- Uzdensky D. A., 2004, Ap&SS, 292, 573
- Uzdensky D. A., Königl A., Litwin C., 2002, ApJ, 565, 1191
- van Ballegoijen A. A., 1994, Space Science Reviews, 68, 299
- Wang Y.-M., 1987, A&A, 183, 257
- Wynn G. A., King A. R., Horne K., 1997, MNRAS, 286, 436



---

## Chapter 3

---

# Long-term Evolution of Discs Around Magnetic Stars

Caroline R. D'Angelo and Hendrik C. Spruit

*Submitted to MNRAS*

WE investigate the evolution of a thin viscous disc surrounding magnetic star, including the spindown of the star by the magnetic torques it exerts on the disc. The transition from an accreting to a non-accreting state, and the change of the magnetic torque across the corotation radius  $r_c$  are included in a generic way, the widths of the transition taken in the range suggested by numerical simulations. In addition to the standard accreting state, two more are found. An accreting state can develop into a 'dead' disc state (SS76), with inner edge  $r_{in}$  well outside corotation. More often, a 'trapped' state develops, in which  $r_{in}$  stays close to corotation even at very low accretion rates. The long-term evolution of these two states is different. In the dead state the star spins down incompletely, retaining much of its initial spin. In the trapped state the star asymptotically can spin down to arbitrarily low rates, its angular momentum transferred to the disc. We identify these outcomes with respectively the rapidly rotating and the very slowly rotating classes of Ap stars and magnetic white dwarfs.

### 3.1 INTRODUCTION

Accreting stars with strong magnetic fields are generally observed to rotate more slowly than their less-magnetic or discless counterparts. In protostars, T Tauri systems (which often have strong surface magnetic fields of  $\sim 10^2 - 10^3$  G) with discs rotate more rapidly than systems without discs (Getman et al. 2008). Most (but not all) mainsequence Ap stars (with surface fields of up to  $10^4$  G) are observed to rotate much slower than normal A stars (Stępień & Landstreet 2002), and recent work has suggests this relationship extends down to their pre-main-sequence progenitors, the Herbig Ae stars (Alecian et al. 2008). In high energy systems the result is similar: accreting neutron stars with weak ( $\sim 10^8$  G) fields rotate up to  $10^4$  times faster than neutron stars with strong ( $\sim 10^{12}$  G) fields. These observations suggest that the interaction between the accretion disc and stellar magnetic field plays a critical role in regulating the spin-rate of the star.

Early theoretical studies of accretion predicted that a strong stellar field would truncate the accretion disc some distance from the surface of the star, with the truncation radius located roughly where the magnetic pressure ( $B^2/4\pi$ ) equals the ram pressure of the infalling gas ( $\dot{m}v_r/2\pi r^2$ ), so that infalling matter is channelled onto the surface via magnetic field lines, causing the star to spin up. (Pringle & Rees 1972). This assumes that the disc is truncated inside the corotation radius ( $r_c \equiv (GM_*/\Omega_*^2)^{1/3}$ ), where the star's spin frequency is equal to the disc's Keplerian frequency). If instead the magnetic field spins faster than the inner edge of the disc, a centrifugal barrier prevents accretion. Interaction between the magnetic field and the disc will then spin down the star (Illarionov & Sunyaev 1975; Mineshige et al. 1991; Lovelace et al. 1999; Romanova et al. 2004; Ustyugova et al. 2006).

The presence of the centrifugal barrier is often equated in the literature with the idea that the accreting gas will be flung out, or 'propellered' out of the system so as to maintain a steady state. This assumption turns out to be both arbitrary and unnecessary. For example, in order for the accreting material to be flung out of the system, the disc must be truncated a sufficient distance away from  $r_c$ . Otherwise the rotational velocity difference between the disc and the magnetosphere is too small (Spruit & Taam (1993)).

Steady disc solutions with a centrifugal barrier at the inner edge were first described by Sunyaev & Shakura (1977), who called them 'dead discs', because even though the disc is actively transporting angular momentum outwards, no accretion onto the star takes place and the disc itself is very dim.

As pointed out already in Sunyaev & Shakura (1977) and Spruit & Taam (1993), in a system with an externally imposed mass flux the likely effect of a centrifugal barrier is to cause the accretion onto the star to be *cyclic*. Accretion phases alternate with quiescent periods during which mass piles up outside the barrier, without mass having to leave the system. In the quiescent phase, the angular momentum extracted from the star by the disc-field interaction is carried outward through the disc by viscous stress. This alters the surface density profile of the disc from the usual accreting solution.

In our previous paper (D'Angelo & Spruit, 2010; hereafter DS10) we studied this form

of cyclic accretion with numerical solutions of the viscous diffusion equation for a thin disc subject to a magnetic torque. As in the (somewhat more ad hoc) model of ST93, limit cycles of the relaxation oscillator type were found. The cycle period of these oscillations depends on the accretion rate, from fast oscillations at higher mass flux to arbitrarily long periods at low accretion rates.

Instead of the two states: accreting and dead as suggested above, the results in DS10 are actually described better by including a third, intermediate state we call here the ‘trapped’ state:

1.  $r_{\text{in}} < r_c$ : accreting state, star spins up,
2.  $r_c - \Delta < r_{\text{in}} < r_c + \Delta$ : trapped state, spinup or spindown,
3.  $r_{\text{in}} - r_c \gg \Delta$  star spins down, no accretion (dead disc),

where  $\Delta \ll r_c$  is a narrow range around corotation, to be specified later. In state (ii), the inner edge of the disc remains close to corotation over a range of accretion rates onto the star, and the net torque on the star can be of either sign, depending on the precise location of the inner edge of the disc.

For a given accretion rate, a disc that starts in state (i) will gradually move into state (ii) or (iii) as the star spins up and  $r_c$  moves inward. In state (ii) accretion can proceed steadily or happen in bursts, depending on the disc-field interaction at  $r_{\text{in}}$ . For steady externally imposed accretion a disc in this state will eventually move into spin equilibrium with the star, so that the net torque on the star is zero. In the dead state (iii) a steady state can exist if the torque exerted by the star is taken up at the outer edge of the disc by a companion star. If we neglect the transition to the propeller regime, then in theory the dead disc solution can exist for a disc truncated at any distance outside  $r_c$ . Such a disc will remain static as the star spins down and  $r_c$  moves outward. Our model is thus qualitatively different from the conventional ‘propeller’ picture since at very low accretion rates a considerable amount of mass remains confined in the disc, and the star can be efficiently spun down.

In the following we study the long-term evolution of the star-disc system by using the description of magnetospheric accretion in DS10, allowing the star’s spin rate to evolve. Of special interest will be the trapped state (ii), since in many cases the evolution of the system ends in it. The accretion cycles found in DS10 also take place essentially within a trapped state.

The inner edge of the disc is near corotation in the trapped state, as is the case also for a disc in spin equilibrium with the accreting star. Spin equilibrium is only a special case of a trapped state, however. In general a trapped state is not one of spin equilibrium, spinup is possible as well as spindown.

Questions we address with the calculations are: under what conditions does the disc get into a trapped state, when does it instead evolve into a dead state? It will turn out that this is determined by the details of the disc-field interaction and the ratio of the spin-down timescale of the star ( $T_{\text{SD}}$ ) to the viscous timescale of the disc ( $T_{\text{visc}}$ ). The initial conditions of the disc

also significantly influence the outcome. In section 3.5.2 we ask how an initially trapped disc could become untrapped as a dead disc state. In particular, does this depend on the initial location of the inner edge of the disc, the initial accretion rate, the presence or absence of a companion or the size of the disc? Finally, in sec. 3.5.3 we ask whether a trapped disc could plausibly regulate the slow spins observed in Ap stars, some of which have spin periods of up to a decade.

In a companion paper we investigate the observable consequences of a trapped disc, focusing in particular on how the burst instability studied in DS10 will change the spin evolution and observable properties of the star. In that paper we also discuss our model's predictions in terms of observations of magnetospherically regulated accretion in both protostars and X-ray binaries.

We use the code developed in DS10, adding the star's moment of inertia as a parameter of the problem in order to follow the spin evolution of the star in response to the disc interaction. We can then simultaneously follow the viscous evolution of the disc and spin evolution of the star as the star's spin changes, and explore how these two interact with each other. We describe our model in more detail in the following section.

## 3.2 MAGNETOSPHERIC INTERACTIONS WITH A THIN DISC

### 3.2.1 Magnetic torque

The interaction between a strong stellar magnetic field and surrounding accretion disc truncates the disc close to the star, and forces incoming matter to accrete along closed field lines onto the surface of the star in a region called the magnetosphere. At the outer edge of the magnetosphere (termed here the magnetospheric radius), the field lines become strongly embedded in the disc over some small radial extent that we term the *interaction region*,  $\Delta r$ . The differential rotation between the star and the Keplerian disc will cause the field lines to be twisted, which will generate a toroidal component to an initially poloidal field (e.g. Ghosh et al. 1977). This will allow the transfer of angular momentum between the disc and star, with the torque per unit area exerted by the field on the disc given by  $\tau = rS_{z\phi}\hat{\mathbf{z}}$ , where:

$$S_{z\phi} \equiv \frac{B_\phi B_z}{4\pi} \quad (3.1)$$

is the magnetic stress generated by the twisted field lines. Both theoretical arguments (e.g. Aly 1985; Lovelace et al. 1995) and numerical simulations (such as Miller & Stone 1997; Goodson et al. 1997; Hayashi et al. 1996) suggest that the strong coupling between magnetic field lines and the disc will cause the field lines to inflate and open. The inflation and opening of field lines limits the growth of the  $B_\phi$  component for the field to  $B_\phi = \eta B_z$ , with  $\eta$  of order unity, and reduces the radial extent of the interaction region, since beyond a given radius the field lines are always open and the disc-field connection will be severed. We take the

interaction region to be narrow,  $\Delta r/r < 1$  (as found in numerical simulations, see section 2 of DS10 for a more detailed discussion). Assuming the star's dipole field strength  $B_d(r)$  as an estimate of  $B_z$ , and taking into account that  $S$  acts on both sides of the disc, (3.1) yields the magnetic torque  $T_0$  exerted on the disc:

$$T_0 = 4\pi r \Delta r r S_{z\phi} = \eta r^2 \Delta r B_d^2. \quad (3.2)$$

This torque exists only if the inner edge  $r_{\text{in}}$  of the disc is outside the corotation radius  $r_c$ . For  $r_{\text{in}} < r_c$ , we have instead a disc accreting on an object rotating slower than the Kepler rate at  $r_{\text{in}}$ . By the standard theory of thin viscous discs, the torque exerted on the disc by the accreting object then vanishes, independent of the nature of the object. The torque  $T_B(r_i)$  thus changes over a narrow range around  $r_c$ . To model this transition we introduce a 'connecting function'  $y_\Sigma$ :

$$T_B(r_{\text{in}}) = y_\Sigma(r_{\text{in}}) T_0(r_{\text{in}}), \quad (3.3)$$

with the properties  $y_\Sigma \rightarrow 0$  ( $r_c - r_{\text{in}} \gg \Delta r$ ),  $y_\Sigma \rightarrow 1$  ( $r_{\text{in}} - r_c \gg \Delta r$ ). As in DS10, we take for this function

$$y_\Sigma = \frac{1}{2} \left[ 1 + \tanh \left( \frac{r_{\text{in}} - r_c}{\Delta r} \right) \right]. \quad (3.4)$$

The width of the transition is thus described by  $\Delta r$ . We take the same value for it as used in eq. (3.2).

### 3.2.2 Model for disc-magnetosphere interaction

In DS10 we derived a description of the interaction between a disc and magnetic-field for a disc truncated either inside or outside  $r_c$ , and introduced two numerical parameters to connect the two regimes. To keep the problem axisymmetric, we assumed a dipolar magnetic field, with the dipole axis aligned with the stellar and disc rotation axis. Since the region of interaction between the disc and the field is small, we use our description of the interaction as a boundary condition for a standard thin accretion disc (Shakura & Sunyaev 1973).

To evolve a thin disc in time, we must choose a description for the effective viscosity ( $\nu$ ) that allows transport of angular momentum. We adopt an  $\alpha$  prescription for the viscosity and assume a constant scale height ( $h$ ) for the disc, so that:

$$\nu = \alpha (GM_*)^{1/2} (h/r)^2 r^{1/2}. \quad (3.5)$$

At the inner edge of the disc the behaviour is regulated by the disc-field interaction. However, since the interaction region is small, we incorporate the interaction as a boundary condition on the inner disc, and assume that the majority of the disc is shielded from the magnetic field and then evolves as a standard viscous disc, albeit with a very different inner boundary condition from the standard one. Below we summarize our analysis of the disc-field interaction and how these translate into boundary conditions on the disc. (For the detailed derivation of our boundary conditions, see sections 2.3, 2.4, and 3.2 of DS10).

### Surface density at $r_{\text{in}}$

In a dead disc, the disc-field interaction prevents matter from accreting or being expelled from the system, instead retaining matter that interacts with the magnetic field. This implies that the angular momentum injected via magnetic torques in the interaction region  $\Delta r$  must be transported outwards by viscous torques in the disc. A dead disc will therefore have a maximum in surface density at  $r_{\text{in}}$ , and  $\Sigma(r_{\text{in}})$  will depend on the amount of angular momentum being added by the disc-field interaction.

By equating the amount of angular momentum added by the field to the amount carried outwards by viscous processes, we can calculate the surface density at the inner boundary of the disc needed to carry away the injected angular momentum. This yields (see DS10) a value for the surface density  $\Sigma$  at the inner edge of a dead disc, proportional to the magnetic torque (eq. 3.3):

$$3\pi\nu\Sigma(r_{\text{in}}) = \frac{T_B}{r^2\Omega_K}\Big|_{r_{\text{in}}}, \quad (3.6)$$

where  $\Omega_K$  is the Keplerian rotation frequency. If the stellar field is a dipole and we use (3.5) to describe the viscosity, then for  $r_{\text{in}} > r_c$ ,  $\Sigma(r_{\text{in}}) \propto r_{\text{in}}^{-4}$ .  $\Sigma(r_{\text{in}})$  thus decreases rapidly with increasing  $r_{\text{in}}$ .

### Accretion rate across $r_c$

If the inner edge is well inside the corotation radius  $r_c$ , we use a standard result to estimate the location of  $r_{\text{in}}$  as a function of the accretion rate  $\dot{m}_a$ . It is obtained from the azimuthal equation of motion for gas at the point at which it is forced to corotate with the star (c.f. Spruit & Taam 1993). This gives:

$$r_{\text{in}}^4 \pi \langle S_{z\phi} \rangle / \Omega_* = \dot{m}_a. \quad (3.7)$$

[Note that we take the sign of  $\dot{m}$  positive for *inward* mass flow.] It is not necessary that stationarity holds: (3.7) can also be applied when the inner edge of the disc moves. However, since it describes the accretion through the magnetosphere-disc boundary  $r_{\text{in}}$ , it has to be applied in a frame comoving with  $r_{\text{in}}$ . If  $\dot{m}$  is the mass flow rate in a fixed frame, it is related to the accretion rate in this comoving frame ( $_{\text{co}}$ ) by

$$\dot{m}_{\text{co}} = \dot{m} + 2\pi r_{\text{in}} \Sigma(r_{\text{in}}) \dot{r}_{\text{in}}, \quad (3.8)$$

where  $\dot{r}_{\text{in}}$  is the rate of change of the inner disc edge.

To connect the accreting case with the dead disc case, for which  $\dot{m} = 0$ , we need one more prescription, this time for the accretion rate as a function of the inner edge radius. We introduce a connecting function  $y_m$  for this (DS10):

$$\dot{m}_{\text{co}}(r_{\text{in}}) = y_m(r_{\text{in}}) \dot{m}_a(r_{\text{in}}), \quad (3.9)$$

with the properties  $y_m \rightarrow 1$  ( $r_c - r_{\text{in}} \gg \Delta r_2$ ),  $y_m \rightarrow 0$  ( $r_{\text{in}} - r_c \gg \Delta r_2$ ), with

$$y_m = \frac{1}{2} \left[ 1 - \tanh \left( \frac{r_{\text{in}} - r_c}{\Delta r_2} \right) \right], \quad (3.10)$$

where  $\Delta r_2$  describes the width of the transition (different in general from  $\Delta r$ ).

With the star's assumed field of dipole moment  $\mu$ ,  $B_d = \mu/r^3$  and Keplerian orbits in the disc, (3.8) becomes, with the viscous thin-disc expression for  $\dot{m}$ :

$$6\pi r_{\text{in}}^{1/2} \frac{\partial}{\partial r} (v\Sigma r^{1/2}) \Big|_{r_{\text{in}}} = y_m \frac{\eta\mu^2}{4\Omega_* r_{\text{in}}^5} - 2\pi r_{\text{in}} \Sigma(r_{\text{in}}) \dot{r}_{\text{in}}, \quad (3.11)$$

where  $\eta$  is a numerical factor of order unity and  $\mu$  the dipole moment of the star (see DS10 for details).

Along with our description for the viscosity, (3.6) and (3.11) define a boundary condition at  $r_{\text{in}}$  and an equation for  $r_{\text{in}}(t)$ , for a disc over a continuous range of accretion rates, from strongly accreting systems ( $r_{\text{in}} \ll r_c$ ) to dead-disc systems ( $\dot{m} \simeq 0$ ).

### Evolution of corotation radius

In order to study the response of a disc to changes in spin of the star, we must incorporate the angular momentum exchange between the star and disc:

$$I_* \frac{d\Omega_*}{dt} = \frac{dJ}{dt}, \quad (3.12)$$

which introduces the moment of inertia of the star,  $I_* = k^2 M_* R_*^2$  as an additional parameter of the problem.

The disc-star angular momentum exchange  $dJ/dt$  has two components: matter accreting onto the star adds angular momentum at a rate  $\dot{m}_{\text{co}} r_{\text{in}}^2 \Omega_{\text{K}}(r_{\text{in}})$ , while the disc-field coupling outside co-rotation extracts angular momentum spinning the star down. The rate of angular momentum exchange between the disc to the star will thus be (with 3.2, 3.3, 3.4):

$$\begin{aligned} \frac{dJ}{dt} &= \dot{m}_{\text{co}} r_{\text{in}}^2 \Omega_{\text{K}}(r_{\text{in}}) - T_B \\ &= \frac{\eta\mu^2}{r_{\text{in}}^3} \left[ \frac{1}{4} \left( \frac{r_c}{r_{\text{in}}} \right)^{3/2} y_m - \frac{\Delta r}{r_{\text{in}}} y \Sigma \right]. \end{aligned} \quad (3.13)$$

The corotation radius (a function of  $\Omega_*$ ) evolves as:

$$\frac{dr_c}{dt} = -\frac{2}{3} \frac{dJ}{dt} I_*^{-1} \left( \frac{GM_*}{r_c^5} \right)^{-1/2}. \quad (3.14)$$

Eq. (3.13) shows that there is a value of  $\dot{m}$  for which there is no net angular momentum exchange with the star. This is the 'spin equilibrium' state discussed in previous work.

This zero-point will depend on our adopted connecting functions, as well as the size of the transition widths,  $\Delta r$  and  $\Delta r_2$ . If  $\dot{m} = 0$ , there is no spin-equilibrium solution: the star will spin down by the magnetic torque.

### Steady-state solutions

In the presence of a magnetic torques at the disc inner edge, the steady solutions ( $\partial/\partial t = 0$ ) of the thin viscous disc diffusion equation with the above boundary conditions have the form (cf. DS10):

$$3\pi\nu\Sigma = \frac{T_B}{\Omega(r_{\text{in}})r_{\text{in}}^2} \left(\frac{r_{\text{in}}}{r}\right)^{1/2} + \dot{m} \left[1 - \left(\frac{r_{\text{in}}}{r}\right)^{1/2}\right], \quad (3.15)$$

where  $\dot{m}$  is the accretion rate onto the star, given by (3.9). If the inner edge is inside corotation ( $T_B = 0$ ),  $\Sigma$  has the standard form for steady accretion on an object rotating below the Keplerian rate (second term on the RHS).

For  $r_{\text{in}}$  well outside corotation ( $r_{\text{in}} - r_c \gg \Delta r$ ),  $\dot{m} \downarrow 0$  and we have a dead disc. The surface density is then determined by the first term on the RHS. The steady outward flux of angular momentum in this case has to be taken up by a sink at some larger distance, otherwise the disc could not be stationary as assumed. This sink can be the orbital angular momentum of a companion star, or the disc can be approximated as infinite. The latter is a good approximation for changes in the inner regions of the disc, if time scales short compared with the viscous evolution of the outer disc are considered.

### 3.2.3 Numerical method

We use the one-dimensional numerical code described in DS10 to evolve the standard diffusive thin-disc equation with our viscosity prescription (3.5) and our description of the disc-field interaction (which gives the inner boundary conditions the boundary conditions (3.6) and (3.11)). At the outer boundary a mass flux and a flux of angular momentum are specified in various combinations (described in sec. 3.2.3).

The calculations are done in dimensionless coordinates and variables. In DS10 we scaled all physical lengthscales to  $r_c$ , and physical time scales to  $t_{\text{visc}}(r_c)$ . Since in this paper we want to follow the evolution of  $r_c$ , we instead use the stellar radius  $r_*$  and  $T_{\text{visc}}(r_*) \equiv t_*$  to scale our physical length and timescales. The grid is logarithmically spaced (to ensure sufficient resolution in the inner disc to capture the disc instability). It is an adaptive mesh, such that the inner boundary moves with  $r_{\text{in}}$ .

Since the grid used is time dependent, the outer boundary condition is also applied at a time-varying location. As discussed in DS10, the artefacts this causes are small, compared to specification at a fixed location (at least for the large discs studied in most cases).

The size of the discs studied range from 10 to  $10^6$  times the inner edge radius, the number of grid points needed for sufficient resolution varies accordingly, from 90 for the smallest to 560 for the largest discs.

Time stepping is done with an implicit method, so the short time scales encountered during episodes of cyclic accretion can be followed, as well as the much slower viscous evolution of the disc as a whole and the spin down the star. It is adapted to the stiff nature of the equation to be solved (see DS10 for details).

### Outer Boundary Condition

The lifetime and evolution of a star surrounded by a dead disc is an inherently time-dependent problem, so the initial conditions in the disc can be critical for its evolution. Since the spin-down timescale for the star can be much larger than viscous timescales throughout the disc, the conditions in the outer disc will also strongly influence the evolution of the system.

We thus consider the effect of varying the outer boundary conditions for the disc. The first condition we study is the simplest: a fixed mass flux  $\dot{m} = \dot{m}_0 (> 0$ , corresponding to accretion). As discussed in the introduction, a key aspect of disc-magnetosphere interaction is that accretion is possible even as the star is spun down. At fixed  $\dot{m} > 0$ , the angular momentum flux can be either inward or outward.

If the mass flux specified vanishes at  $r_{\text{out}}$ , the boundary condition is

$$\left. \frac{\partial}{\partial r} (r^{1/2} v \Sigma) \right|_{r_{\text{out}}} = 0. \quad (3.16)$$

On long evolution timescales, the finite extent of the disc itself could be relevant in a star without a companion where the disc can spread outwards. To model this, as our final boundary condition we take  $\Sigma(r_{\text{out}}) = 0$ , so that the angular momentum added at  $r_{\text{in}}$  is carried away by the outer parts of the disc, causing the disc to spread outwards. In section 3.5.2 we discuss the consequences of these assumptions in limiting the lifetime of a trapped disc.

### The Evolution of $r_c$

The final modification to our code used in DS10 is to allow  $r_c$  to evolve as the spin rate of the star changes (3.14). The characteristic evolution timescale for  $\dot{r}_c$ , the spin-down timescale for the star, is much longer than the nominal viscous timescale in the disc (see the next section). The code updates  $r_c$  by an explicit time step, rather than implicitly, as we do the other variables. Rather than discretizing (3.14) and add it to our system of linearized equations that are solved numerically at each timestep, we instead approximate the evolution in  $r_c$  to first order in time, that is:

$$r_c(t_0 + \Delta t) = r_c(t_0) + \left. \frac{dr_c}{dt} \right|_{t_0} \Delta t \quad (3.17)$$

This scheme is simpler than adding additional equations to the code, and is sufficient to describe the co-evolution of the disc and stellar spin-rate. However, as we discuss in sec. 3.4.3, it is not accurate enough when  $r_{\text{in}}$  is close to  $r_{\text{c}}$  and the spindown timescale comparable to the viscous timescale in the inner regions of the disc.

### 3.3 CHARACTERISTIC TIMESCALES OF DISC-STAR EVOLUTION

Three kinds of time scale play a role in the evolution of a star coupled magnetically to an accretion disc. These are the spin period of the star, the time scale for changes in spin period of the star, and viscous evolution timescales of the disc. The viscous evolution does not have a single characteristic time scale; it can vary over many orders of magnitude depending on which regions in the disc participate in the evolution.

The spin period of the star ( $P_*$ ) determines the location of the corotation radius. This then sets the accretion rate at which the transition from accreting to non-accreting disc takes place. It also determines the timescale for magnetospheric variability (from processes like reconnection of field lines), which can lead to variability  $\dot{m}$ ,  $\Delta r$ ,  $\Delta r_2$  and the  $B_\phi$  component of the magnetic field (which sets the magnitude of the torque).  $P_*$  is much shorter than the other characteristic timescales studied in this paper, and the complex variability processes are best studied with detailed MHD simulations, so in this work we assume time-averaged values for  $\dot{m}$ ,  $\Delta r$ ,  $\Delta r_2$  and  $B_\phi$  and neglect shorter timescales.

A convenient unit of time for measuring changes in a viscous disc at a distance  $r$  from the center is  $t_a = r^2/v(r)$ , sometimes called the accretion- or viscous time scale at distance  $r$ . If  $\alpha$  is the viscosity parameter and  $H$  the disc thickness, it is longer than the orbital time scale  $\Omega_K^{-1}$  by a factor  $\alpha^{-1}(r/H)^2$ , a large number for most observed discs. Natural choices for  $r$  in this expression would be the inner edge radius  $r_{\text{in}}$  or the corotation radius  $r_{\text{c}}$ . Both of these are functions of time. The actual time scales of variation in our discs can be much shorter than  $t_a$ , however, since the extent of the disc that participates in the variation can be much smaller than  $r_{\text{in}}$ . In the cyclic accretion mode described in DS10, for instance, cycle times as short as  $0.01t_a$  are found. The time scale for viscous adjustment in the outer disc regions, on the other hand, can be very large compared to  $t_a$ .

The longest timescale is the rate at which the star's spin will change, which is determined both by the rate of angular momentum exchange with the disc and the star's moment of inertia. The spin-down torque of a dead disc (with  $\dot{m} = 0$  and  $r_{\text{in}} = r_{\text{c}}$ ) is, from eq. (3.13):

$$I_* \frac{d\Omega_*}{dt} = -\frac{\eta\mu^2\delta}{r_{\text{in}}^3}, \quad (3.18)$$

where  $\delta = \Delta r/r_{\text{in}}$ . The characteristic spindown time is:

$$T_{\text{SD}} \equiv P_*/\dot{P} \sim \frac{I_*\Omega_*r_{\text{in}}^3}{\eta\mu^2\delta}. \quad (3.19)$$

**Table 3.1:** Spindown and viscous timescales for different type of magnetic stars

Source	Mass ( $M_{\odot}$ )	Radius ( $R_{\odot}$ )	$B_*$ (G)	$P_*$	$I_*$ ( $M_{\odot}R_{\odot}^2$ )	$T_{\text{SD}}$ (years)	$T_{\text{visc}}(r_c)/T_{\text{SD}}$
slow Pulsar	1.4	$1.4 \times 10^{-5}$	$10^{12}$	5.0s	$2.9 \times 10^{-11}$	4400	$3 \times 10^{-7}$
ms Pulsar	1.4	$1.4 \times 10^{-5}$	$10^8$	0.1s	$2.9 \times 10^{-11}$	$2.6 \times 10^{11}$	$2 \times 10^{-17}$
Magnetic Ae star <sup>a</sup>	3.0	5.5	$10^4$	10 yrs	4.0	$3 \times 10^5$	0.06
T Tauri Star <sup>b</sup>	0.6	3.0	1500	7 days	0.54	$2.3 \times 10^4$	0.001

<sup>a</sup> $B_*$  and  $I_*$  from Stępień (2000)

<sup>b</sup>Sipos et al. (2009)

If the inner edge stays near corotation,  $\Omega_K = \Omega_*$ , replacing  $r_{\text{in}}$  by  $r_c$ , this yields:

$$T_{\text{SD}} = \frac{GM_* I_*}{2\pi\eta\mu^2\delta} P_*, \quad (\Omega_K(r_{\text{in}}) = \Omega_*). \quad (3.20)$$

The spindown timescale varies considerably between different sources. Adopting  $\eta = 1$  and  $\Delta r/r_{\text{in}} = 0.3$ , this spindown timescale is short enough to account for spin-regulation in slowly rotating magnetic stars. In Table 3.3 we summarize the predicted spin-down timescales for a slowly rotating X-ray pulsar, a millisecond pulsar, a slowly rotating Ap star, and a typical T Tauri star. For all these examples but the millisecond pulsar the spin-down timescale is much shorter than the lifetime of the star. Provided the conditions are such that the inner edge of the disc can stay near corotation (i.e. what we have called the ‘trapped disc’ state), it will be able to spin down a star to very slow rotation periods. In the next sections we will explore how this could work in detail by evolving a viscous disc in time numerically.

The last column of Table 3.3 lists the ratio of the viscous time scale  $r_c^2/\nu$  and (3.19). Note that for our description of viscosity, the viscous and spin-down timescales both scale as  $r^{-3/2}$ . The quantity  $T_{\text{visc}}/T_{\text{SD}}$  thus defines the ratio of the time that gas at that radius takes to travel inwards onto the star and the time it would take to spin-down, independent of radius. In all cases, the spin-down timescale is much longer than the viscous timescales in the disc, so that at least part of the disc is able to adjust to the new spin rate of the star. However, the exact ratio between the two timescales varies over ten orders of magnitude, from 0.06 for a strongly magnetic Herbig Ae star to  $10^{-17}$  for an accreting millisecond pulsar. This ratio implies that the extent of spin-down will be influenced by the viscous evolution of the disc itself in response to the disc-field interaction, and that this evolution will vary substantially between different systems, breaking the scale invariance usually assumed in disc-magnetospheric interactions. In section 3.4.3 we demonstrate how the ratio of these two timescales is critical in determining the ratio of  $r_{\text{in}}$  to  $r_c$  in a trapped disc.

### 3.3.1 Representative Model

In sections 3.4 and 3.5.2 we study how a trapped disc can form and evolve, as well as how it can become untrapped. In order to simplify comparison between different simulations, we adopt a set of parameters for a representative model, which we then vary between solutions as necessary.

For the dimensionless parameters we adopt  $\Delta r/r_{\text{in}} = 0.1$ ,  $\Delta r_2/r_{\text{in}} = 0.04$ , and  $B_\phi/B_z \equiv \eta = 0.1$ . The values of  $\Delta r/r_{\text{in}}$  and  $\Delta r_2/r_{\text{in}}$  are small enough to provide an abrupt transition between an accreting and non-accreting disc, but do not show the cyclic instability discussed in DS10. Neglecting the star's spin change, the problem has a scale invariance (DS10), whereby the parameters  $\mu$ ,  $M_*$ ,  $\Omega_*$  and  $\dot{m}$  can be re-written as the ratio  $\dot{m}/\dot{m}_c$ , and  $\dot{m}_c$  is the accretion rate in (3.7) that puts the magnetospheric radius at  $r_c$ , a natural unit of  $\dot{m}$  for magnetospheric accretion. The results in DS10 were presented in this unit.

As discussed in the previous section, the variation of  $r_c$  with time during spindown of the star makes this unit impractical. Instead, we present the representative model in units suitable for a protostellar system with  $T_{\text{visc}}/T_{\text{sd}} = 2.6 \times 10^{-3}$  (which is as large a ratio as the present version of the code allows), and explore the effect of varying this ratio. As unit of length we use  $r_*$ , the star's radius, and for timescale  $t_*$ , the nominal viscous timescale of the disc at the star's radius.

## 3.4 TRAPPED DISCS

### 3.4.1 Trapped disc evolving from an accreting disc

For our description of the disc-field interaction (which ignores outflows), once the accretion rate falls to zero, the inner edge of the disc could be located anywhere outside  $r_c$ , depending on the amount of mass in the disc. What then determines the location of the inner radius of a dead disc? To answer this question, we simulate an initially steadily accreting disc in which the accretion rate at  $r_{\text{out}}$  suddenly decreases to zero. As the reservoir of gas in the disc runs out, the accretion rate onto the star declines, and the inner radius of the disc moves outwards.

In the simulation we use our representative disc parameters described above, and set the initial inner radius of the disc to be just inside  $r_c$ ,  $r_{\text{in}}(t = 0) = 0.88$ , and the outer radius  $r_{\text{out}} = 100r_{\text{in}}$ . We can calculate the corresponding accretion rate from (3.7), and use the static solution for  $\Sigma$  given by (3.15) as our initial surface density profile. At  $t = 0$ , we set  $\partial_r(\nu\Sigma r^{1/2})|_{r_{\text{out}}} = 0$ , so that no mass is added to the disc or allowed to escape. This sets a constant angular momentum flux at  $r_{\text{out}}$ .

The results are shown in Fig. 3.1. The bottom panel of Fig. 3.1 shows the change in accretion rate onto the star, scaled to  $\dot{m}_c$ . The top panel of Fig. 3.1 shows the evolution of the inner radius (solid black curve) and  $r_c$  (dashed red curve) in response to the changing accretion rate. After initial steady accretion over about  $30 t_*$  (less than 1/10th the viscous

timescale at  $r_{\text{out}}$ ),  $\dot{m}$  through the inner edge of the disc begins to decrease as the reservoir of mass in the disc is accreted onto the star, and  $r_{\text{in}}$  begins to move outward. From  $30 - 1500 T_*$ ,  $\dot{m}$  decreases exponentially with a decay timescale of about  $240 t_*$  and the disc moves outwards. However,  $r_{\text{in}}$  increases by only about 20% as the accretion rate decreases by three orders of magnitude. (The structure of  $r_{\text{in}}$  around  $r_c$  is an artifact of the tanh connecting functions we adopted to describe  $r_{\text{in}}$  and  $\dot{m}$  across the transition region).

After  $\sim 1500 t_*$  the star begins to spin down (so that  $r_c$  moves outwards), and the inner radius of the disc begins to track  $r_c$ , so that the ratio  $r_{\text{in}}/r_c$  remains nearly constant thereafter. The behaviour of the accretion rate at this point also changes. Although it continues to decrease exponentially, the decay timescale lengthens considerably and the accretion rate ( $\sim 10^{-4}$  of the initial  $\dot{m}$ ) is regulated by the spin-down rate of the star. Instead of continuing to move away from  $r_c$  into the ‘dead disc’ regime (in which  $\dot{m} = 0$ ), the inner radius instead remains *trapped* at nearly a constant fraction of  $r_c$  while the star continues to spin down. We thus call this disc solution a ‘trapped disc’, since rather than continue to move outwards,  $r_{\text{in}}$  becomes trapped at a nearly constant fraction of  $r_c$ .

At the outer edge of the disc  $\dot{m} = 0$  and there is an outward angular momentum flux. The accretion onto the star comes from the disc being slowly eroded (although at a very low rate) as  $r_{\text{in}}$  moves outward. The evolution of  $r_{\text{in}}$  and the inner parts of the disc is determined by the spin down rate of the star itself, which is itself influenced by how close  $r_{\text{in}}$  can stay near  $r_c$ . In Sec. 3.4.3 we demonstrate how  $r_{\text{in}}/r_c$  is mostly determined by the parameters  $\Delta r$  and  $\Delta r_2$ , and the ratio  $T_{\text{visc}}/T_{\text{SD}}$ . However, the main conclusion of this section is clear: if a trapped disc forms and can efficiently carry away the angular momentum of the star, over spin-down timescales the disc will accrete at such a rate so as the inner edge of the disc can move outwards together with  $r_c$  and the star could in theory spin down completely.

### 3.4.2 Trapped disc evolving from a dead disc

Consider next a case where the initial condition is a dead disc, ( $r_{\text{in}} > r_c$ ) given by the steady profile ((3.15) with  $\dot{m} = 0$  and  $y_\Sigma = 1$ ). As the star spins down,  $r_c$  moves out until it catches up with the inner edge  $r_{\text{in}}$ . From then on, the same evolution is as in the previous case:  $r_{\text{in}}$  and  $r_c$  move outward together indefinitely. A small amount of mass is accreting while the star’s angular momentum is transferred to the disc.

The asymptotic evolution of this dead disc can be compared with the case when a fixed mass flux is imposed at the outer edge. The asymptotic state is then a steady state with *spin equilibrium*: the spin-up torque due to the accreted mass is balanced by the magnetic torque at  $r_c$  transferring angular momentum outward.

We illustrate the distinction between these two cases in figure 3.2. This shows the evolution of an initially dead disc (black, thick curves) and accreting disc (red, thin curves). Both discs have the same representative parameters (Sec. 3.3.1) and  $r_{\text{out}} = 100 r_{\text{in}}$ , but with different initial inner radii (a few times the stellar radius), accretion rates and appropriate initial surface density profiles given by (3.15). For the dead disc, we take  $r_{\text{in}} = 1.3 r_{c,0}$  (where  $r_{c,0}$

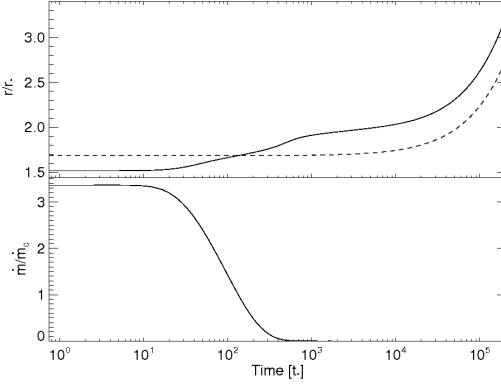


**Figure 3.1:** Transition from an accreting to a ‘trapped disc’ state. The initial  $\Sigma$  profile of the disc sets  $r_{\text{in}} = 1.5r_*$ , but the accretion rate through  $r_{\text{out}}$  is set to zero at  $t = 0$ . As a result of mass loss by accretion through  $r_c$ , the disc quickly evolves away from a steady accretion state and after about  $1500 t_*$  settles into a slowly evolving state in which  $r_{\text{in}}$  tracks  $r_c$ . Top: The black solid curve shows the evolution of the inner radius in time, while the red dashed curve shows the evolution of  $r_c$ . Bottom: The accretion rate onto the star, which decreases sharply as  $r_{\text{in}}$  moves outwards across the corotation radius.

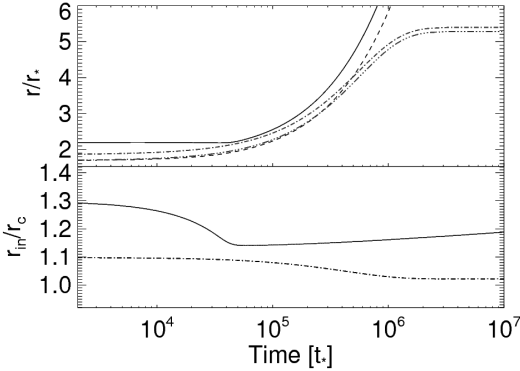


**Figure 3.2:** Comparison of the evolution of  $r_{\text{in}}$  and  $r_c$  between a dead disc (black solid and dashed curves) and accreting disc (red dot-dashed curves). Top: The evolution of  $r_c$  and  $r_{\text{in}}$  in units of the stellar radius. Black curves:  $r_{\text{in}}$  (solid) and  $r_c$  (dashed) in the dead disc; red curves: the accreting disc ( $r_{\text{in}}$ , dot-dashed curve;  $r_c$ , triple-dot dashed curve). Bottom: The ratio  $r_{\text{in}}/r_c$  for the dead disc (solid) and the accreting disc (dot-dashed). The dead disc keeps evolving indefinitely, the accreting case reaches a steady state in spin equilibrium with the star around  $t \sim 10^6$ .

is the initial corotation radius) which corresponds to  $\dot{m} \simeq 0$  for our chosen value of  $\Delta r_2/r_{\text{in}}$ . For the accreting disc, we choose  $r_{\text{in}} = 1.1r_{c,0}$ , which corresponds to a low but non-zero accretion rate ( $\dot{m} = 8 \times 10^{-3}\dot{m}_c$ ).

Since  $\dot{m}$  for the accreting disc is initially low compared to  $\dot{m}_c$ , at early times  $r_c$  evolves at the same rate in both simulations (accreting: red, triple-dashed curve; non-accreting: black,

dashed curve), and the star spins down. Eventually, however, the amount of angular momentum added by the accreted gas becomes comparable to the amount removed, and spin equilibrium is reached at  $\sim 10^6 t_*$ . In contrast, for the  $\dot{m} = 0$  case, the disc at first remains unaffected, while  $r_c$  moves outwards. (This is because the magnetic torque depends only on distance, not on the rotation rate of the star). After  $r_c$  moves close enough to  $r_{in}$  that accretion can begin (around  $4 \times 10^4 t_*$ ), the two start to move outwards at approximately the same rate. The (low) accretion rate onto the star is determined by the (slow) rate at which  $r_c$  moves outwards, and the star continues to spin down indefinitely. The bottom panel of fig. 3.2 shows the ratio of  $r_{in}/r_c$  for the accreting (dashed) and non-accreting disc (solid). After the non-accreting disc passes out of the dead disc phase (at  $\sim 4 \times 10^4$ ), in both systems the ratio changes by less than 10%, and  $r_{in}$  always remains close to  $r_c$ . The non-accreting disc, however, differs in that it never reaches spin equilibrium.

The main difference between the evolution of a dead disc and an accreting disc is the behaviour of the inner edge radius. As seen in sec. 3.4.2, in the initially dead disc the accretion rate onto the star is determined by the disc's behaviour when it reaches  $r_{in} \simeq r_c$ , while in an accreting disc the accretion rate is governed by the value set at the outer boundary.

Both the accretion rate on the star and the outward angular momentum flux in our trapped discs depend sensitively on the distance between  $r_{in}$  and  $r_c$  compared with the transition widths  $\Delta r$  and  $\Delta r_2$ . In the results of figure 3.2,  $r_{in} - r_c$  is of the order  $0.5 - 2\Delta r$ . In the next section we develop an analytic estimate of this number and compare it with the numerical results.

### 3.4.3 Analytic estimates for a trapped disc

As we showed above, an initially dead disc will eventually start accreting at a low rate, in such a way that  $r_{in}$  moves outwards together with  $r_c$  at a nearly constant ratio. The accretion rate onto the star is determined by how close  $r_c$  can move to  $r_{in}$  before the disc moves outwards in response. The actual distance on which  $r_{in}$  settles in cases like those show in the previous section depends on the details of the disc-field interaction (namely the parameters  $\Delta r$  and  $\Delta r_2$ ) and the ratio of timescales,  $T_{\text{visc}}/T_{\text{SD}}$ .

The spin-down timescale derived above assumes that  $r_{in}$  moves steadily outwards at the same rate as  $r_c$ . This timescale is an upper limit, since as  $r_c$  approaches  $r_{in}$  there is reduced transport of angular momentum through  $r_{in}$  and accretion onto the star begins. In addition, in order for spin-down to remain efficient, the angular momentum added by the disc-field interaction can be transported through the disc and carried away at  $r_{out}$ , otherwise  $r_{in}$  will move quickly away from  $r_c$  and spin-down will effectively cease.

When  $r_{in}$  is far enough from  $r_c$  that  $\dot{m} \simeq 0$ ,  $r_{in}$  stays fixed as the star is spun down and  $r_c$  moves outwards (3.15). However, once  $r_{in}$  moves closer to  $r_c$  (within  $\Delta r$  or  $\Delta r_2$ ), this static state is no longer possible: either matter at  $r_{in}$  starts accreting onto the star ( $y_m \neq 0$ ), or the surface density at  $r_{in}$  declines ( $y_\Sigma \neq 1$ ), which causes  $r_{in}$  to move closer to  $r_c$  until accretion through  $r_{in}$  can begin. Since the viscous timescale in the inner part of the disc

is much shorter than the spindown timescale, after accretion through  $r_{\text{in}}$  begins, a pseudo-steady-state develops, and  $r_{\text{in}}$  moves slowly outwards with  $r_c$ . If the disc can maintain a steady-state for the given  $\dot{m}$ , then  $r_{\text{in}}$  will track  $r_c$ , and the disc will remain a nearly dead disc as the star spins down to a small fraction of its initial spin period.

We can study this quantitatively by considering the equations for  $\dot{r}_{\text{in}}$  and  $\dot{r}_c$ . The evolution of the inner edge of the disc ((3.11) from Sec. 3.2.2), defining  $u \equiv \Sigma r$  for convenience is:

$$2\pi u(r_{\text{in}})\dot{r}_{\text{in}} = y_m \frac{\eta\mu^2}{4\Omega_* r_{\text{in}}^5} - 6\nu_0\pi r_{\text{in}}^{1/2} \left. \frac{\partial u}{\partial r} \right|_{r_{\text{in}}}. \quad (3.21)$$

As long as the two terms on the right of (3.21) balance,  $\dot{r}_{\text{in}} = 0$  even after accretion through  $r_{\text{in}}$  begins. This will continue until the surface density profile near  $r_{\text{in}}$  no longer satisfies (3.15). Since the change in  $r_c$  is the only source of variability in the problem,  $r_{\text{in}}$  will approximately track  $r_c$ .

Eq. (3.21) cannot be solved as is, since  $\partial u/\partial r$  depends on solving the full time dependent diffusion problem. As an estimate we assume that  $u$  changes as a result of the changing boundary condition (which will increase the surface density gradient), divided by the rate at which the rest of the disc can respond to that change (which will smooth it out). This can be approximated by:

$$\left. \frac{\partial u}{\partial r} \right|_{r_{\text{in}}} \sim - \frac{\partial u(r_{\text{in}})}{\partial t} v_{\text{visc}}^{-1}, \quad (3.22)$$

where  $v_{\text{visc}}$  is the viscous speed at  $r_{\text{in}}$ , of order:  $v_{\text{visc}} \sim \nu/r$ .

The time derivative for  $u(r_{\text{in}})$  follows from the boundary condition for  $u$ :

$$\left. \frac{\partial u}{\partial t} \right|_{r_{\text{in}}} = \frac{\partial u}{\partial r_{\text{in}}} \dot{r}_{\text{in}} + \frac{\partial u}{\partial r_c} \dot{r}_c. \quad (3.23)$$

The equation for  $\dot{r}_{\text{in}}$  then becomes:

$$\dot{r}_{\text{in}} = \left( \frac{\nu_0 y_m f^{3/2}}{8 r_{\text{in}} \partial_{r_{\text{in}}} y_{\Sigma}} \left( \frac{\Delta r}{r} \right)^{-1} r_{\text{in}}^{-1/2} - \dot{r}_c \right) \left( \frac{10}{3} \frac{y_{\Sigma}}{\partial_{r_{\text{in}}} y_{\Sigma} r_{\text{in}}} - 1 \right)^{-1}, \quad (3.24)$$

where  $f \equiv (r_c/r_{\text{in}})$ , and we have used the definition of  $y_{\Sigma}$  from Sec. 3.2.2 so that  $\partial_{r_{\text{in}}} y_{\Sigma} = -\partial_{r_c} y_{\Sigma}$ .

The evolution of  $\dot{r}_c$  depends on the rate of angular momentum exchange with the star. Matter falling onto the star spins it up, while the interaction with the disc outside  $r_c$  transfers angular momentum outward and spins the disc down. The equation for this evolution is given by (3.14), which can be re-written:

$$\dot{r}_c = \frac{2}{3} \frac{\eta\mu^2}{(GM_*)^{1/2} I_*} f^{7/2} \left[ \frac{\Delta r}{r_{\text{in}}} y_{\Sigma} - \frac{y_m}{4} f^{1/2} \right] r_{\text{in}}^{-1/2}. \quad (3.25)$$

We can study the evolution of  $\dot{r}_c$  and  $\dot{r}_{in}$  in two limiting cases. In the limit where  $r_{in} - r_c \gg \Delta r, \Delta r_2$ :

$$\begin{aligned}\dot{r}_c &\rightarrow \frac{2}{3} \frac{\eta \mu^2 r_{in}^{-4}}{(GM_*)^{1/2} I_*} \frac{\Delta r}{r_{in}} r_c^{7/2} \\ \dot{r}_{in} &\rightarrow 0,\end{aligned}\quad (3.26)$$

so that:

$$\begin{aligned}r_c &= \left( -\frac{5}{3} \frac{\eta \mu^2 r_{in}^{-4}}{(GM_*)^{1/2} I_*} \frac{\Delta r}{r_{in}} t + r_{c,0}^{-5/2} \right)^{-2/5} \\ r_{in} &= r_{in,0}.\end{aligned}\quad (3.27)$$

This is the limiting ‘dead disc’ case, where the amount of angular momentum being injected at  $r_{in}$  can be extracted at  $r_{out}$  and the disc remains steady while the star is spun down. It predicts a slightly smaller spin-down torque than was estimated in Sec. 3.3 because the torque scales with  $r_{in}$ .

The inner radius of the disc will remain approximately constant until either  $\frac{y_m}{y_\Sigma}$  or  $\frac{\partial_r y_\Sigma}{y_\Sigma} \left( \frac{\Delta r}{r_{in}} \right)^{-1}$  become non-negligible (3.24). Based on our assumption that the disc will remain in a quasi-steady-state while  $r_{in}$  moves,  $r_{in}$  will evolve only in response to changes in  $r_c$ , which means that  $f$  is a constant. This simplifies (3.24) and (3.25) considerably:

$$\begin{aligned}\dot{r}_c &= (A_0 f^{7/2} - A_1 f^4) r_{in}^{-1/2} \\ \dot{r}_{in} &= \frac{B_0 f^{3/2} r_{in}^{-1/2} - \dot{r}_c}{B_1 - 1},\end{aligned}\quad (3.28)$$

where,

$$\begin{aligned}A_0 &= \frac{2}{3} \frac{\eta \mu^2}{(GM_*)^{1/2} I_*} \frac{\Delta r}{r_{in}} y_\Sigma \\ A_1 &= \frac{1}{6} \frac{\eta \mu^2}{(GM_*)^{1/2} I_*} y_m \\ B_0 &= \frac{v_0 y_m}{8 r_{in} \partial_{r_{in}}(y_\Sigma)} \left( \frac{\Delta r}{r_{in}} \right)^{-1} \\ B_1 &= \frac{10 y_\Sigma}{3 r_{in} \partial_{r_{in}}(y_\Sigma)}.\end{aligned}\quad (3.29)$$

The solution is then:

$$\begin{aligned}r_c &= \left( \frac{3}{2} (A_0 f^3 - A_1 f^{9/2}) t + r_{c,0}^{3/2} \right)^{2/3} \\ r_{in} &= \left( \frac{3}{2} \left( \frac{B_0 f^{3/2} - A_0 f^{7/2} + A_1 f^4}{B_1 - 1} \right) t + r_{in,0}^{3/2} \right)^{2/3}.\end{aligned}\quad (3.30)$$

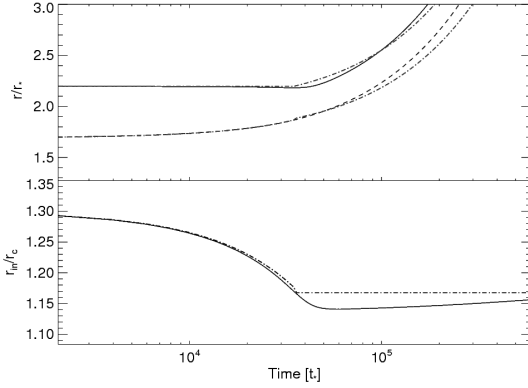


**Figure 3.3:** Comparison between numerical solution and analytic estimate for an idealized dead disc around a star spinning close to break-up  $r_c = 1.7$ , with  $\Delta r/r_{in} = 0.1$  and  $\Delta r_2/r_{in} = 0.05$ . Top: Numerical solution of the evolution of  $r_c$  (black, dashed curve) and  $r_{in}$  (black, solid curve) in time. Overplotted is our analytic estimate for  $r_{in}$  (red dash-dotted curve) and  $r_c$  (red dash-triple dotted curve) for the same physical conditions. Bottom: The ratio  $r_c/r_{in}$  for our numerical solution (solid curve) and analytic estimate (dash-dotted curve). The disagreement in the two solution arises from our simplified treatment of the viscous disc.

We can use (3.28) to calculate  $f$ , that is, how close  $r_c$  can move towards  $r_{in}$  before the disc will start moving outwards in response. Setting  $\dot{r}_c = f\dot{r}_{in}$ , we can re-express the constants in (3.30) as:

$$\left(2\frac{\Delta r}{r_{in}}f\gamma_{\Sigma} - \frac{y_m f^{3/2}}{2}\right) \left(\frac{10y_{\Sigma}}{3r_{in}\partial_{r_{in}}\gamma_{\Sigma}} + f - 1\right) \quad (3.31)$$

$$\left(\frac{r_{in}\partial_{r_{in}}\gamma_{\Sigma}}{y_m}\right) = \frac{3}{8}\frac{T_{SD}}{T_{visc}},$$

and solve  $f$  numerically to give the approximate evolution for  $r_c$  and  $r_{in}$  in time.

In Fig. 3.3 we compare our estimates for the evolution of  $r_c$  and  $r_{in}$  to the solution from our numerical simulation. We consider a rapidly spinning star ( $r_c = 1.7$ ), with  $\Delta r/r_{in} = 0.1$  and  $\Delta r_2/r_{in} = 0.05$ . In the top panel we compare the two solutions for  $r_{in}$  (estimate: dot-dashed red curve vs. numerical solution: black solid curve) and  $r_c$  (estimate: triple-dotted-dashed red curve vs. numerical solution: black dashed curve). In the bottom panel we plot the ratio  $r_{in}/r_c$  for the numerical (solid curve) and analytic (dashed curve) result. At early times,  $r_c < r_{in}$  (3.27), and the solutions match exactly. However, at late times the solutions disagree somewhat. Most obviously, the value for  $f$  calculated by (3.30) is smaller than the numerical solution, that is that  $\dot{r}_{in} = 0$  for longer than we predict, and there is some evolution in  $f$  over long timescales. This mismatch comes from our simplified treatment for  $\partial_r u|_{r_{in}}$ , which over long timescales will depend on the surface density gradients in the entire disc.

By comparing the sizes of each term on the left-hand side of (3.31), some insightful approximations can be made. Since the solution is nearly a dead disc, the disc's accretion

rate will be very low, so that  $y_m \ll 1$ ,  $y_\Sigma \sim O(1)$ , and  $\partial_{r_{\text{in}}} y_\Sigma \ll 1$ . As well,  $r_{\text{in}}$  is close to  $r_c$  so that  $f \sim O(1)$ . Since in general  $T_{\text{visc}}/T_{\text{SD}} \ll 1$ , (3.31) can be approximated:

$$\frac{160}{9} \frac{\Delta r}{r_{\text{in}}} f \frac{y_\Sigma^2}{y_m} \simeq \frac{T_{\text{SD}}}{T_{\text{visc}}}, \quad (3.32)$$

and used to estimate  $f$ . The left-hand side of (3.32) is dominated by  $y_m^{-1}$ , which quickly grows as  $r_{\text{in}}$  moves away from  $r_c$ , and must balance the right-hand side. The ability to sustain a dead disc will thus depend on *both* the interaction between the disc and the field (through the parameter  $\Delta r_2$ ), *and* the ratio between the spin-down timescale and the accretion timescale.

For a given  $T_{\text{SD}}/T_{\text{visc}}$ , if  $\Delta r_2/r_{\text{in}} \ll 1$ , then  $y_m$  is nearly a step function, and  $f$  will stay close to 1 even if  $T_{\text{SD}}/T_{\text{visc}}$  is very large. On the other hand, if  $\Delta r_2/r_{\text{in}} \sim 1$ , and accretion continues even when  $r_{\text{in}}$  moves a fair distance from  $r_c$ , then it is possible that the solution to (3.31) will predict a larger value for  $r_{\text{in}}$  than can support a dead disc. In this case no dead disc solution exists: even if the disc initially begins as a dead disc, once  $r_c$  moves close enough to  $r_{\text{in}}$  that accretion begins, the disc will begin to move outwards until matter at  $r_{\text{in}}$  can be expelled from the system. The outflow of material will then proceed at a moderate rate as the surface density profile of the disc evolves away from the dead disc solution (3.15 with  $\dot{m} = 0$ ) to the standard disc solution, with outflow rather than accretion onto the star.

## 3.5 TRAPPED AND UNTRAPPED

### 3.5.1 Accreting discs evolving to trapped or dead disc states

The results found so far and in DS10 indicate the strong tendency for the inner edge of the disc to track the corotation radius, what we call here a ‘trapped disc’. This does not happen in all cases, however. We would like to find out under what conditions a disc gets stuck in this way, and when instead the inner edge proceeds to move well outside corotation into the ‘dead disc’ state.

Armed with qualitative understanding from the previous section, we can address this question with a few numerical experiments. We take the case of a neutron star with field strength  $B_S = 10^{12}$ , initial spin period  $P_* = 5\text{s}$ , and initial inner edge radius  $r_{\text{in}} = 0.95r_{c,0}$ . The disc is thus initially in an accreting state. The (initial) outer boundary is located at  $r_{\text{out}} = 100r_{\text{in}}$ , and we set  $\dot{m} = 0$  there so that no matter can escape the system. The other parameters are the same as for our representative model.

We first investigate the effect of varying the viscosity on the way the transition from an accreting to a dead disc takes place. This is shown in fig. 3.4. The spindown timescale (3.20) for the initial  $r_c$  is  $T_{\text{SD}} = 10^5$  years. From top to bottom, we plot this transition for decreasing values of viscosity (and hence increasing viscous timescales). To compare these

two quantities we define  $T_{\text{visc}}$  as the viscous timescale at the initial  $r_c$ . In the different plots, the ratio  $T_{\text{visc}}/T_{\text{SD}}$  increases from  $2.5 \times 10^{-9}$  to  $10^{-4}$ .

The most striking change in behaviour occurs between the top panel and the second panel. At the shortest viscous time scale, the disc does not get into a trapped state, but evolves directly through corotation, while at lower viscosity it always settles into the trapped state, with the inner edge moving in step with with the corotation radius.

In all the discs, the initial evolution is the same: as  $\dot{m}$  decreases,  $r_{\text{in}}$  moves outwards, crossing  $r_c$  over about  $10^3$  years. Once that happens, however, the subsequent evolution of the disc and star differs substantially between simulations. In the most viscous discs (top),  $r_{\text{in}}$  continues moving steadily outwards over  $10^{10}$  years – roughly  $10^5$  times longer than the nominal spin-down timescale of the disc. Since  $r_{\text{in}}$  keeps moving outwards, the torque on the star decreases too, so that the disc moves far away from  $r_c$  before it is able to spin down the star.

As the viscosity is reduced, the ratio between the two timescales becomes smaller, and  $r_{\text{in}}$  does not move so far away from  $r_c$  before  $\dot{r}_{\text{in}} \sim \dot{r}_c$ . Thus for the disc with the lowest viscosity (bottom),  $r_{\text{in}}$  and  $r_c$  begin to move outwards after about  $10^5$  years, and the trapped disc (where  $\dot{m}$  is regulated by  $\dot{r}_c$ ) has a much larger accretion rate onto the star (seven orders of magnitude larger after  $10^4$  years) than for higher viscosities.

By the initial condition chosen, the magnetic torque pushes the inner edge out across corotation. This causes mass to pile up outside  $r_{\text{in}}$ . The higher the viscosity, the faster this pile is reduced again by outward spreading, and the faster the inner edge can continue to move outward in response. The experimental result is then that trapping behavior is avoided when the transition takes place fast enough. We return to this in the discussion.

The pile up is also influenced by the way in which accretion on the star changes as  $r_{\text{in}}$  crosses  $r_c$ , hence we expect that the parameter controlling this,  $\Delta r_2$ , will have a strong effect as well.

In fig. 3.5 we show three discs in which the initial ratio  $T_{\text{SD}}/T_{\text{visc}}$  is kept fixed, but the value of  $\Delta r_2$  changes, from top to bottom,  $\Delta r_2/r_{\text{in}} = [0.4, 0.04, 0.004]$ . The larger  $\Delta r_2$ , the further away  $r_{\text{in}}$  must move from  $r_c$  in order for the accretion rate to decrease sufficiently to form the trapped disc. In the top panel (when  $\Delta r_2$  is largest), the disc must move out a considerable distance before becoming trapped, sufficiently far to significantly decrease the efficiency of the spin-down torque (and hence increase the spin-down timescale of the star). As well as decreasing the spin-down efficiency, if  $\Delta r_2$  is large enough, the inner radius could move far enough away from  $r_c$  that material could begin to be launched from the disc in an outflow, and the disc would become untrapped.

As was shown in Section 3.3, the ratio  $T_{\text{visc}}/T_{\text{SD}}$  itself can vary over many orders of magnitude in different systems, from  $10^{-17}$  in neutron stars with weak magnetic fields to  $10^{-2}$  in discs around massive young stars. The size of this ratio will also determine whether a trapped disc can form.

This analysis would suggest that, assuming  $\Delta r_2/r_{\text{in}}$  does not vary much from system to system, trapped discs are much more likely to form in protostellar discs than in strongly ion-

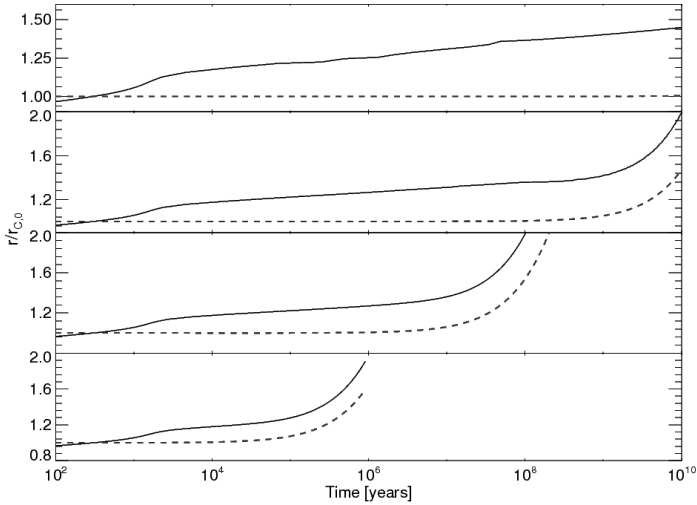


**Figure 3.4:** The evolution from an accreting to a non-accreting disc, for increasing (top to bottom) ratios of  $T_{\text{visc}}/T_{\text{SD}}$  (with  $\Delta r/r_{\text{in}} = 0.1$ ,  $\Delta r_2/r_{\text{in}} = 0.04$ ). From top to bottom, the ratio  $T_{\text{visc}}/T_{\text{SD}}$  is  $2.5 \times [10^{-9}, 10^{-7}, 10^{-5}, 10^{-4}]$ . As the ratio between the two timescales decreases, the disc is not able to move outwards as quickly before the star begins to spin down, so that  $r_{\text{in}}$  will always remain close to  $r_c$ . Black solid curve: evolution of  $r_{\text{in}}$ . Red dashed curve: evolution of  $r_c$ .

ized discs around neutron stars. Furthermore, the closer  $r_{\text{in}}$  is to  $r_c$ , the higher the accretion rate in the trapped disc. Conceivably, especially if the viscosity in the disc were very low, this accretion rate could be larger than the average accretion rate in the disc itself, so that the disc could spin down the star for a long time without ever reaching spin equilibrium, even with a finite accretion rate onto the star.

As the results reported above show, the evolution can end either in a dead disc state in which the star has lost only a fraction of its angular momentum, or a trapped state in which corotation is maintained and the star can spin down much further. Which outcome results depends on details of the interaction between the star and the disc, parametrized in our model by the transition widths  $\Delta r$  and  $\Delta r_2$ . It also depends on the rate at which the disc can respond viscously compared to the spin change rate of the star. A fast response of the disc makes the transition through corotation faster than  $r_c$  changes, and the disc is more likely to enter the dead state. This makes it far more likely to occur in young stellar systems than in neutron star binaries.

In the results presented above, the initial conditions were taken from steady solutions of the viscous thin disc equation. These included dead discs in which a steady state was made

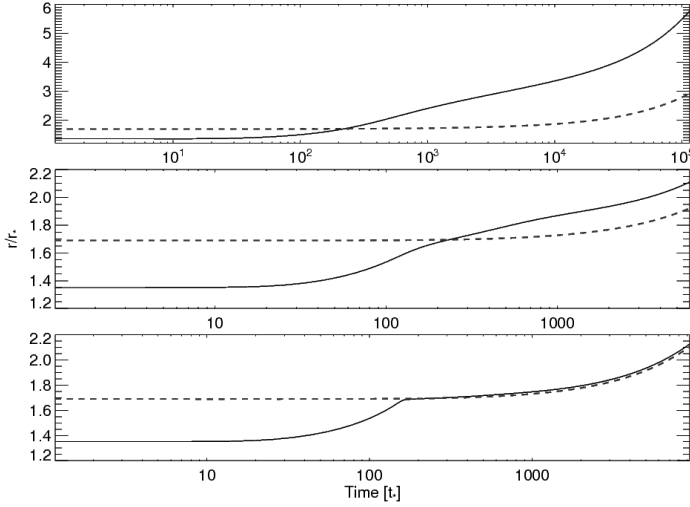


**Figure 3.5:** The evolution from an accreting to a non-accreting disc, for stable discs ( $\Delta r/r_{\text{in}} = 1$ ) with different  $\Delta r_2$ . From top to bottom,  $\Delta r_2/r_{\text{in}} = [0.4, 0.04, 0.004]$ . Curves show  $r_{\text{in}}$  and  $r_c$  as in fig. 3.4.

possible by a sink of angular momentum at the outer boundary of the numerical grid, which takes up the angular momentum added by the magnetic torques at the inner edge.

### 3.5.2 Dead discs evolving into trapped discs

In this example we investigate the opposite case of section 3.5: discs with  $r_{\text{in}}$  initially outside corotation, and conditions chosen such that the disc begins by spreading inward. The mass flux at the outer boundary is set to zero. Varying the initial outer radius,  $r_{\text{out},0}$  varies the amount of mass in it, and the time scale of its long-term evolution can change.

We adopt the representative model parameters used before, with an initial inner radius set to  $1.3r_c$  (corresponding to a negligible accretion rate for our chosen  $\Delta r_2/r_{\text{in}}$ ), and set  $r_{\text{out},0} = [10, 100, 10^3, 10^4]r_{\text{in},0}$ . The evolution of  $r_{\text{in}}$  and  $r_c$  is plotted in Figs. 3.6 and 3.7. Fig. 3.6 compares the evolution of  $r_{\text{in}}/r_c$  for different sizes of disc, while fig. 3.7 compares the evolution of  $r_{\text{in}}$  and  $r_c$  for different disc sizes to the simulation where  $r_{\text{out},0} = 10r_{\text{in},0}$ . In both simulations, the different curves correspond to different initial  $r_{\text{out}}$ :  $10 r_{\text{in}}$  (dotted curve),  $100 r_{\text{in}}$  (dashed curve),  $1000 r_{\text{in}}$  (dash-dotted curve),  $10^4 r_{\text{in},0}$  (dash-triple-dotted curve).

Fig. 3.6 shows the evolution of  $r_{\text{in}}/r_c$  in time for different initial  $r_{\text{out}}$ . For the simulations with  $r_{\text{out},0}/r_{\text{in},0} = [10, 100, 1000]$ , the ratio  $r_{\text{in}}/r_c$  declines to a minimum value that decreases

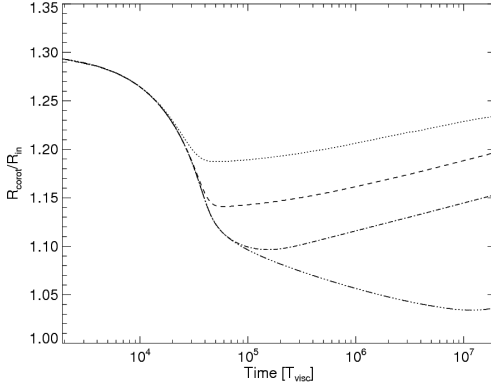


**Figure 3.6:** Discs starting outside corotation and spreading inward. Evolution of  $r_{\text{in}}/r_c$  for different initial  $r_{\text{out}}$ . From top to bottom:  $r_{\text{out},0} = 10r_{\text{in},0}$  (dotted curve),  $10^2$  (dashed curve),  $10^3$  (dash-dotted curve), and  $10^4$  (triple dash-dotted curve)  $r_{\text{in}}$  at  $t = 0$ . Larger discs have a larger reservoir of matter, so that they can sustain a larger  $\dot{m}$  (so smaller  $r_{\text{in}}$ ) as  $r_c$  increases due to spindown of the star.

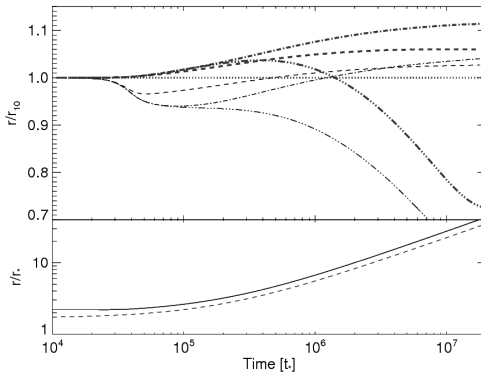


**Figure 3.7:** Evolution of  $r_{\text{in}}$  and  $r_c$  in a dead disc with different  $r_{\text{out}}$ . Bottom: The evolution of  $r_{\text{in}}$  (solid black curve) and  $r_c$  (dashed red curve) for the smallest disc,  $r_{\text{out},0} = 10 r_{\text{in},0}$ . Top: The evolution of  $r_{\text{in}}$  (thin black curves) and  $r_c$  (thick red curves) for different sizes of disc, divided by the  $r_{\text{out},0} = 10 r_{\text{in},0}$  solution. The individual curves are the same as in Fig. 3.6.

as  $r_{\text{out}}$  is taken larger, before again increasing approximately logarithmically. In the largest disc,  $r_{\text{out},0}/r_{\text{in},0} = 10^4$ , the evolution is the same as in the smaller discs at early times, but  $r_{\text{in}}/r_c$  continues to decline for much longer until it reaches a minimum at around  $10^7 t_*$  when it finally turns over.

The minimum value of  $r_{\text{in}}/r_c$  is determined by the amount of mass in the disc available for accretion. The larger discs have more mass, which sustains the accretion rate onto the star for a longer time before the drop in surface density causes  $r_{\text{in}}$  to move outward again.

The bottom panel of Fig. 3.7 shows the evolution of  $r_{\text{in}}$  and  $r_c$  for  $r_{\text{out},0} = 10 r_{\text{in},0}$ . The evolution is qualitatively the same as we derived in the analytic approximation in Sec. 3.4.3. Initially  $r_{\text{in}}$  remains fixed as  $r_c$  starts to evolve outwards, until  $r_c$  moves close enough to  $r_{\text{in}}$  that accretion can begin. The inner radius then evolves outward at approximately the same

rate as  $r_c$  as the star spins down. The variation between different simulations is emphasized in the top panel of Fig. 3.7. Here we plot the evolution of  $r_c$  (thick curves, red) and  $r_{in}$  (thin curves, black) for the discs with  $r_{out,0}/r_{in,0} = [10^2, 10^3, 10^4]$ , divided by the solution for  $r_{out,0}/r_{in,0} = 10$ . For larger discs the accretion rate is higher, so that  $r_{in}$  can move closer to  $r_c$ . In the three smaller discs, the accreted mass adds a negligible amount of angular momentum to the star, so that as  $r_{in}$  moves closer to  $r_c$ . As a result, the spin-down torque simply becomes more efficient, and  $r_c$  spins down faster. After  $10^7 t_*$   $r_c$  for the disc with  $r_{out,0}/r_{in,0} = 10^3$  is more than 10% larger than in the smallest disc. However, for the largest disc, the accretion rate puts  $r_{in}$  close enough to  $r_c$  that the spin-down torque starts to drop in efficiency and the spin-up from accretion becomes non-negligible. Although  $r_c$  still increases, after  $10^7 t_*$   $r_c$  is 30% smaller than for a small disc.

These results show that size of the disc can considerably influence the efficiency of spin-down, emphasizing the fact that the spin-down of a star is an initial value problem. The initial size of the disc can be as important as the ratio  $T_{SD}/T_{visc}$  and the parameter  $\Delta r_2$  in determining whether the disc can become trapped, and the efficiency of the spin-down torque. The results of this section would suggest that larger discs (with their larger reservoirs of mass) are more likely to become trapped than smaller discs.

### 3.5.3 Long-term behaviour of discs of finite size

As we found in section 3.5, the long-term evolution of the disc+star system tends to ‘bifurcate’. The end state is either a star that has lost little angular momentum, surrounded by a dead disc, or a star continuously spun down by a disc trapped at corotation with the star.

We investigate this by a set of simulations in which the initial state is a disc of finite size  $r_0$ , evolving in a grid that is 10 times larger,  $r_{out} = 10r_0$ . Apart from this change we use the standard parameters (section 3.3.1), setting the initial value of  $r_{in}/r_c$  at 1.3 (for comparison with the results of the previous section). Whether the disc will be able to substantially spin down the star depends on the ratio the timescales  $T_{visc}(r_0)$  to  $T_{SD}$ . If the disc is very small ( $T_{visc}(r_0) \ll T_{SD}$ ),  $r_{in}$  will move outward too quickly to spin down the star, while if  $T_{visc}(r_0) \gg T_{SD}$ , the moment of inertia in the disc is sufficiently high to be able to absorb much more angular momentum from the star, so that the disc can operate as an efficient sink for the star’s angular momentum.

Fig. 3.8 shows results for three different sizes of disc. In each curve, the dashed red line shows the evolution of  $r_c$ , while the solid black curve shows the evolution of  $r_{in}$ . The top panel of fig. 3.8 shows the disc evolution when the viscosity is chosen such that  $T_{visc}(r_0) \ll T_{SD}$ , with  $r_0 = 100r_{in}$ . Since the angular momentum injected at  $r_{in}$  is carried away by viscous spreading of the disc, the disc quickly evolves away from its initial configuration. Since the moment of inertia in the disc is much smaller than in the star, the disc becomes too spread out to absorb the angular momentum injected at  $r_{in}$ , and  $r_{in}$  moves outward before the star is able to slow down substantially.

In the middle panel of 3.8 we show the evolution of  $r_{in}$  and  $r_c$  when the spin-down

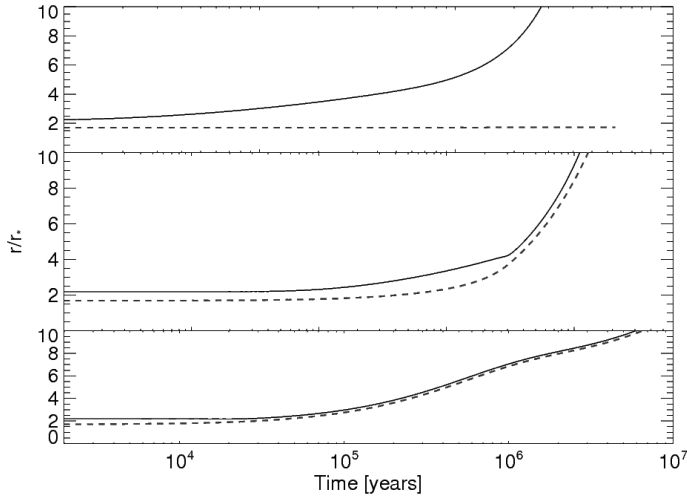


**Figure 3.8:** Top: Evolution of  $r_{\text{in}}$  and  $r_{\text{c}}$  in a dead disc with mass transport through  $r_{\text{out}}$ , where  $T_{\text{visc}}(r_{\text{out},0}) \gg T_{\text{SD}}$ . The moment of inertia in the disc is sufficiently large to prevent  $r_{\text{in}}$  from moving out as  $r_{\text{c}}$  evolves. Middle: Evolution of  $r_{\text{in}}$  and  $r_{\text{c}}$  in a dead disc with mass transport through  $r_{\text{out}}$ , where  $T_{\text{visc}}(r_{\text{out},0}) \sim T_{\text{SD}}$ . The disc is initially massive enough to spin down the star, but after some time evolves away from the equilibrium solution and  $r_{\text{in}}$  moves rapidly out. Bottom: Evolution of  $r_{\text{in}}$  and  $r_{\text{c}}$  in a dead disc with mass transport through  $r_{\text{out}}$ , where  $T_{\text{visc}}(r_{\text{out},0}) \gg T_{\text{SD}}$ . The moment of inertia in the disc is sufficiently large to prevent  $r_{\text{in}}$  from moving out as  $r_{\text{c}}$  evolves. Curves show  $r_{\text{in}}$  and  $r_{\text{c}}$  as in fig. 3.4.

timescale is comparable to the viscous timescale at  $r_0$ . The disc also initially diffuses outwards (as seen by the increase in  $r_{\text{in}}$  around  $t = 5 \times 10^5$ ), so that the rate of angular momentum exchange from the star to  $r_{\text{in}}$  decreases. This allows  $r_{\text{c}}$  to catch up, and the two radii start to evolve together. Eventually, however, viscous spreading of the disc wins, and  $r_{\text{in}}$  begins to move outwards.

The bottom panel of 3.8 shows the evolution of  $r_{\text{in}}$  and  $r_{\text{c}}$  when  $T_{\text{visc}}(r_0) \gg T_{\text{SD}}$ . The result is essentially the same as in Sec. 3.5.2, since the disc is now so large that additional angular momentum from the star does not reach  $r_{\text{out}}$  on the spindown timescale. In other words, the moment of inertia of the disc itself is large enough that the star is able to spin down without causing  $r_{\text{in}}$  to move rapidly outward.

### The rotation of Ap stars and magnetic white dwarfs

An intriguing clue to the spindown of magnetic stars comes from slowly rotating Ap stars. As a class these stars are observed to have very strong dipolar magnetic fields (up to 10 kG). A few of them have extremely long rotation periods (up to 10-100 years), while others have rotation periods as short as 0.5 d. A similar phenomenon is observed in the magnetic white dwarfs. Most of these have periods of a few days or weeks, but some rotate as slowly as the slowest Ap stars. We suggest that the bifurcation of outcomes we found in the above is the underlying reason for the remarkable range of spin periods of magnetic stars.

## 3.6 CONCLUSIONS

As found before in SS and DS10, a disc in contact with the magnetosphere of a star can be in a ‘dead’ state, with its inner edge well outside the corotation radius so the accretion rate onto the star vanishes, and the torque exerted by the magnetic field transmitted outward by viscous stress. In the calculations reported in DS10, an additional state was found, intermediate between the accreting and dead state. In this state, the inner edge of the disc stayed close to the corotation radius  $r_c$ , even as the accretion rate onto the star varied by large factors. We call this phenomenon *trapping* of the disc. Accretion can be stationary or in the form of a limit cycle in this state.

One of the goals of this investigation was to find out under what conditions this trapping takes place, using a series of numerical experiments with varying initial and boundary conditions. If initial conditions are such that the inner edge starts inside corotation and slowly moves outward, we find that the disc gets stuck in a trapped state for a long time if the disc viscosity  $\nu$  is low (up to about  $10^3$  times shorter than the spindown timescale of the star). The accretion rate then slowly vanishes but the inner edge always stays close to corotation. At higher viscosity ( $> 10^5 \times$  the spindown timescale) on the other hand, the disc evolves through corotation into a ‘dead’ disc state, with inner edge well outside the corotation radius. In terms of the standard viscosity parametrization  $\nu = \alpha(H/r)^2$ , compared with the spin-down timescale of the disc, a trapped state is more likely to happen in strongly magnetic ( $B_S \sim 10^{12}G$ ) X-ray pulsars and protostellar discs than the weaker magnetic fields ( $B_S \sim 10^8G$ ) of millisecond X-ray pulsars.

Our second goal was to find out how a star spins down in the long term, under the influence of the angular momentum it loses by the magnetic torque exerted on the disc. The results show an interesting ‘bifurcation’ of long-term outcomes: if the disc evolves into a dead state, the star loses only a fraction of its initial angular momentum, and can remain spinning rapidly throughout its life. If on the other hand it enters a trapped state at some point, it remains in this state. The star can then slow down to very low rotation rates, the inner edge of the disc tracking the corotation radius outward. We suggest that these two outcomes can be identified respectively with the rapidly rotating and slowly rotating classes of magnetic Ap stars and magnetic white dwarfs. The evolution of the trapped state could also

be reproduced with a simplified model that does not require solving the full viscous diffusion equation.

This picture of magnetosphere-disc interaction differs from the standard view that mass will be ‘propellered’ out of the system instead of accreting, once the star rotates more rapidly than the inner edge of the disc. As shown already by Sunyaev & Shakura (1977) and again argued in Spruit & Taam (1993) and DS10 this assumption is not necessary, in many cases unlikely, and ignores some of the theoretically and observationally most interesting aspects of the disc-magnetosphere interaction.

Though the dead state is a regime where a significant fraction of the disc mass could in principle be expelled ( $r_{\text{in}} \gg r_c$ ), the results presented here show that magnetospherically accreting systems often avoid this regime. Instead, they end up in the trapped state, in which the disc-field interaction keeps the inner radius truncated very close to the co-rotation radius, even at very low accretion rates. Both the trapped and ( $r_{\text{in}} \approx r_c$ ) and the dead state ( $r_{\text{in}} \gg r_c$ ) allow the disc to efficiently spin down the star. The disc retains a large amount of mass, but in the absence of accretion onto the central star appears quiescent.

### 3.7 DISCUSSION

By assuming a given dependence of viscosity on distance, we have bypassed the physics that determines it. In terms of the standard  $\alpha$ -parametrization of viscosity, we have left out the physics that determines the disc temperature and hence its thickness  $H/r$ . Additional time dependence or instabilities may arise from feedback between accretion and disc temperature. The radiation produced by matter accreting on the star could be large enough to change temperature, the ionization state and hence the thickness at the inner edge of the disc. In a trapped disc, this is just the region that controls the accretion rate onto the star. The size of the transition region, which we have parametrized with the widths  $\Delta r, \Delta r_2$  may well depend on disc thickness. Positive feedback may be thus possible. We leave this possibility for future work.

In systems such as the accreting X-ray pulsars the accretion is episodic on long time scales. This is attributed to the instability of viscous discs that is also responsible for the outbursts of cataclysmic variables. In these cases, in which there is a large change in  $\dot{m}$  and  $r_{\text{in}}$  is far from  $r_c$  in the quiescent phase, there is the possibility of hysteresis: the same accretion rate will lead to a different value of  $r_{\text{in}}$  (and therefore disc torque) depending on whether the source is moving into or out of outburst. As the source goes into outburst, the disc will not have as much mass in its inner regions, so that  $r_{\text{in}}$  will move inward gradually from large radii until it crosses  $r_c$  and the outburst begins. In the decline phase, however, the disc will become trapped around the inner radius of the disc when the accretion rate drops, allowing for a larger spin-down in the disc and accretion bursts via the instability of DS10. The net effect of such episodic accretion on the spin history of the star, as compared with the case of steady accretion, is not obvious. We discuss this in more depth in the companion

paper.

Some work on disc-magnetosphere interaction assumes magnetic torques to act over a significant part of the disc (Königl 1991; Armitage & Clarke 1996). More recent work (and in particular numerical MHD simulations of the disc-field interaction) finds the interaction region to be much narrower (as we have also assumed here), and spindown torques on the star are correspondingly smaller. The difference for the long-term spin evolution is not dramatic, however, as our trapped disc results demonstrate.

Interestingly, Armitage & Clarke (1996) also observed that their discs would become trapped around  $r_c$  as the accretion rate in the disc decreased by several orders of magnitude. In their model, the magnetic field-disc interaction also acts like a boundary condition at low accretion rates and the disc evolved viscously in response. This is presumably because although the disc in their model is threaded by a magnetic field everywhere, the disc-field interaction is by far the strongest in the inner regions, so that they see a similar behaviour to the one described in this paper.

MHD simulations of interaction between the disc and the magnetic field are becoming increasingly realistic. These simulations can only run for very short timescales (the longest of order  $T_{\text{visc}}$  at  $r_{\text{in}}$ ), so they tend to emphasize initial transients. Still, they offer insight in how the disc and magnetic field will interact. To date, most simulations have concentrated on strongly accreting (Hayashi et al. 1996; Goodson et al. 1997; Miller & Stone 1997) or propeller (Romanova et al. 2004) cases. Simulations that come closest to the conditions of a trapped disc are the study of a so-called ‘weak propeller’ regime by Ustyugova et al. (2006). The authors found that discs in which  $r_{\text{in}}$  was initially truncated close to  $r_c$  launch much weaker outflows than discs truncated further away. They also found some evidence of the field changing the disc structure (as shown from mass piling up in the inner regions), although in their simulation the majority of the angular momentum in the star was carried away via a wind, rather than through the disc. These simulations also did not run for very long, however, so it is hard to separate transient behaviour due to the initial conditions from the longer-term systematic effects we are interested in.

Perna et al. (2006) did calculations where the star’s field is inclined with respect to the disc axis. The authors’ results suggest that the transition width which we have parametrized by  $\Delta r_2$  would increase with the inclination of the magnetic field, since there will be some values for  $r_{\text{in}}$  at which both accretion and disc mass trapping can occur. This then would suggest that dead discs are more likely to form in systems with small inclinations between the spin axis and magnetic axis, and also that the disc instability studied in DS10 (which also tends to occur for smaller values of  $\Delta r_2$ ). This prediction is supported by the observation that Ap stars with the longest periods tend to have the lowest inclination angles for the magnetic field (Landstreet & Mathys 2000).

The transition widths of disc-magnetosphere interaction that can be inferred from these simulations are significant, and are in the range we have assumed here. They are much larger than the very narrow interaction regions assumed by Matt et al. (Matt & Pudritz 2004, 2005; Matt et al. 2010).

We have found that the distance from  $r_c$  at which the inner edge of the disc gets trapped is determined by the ratio of two timescales for the disc's evolution: the viscous evolution timescale in the disc (which determines the rate at which disc density profile can change) and the star's spin-down timescale (which sets the rate at which  $r_c$  moves outwards). The viscous timescale is in general much shorter than the spin-down timescale, and the ratio of the two timescales varies from  $\sim 10^{-3}$  (in protostellar discs) to  $\sim 10^{-17}$  (in millisecond X-ray pulsars). The larger the ratio, the longer the disc will take to respond to changes in  $r_c$ . As a result  $r_{in}$  remains closer to  $r_c$  than it would if the ratio were smaller, and the trapped disc has a higher accretion rate onto the star. If the ratio is too low, then  $r_{in}$  moves much further away from  $r_c$ , and the system likely enters the dead disc regime.

For the parameters characterizing the interaction region between disc and magnetosphere in our model, we have used here values such that the cyclic accretion behavior found in DS10 does not develop. This was done for convenience, since the short time steps needed to follow these cycles makes it harder to calculate the long-term evolution. The time-averaged effect of these cycles is not expected to make a big difference for the long-term evolution.

These cyclic accretion bursts can persist in the trapped state, when the star is spinning down efficiently. They are observed to occur both over several orders of magnitude of accretion rates and transiently (over a small range of accretion rate), and depend on the ratio of timescales discussed above. Whether or not the instability occurs is determined by the detailed disc-field interaction (the parameters  $\Delta r$  and  $\Delta r_2$  in our model). The peak of the accretion bursts is typically much larger ( $> 10\times$ ) than the mean accretion rate for the system, and the period is typically between  $0.01 - 10^2 T_{\text{visc}}(r_{in})$ . The properties and conditions for occurrence of these cycles are studied further in a companion paper.

### 3.7.1 'Propellering'

In our calculations we have left out the possibility that interaction of the magnetosphere with the disc will cause of mass ejection from the system. The point being that, contrary to common belief, such interaction can function without mass ejection by 'propellering', as pointed out already by (SS76). Understanding of this restricted case, as we have developed here, is prerequisite for understanding the much less well defined case of mass losing discs.

On energetic grounds, mass loss from the system is necessarily limited, unless the inner edge is well outside corotation (ST93). This point has also been made by Perna et al. (2006), who propose that mass lifted at  $r_{in}$  may fall back on the disc at some finite distance. This would create a feedback loop in the mass flux through the disc, opening the possibility of additional forms of time-dependent behaviour that do not exist in accretion onto non-magnetic stars. In the trapped disc state we have studied here the difference in rotation between disc and star is small, so any significant amount of mass kicked up from the interaction region cannot move very far before returning to the disc. Its effects are then secondary, at least for the long-term evolution of the disc.

The possibility of significant effects of mass loss is more realistic for the dead disc states, where the distance of the inner edge from corotation can become much larger.

Real propellering is expected to happen when mass transfer from a companion star sets in for the first time onto a rapidly spinning magnetic star. The cataclysmic binary AE Aqr is evidently such a case (Pearson et al. 2003). A disc is absent in this CV, and all mass transferred appears to be ejected in a complex outflow associated with strong radio emission.

#### REFERENCES

- Alecian E., Wade G. A., Catala C., Folsom C., Grunhut J., Donati J., Petit P., Bagnulo S., Marsden S. C., Ramirez Velez J. C., Landstreet J. D., Boehm T., Bouret J., Silvester J., 2008, *Contributions of the Astronomical Observatory Skalnaté Pleso*, 38, 235
- Aly J. J., 1985, *A&A*, 143, 19
- Armitage P. J., Clarke C. J., 1996, *MNRAS*, 280, 458
- Getman K. V., Feigelson E. D., Micela G., Jardine M. M., Gregory S. G., Garmire G. P., 2008, *ApJ*, 688, 437
- Ghosh P., Pethick C. J., Lamb F. K., 1977, *ApJ*, 217, 578
- Goodson A. P., Winglee R. M., Boehm K., 1997, *ApJ*, 489, 199
- Hayashi M. R., Shibata K., Matsumoto R., 1996, *ApJ*, 468, L37+
- Illarionov A. F., Sunyaev R. A., 1975, *A&A*, 39, 185
- Königl A., 1991, *ApJ*, 370, L39
- Landstreet J. D., Mathys G., 2000, *A&A*, 359, 213
- Lovelace R. V. E., Romanova M. M., Bisnovaty-Kogan G. S., 1995, *MNRAS*, 275, 244
- Lovelace R. V. E., Romanova M. M., Bisnovaty-Kogan G. S., 1999, *ApJ*, 514, 368
- Matt S., Pudritz R. E., 2004, *ApJ*, 607, L43
- Matt S., Pudritz R. E., 2005, *ApJ*, 632, L135
- Matt S. P., Pinzón G., de la Reza R., Greene T. P., 2010, *ApJ*, 714, 989
- Miller K. A., Stone J. M., 1997, *ApJ*, 489, 890
- Mineshige S., Rees M. J., Fabian A. C., 1991, *MNRAS*, 251, 555
- Pearson K. J., Horne K., Skidmore W., 2003, *MNRAS*, 338, 1067
- Perna R., Bozzo E., Stella L., 2006, *ApJ*, 639, 363
- Pringle J. E., Rees M. J., 1972, *A&A*, 21, 1
- Romanova M. M., Ustyugova G. V., Koldoba A. V., Lovelace R. V. E., 2004, *ApJ*, 616, L151
- Shakura N. I., Sunyaev R. A., 1973, *A&A*, 24, 337
- Sipos N., Abraham P., Acosta-Pulido J., Juhász A., Kóspál Á., Kun M., Moór A., Setiawan J., 2009, *A&A*, 507, 881

Spruit H. C., Taam R. E., 1993, *ApJ*, 402, 593

Stępień K., 2000, *A&A*, 353, 227

Stępień K., Landstreet J. D., 2002, *A&A*, 384, 554

Sunyaev R. A., Shakura N. I., 1977, *Pisma Astronomicheskii Zhurnal*, 3, 262

Ustyugova G. V., Koldoba A. V., Romanova M. M., Lovelace R. V. E., 2006, *ApJ*, 646, 304



---

## Chapter 4

---

# Accretion Discs Trapped Near Corotation

Caroline R. D'Angelo and Hendrik C. Spruit

*to be submitted to MNRAS*

Discs accreting onto the magnetosphere of a rotating star can end up in a 'trapped' state, in which the inner edge of the disc stays near the corotation radius, even at low accretion rates. The accretion in these trapped states can be steady or cyclic. The conditions for occurrence of such cycles, their amplitudes, cycle periods, and their effect on the average torque on the accreting star are investigated. Two forms of cycle are found, one of them corresponding to those proposed by Sunyaev and Shakura (1976) and Spruit and Taam (1993). The presence of cycles depends on the details of the interaction between disc and magnetosphere, in particular the width of the region of interaction. Observational evidence of such cycles would provide important clues on the physics of magnetospheric accretion. Recent observations of cyclic and other unusual variability in T Tauri stars (EXors) and X-ray binaries are discussed in this context.

## 4.1 INTRODUCTION

Many accreting stars show evidence of the effects of a strong stellar magnetic field regulating the accretion flow onto the star. Accreting X-ray pulsars, for example, show flux modulation on timescales between  $\sim 10^{-3} - 10^2$  seconds, which is attributed to the magnetic pole sweeping through our line of sight, illuminated by matter accreting along field lines (Davidson & Ostriker 1973). In some pulsars, this probe of the star's period has shown an evolution in the spin period of the star in time (e.g. Bildsten et al. 1997), which is attributed to the interaction with the surrounding material. On the other end of the energy scale, T Tauri stars also often have strong magnetic fields (up to 1-2 kG), and show some evidence that their period is regulated by the disc-field interaction (Getman et al. 2008).

From the earliest studies of stellar accretion researchers recognized that a strong magnetic field could substantially influence an accretion disc surrounding the star. Pringle & Rees (1972) estimated the 'magnetospheric radius' of the disc – the radius at which the magnetic field would truncate the disc – by equating the ram pressure of free-falling gas to the magnetic pressure of the field. The inner radius of the disc will thus be determined by the magnetic field strength (assumed dipolar with a magnetic moment  $\mu \equiv B_S r_*^3$ ), stellar mass and the accretion rate onto the star:  $r_m^{7/2} \propto \mu^2 M_*^{-1/2} \dot{m}^{-1}$ . The infalling material will then add its angular momentum to the star, causing it to spin faster. Illarionov & Sunyaev (1975) noted that if the magnetospheric radius extends beyond the corotation radius ( $r_c \equiv (GM_*)^{1/3} \Omega_*^{-3/2}$ , where the Keplerian frequency of the disc equals the star's rotation frequency), the stellar magnetic field will spin faster than the gas at the inner edge of the disc. This is generally called the 'propeller' regime. A standard view expressed in the literature is that in this case the accreting mass is expelled from the system (see below).

Analytic (Aly & Kuijpers 1990; Lovelace et al. 1995; Matt et al. 2010) and numerical (Hayashi et al. 1996; Miller & Stone 1997; Goodson et al. 1997; Romanova et al. 2008) has demonstrated that embedded field lines in the disc will rapidly open, decoupling the majority of the disc from the star, in contrast with what has been assumed in most of the early literature. The small radial extent of the interaction between the disc and the field has led some authors to question whether the disc is able to regulate the spin rate of the star altogether (Matt & Pudritz 2005; Matt et al. 2010).

A number of persistent X-ray pulsars show spin-down as well as spin-up (e.g. Bildsten et al. 1997), or a rate of spin-up much lower than expected based on the accretion rate. In addition, many sources show hysteresis, where the luminosity differs between spin-up and spin-down phases (Camero-Arranz et al. 2010), or even anti-correlates with spin-down (Chakrabarty et al. 1997). Finally, in persistent sources that show both spin-up and spin-down, the magnitude of  $|\dot{\nu}|$  often stays nearly constant when the torque changes sign, which is not naturally explained in a model where the torque scales as a power of  $\dot{m}$ .

More recently, two transient X-ray pulsars were observed to undergo brief weak outbursts (lasting about 6-7 days) followed by a short period of quiescence (Heinke et al. 2010; Hartman et al. 2010). The outburst recurrence time (on the order of a month in both sources)

is too short to be naturally explained by the ionization instability model (e.g. Lasota 2001), and Hartman et al. (2010) have suggested (based on the total outburst luminosity) that mass could remain stored in the disc when the accretion rate onto the star drops by at least 3-4 orders of magnitude. This explanation is inconsistent with the standard relation between accretion rate and inner radius, in which  $r_{\text{in}} \propto \dot{m}^{2/7}$ , so that a change of  $10^4$  in accretion rate corresponds to an increase of  $\sim 10 \times$  in  $r_{\text{in}}$ . In one of these sources, NGC 6440 X-2, Patruno et al. (2010) recently reported the detection of a strong QPO at 1Hz. A similar QPO was previously detected in SAX J1808.4-3658 (Patruno et al. 2009). This QPO period is of the order of  $10^{-2} - 10^{-1}$  times the viscous timescale at the the corotation radius  $r_c$ .

Similar outburst time scales, in units of the viscous time scale, are seen in a class of young stars called ‘EXors’. These stars typically show episodic changes in luminosity (of between 2-5 magnitudes) on timescales of a few years. The variability timescale implies accretion rate variability in the inner regions of the accretion disc, where it interacts with the magnetic field.

Together, these puzzling observations suggest that significant physics is missing in current interpretations of the phenomena seen in accreting magnetospheric systems.

#### 4.1.1 Accretion at a centrifugal barrier

One of the things missing in these interpretations is the insight that mass prevented from accreting by the presence of a ‘centrifugal barrier’ does not necessarily have to leave the system at all. In other words, that mass transferred from a binary companion onto a spinning magnetosphere does not have to be ‘propellered’ out.

This was already noted by (Sunyaev & Shakura 1977) and (Spruit & Taam 1993). Without mass loss, accretion on the magnetosphere can just be *cyclic*, with periods of accumulation outside the corotation radius alternating with accreting phases. Mass loss in a magnetically driven wind may happen as well, but this bit of (still poorly known) physics is separate from the effect of a centrifugal barrier on a viscous disc. The problem of disc responding to the torque exerted at its inner edge by a spinning magnetosphere has a well-defined solution within the standard thin viscous disc formalism without mass loss.

This is the problem we have studied in D’Angelo & Spruit (2010a) and D’Angelo & Spruit 2010b (hereafter DS10a and DS10b respectively [chapters 2 and 3]). There we classified the properties of time dependent solutions of the thin disc diffusion equation with a magnetic torque acting at its inner edge (DS10a), and studied the long term evolution of discs with such torques, including the spindown of the star (DS 10b).

Due to the magnetic torques transporting angular momentum outward, the density profile of the disc is altered substantially. The disc remains truncated only slightly outside  $r_c$  even when the accretion rate declines by several orders of magnitude. We found that the formation of a dead disc often results in the instability described by Spruit & Taam (1993), which we suggested could be operating in EXors as in SAX J1808.4-3658 and NGC 6440 X-2. In the instability, the disc is initially truncated outside  $r_c$  and accretion is suppressed, causing

material to build up in the inner regions of the disc. Eventually, the surface density in the disc becomes high enough to overcome the centrifugal barrier and accrete onto the star. Once the reservoir is emptied, the disc again moves outside  $r_c$  and the cycle begins again. In that paper we concluded that the presence of the instability depended on the mean accretion rate,  $\dot{m}$  and the details of the disc-field interaction.

The modes of accretion of a viscous disc on a rotating magnetosphere can be classified in three states, all of which have a different appearance and effect on the star's evolution. We explicitly neglect the possibility of outflows, so that the disc never crosses into the propeller regime for any  $\dot{m}$ .

The disc state depends on the ratio of the mean accretion rate through the disc to  $\dot{m}_c$ , the accretion rate that puts  $r_{in}$  at  $r_c$ :

1.  $\dot{m} \gg \dot{m}_c$ :  $r_{in} < r_c$ , star spins up
2.  $\dot{m} \simeq \dot{m}_c$ :  $r_{in} \approx r_c$ , star spins either up or down, inner edge stays near corotation while  $\dot{m}$  varies.
3.  $\dot{m} \sim 0$ :  $r_{in} > r_c$ , star spins down, negligible accretion (dead disc).

State ii) can be further divided into cases where accretion takes place in a continuous way, and cases where accretion is cyclic, with bursts of accretion alternating with quiescent phases. The latter case will be the main subject of interest in the following. If there is a long-term imposed accretion rate at the outer edge of the disc, as in a mass transferring binary, dead disc states can occur as part of the cycle, as suggested by Sunyaev & Shakura (1977).

#### 4.1.2 Trapped discs

In DS10b, we turned our attention to the long-term evolution of a viscous disc, and its effect on the spin evolution of the star. This added a new parameter to the problem, the moment of inertia  $I_*$  of the star, and introduced a new characteristic timescale,  $T_{SD}$ , the spin-down timescale of the star.

When initial conditions are chosen such that  $r_{in}$  is initially inside  $r_c$  but moves gradually outward, we found that the evolution of the disc often gets 'stuck' with  $r_{in}$  near corotation, with slowly decreasing accretion rate. The same happens when  $r_{in}$  is initially outside  $r_c$ , but spindown of the star causes  $r_c$  to move out. When it catches up, the following evolution again tends to be one in which the inner edge hovers slightly outside corotation. The outward angular momentum transport due to the magnetic torque is accompanied by low-level accretion onto the star. We called this phenomenon of a disc with inner edge stuck at the corotation radius a 'trapped disc'. It is the intermediate state ii) mentioned above.

The disc does not stay trapped in all cases, however;  $r_{in}$  can also evolve well beyond  $r_c$ , the end result being a 'dead disc': the state iii) above. Whether or not the disc becomes trapped depends on the details of the disc-field interaction (see below) and on the ratio  $T_{visc}/T_{SD}$  (where  $T_{visc}$  is the viscous accretion timescale of the disc measured at  $r_c$ ).

The trapped disc state presents a very different picture from the traditional accreting/propeller view. For one, the small velocity difference between disc and magnetosphere in this state makes significant mass loss unlikely. It also leads to different observational characteristics, in particular modification to the expected relationship between spin-down torque and luminosity, and the appearance of cyclic accretion. These are the focus of this paper.

Accretion in the trapped state can be continuous or cyclic. In DS10b we limited ourselves mostly to parameter regimes that lead to continuous accretion, since the short time scale of the cycles makes it difficult to follow the long-term evolution of the disc. Here we study the cyclic case of trapped discs in more detail, with less emphasis on long-term evolution. In DS10a, we found two forms of cyclic behavior. Their nature and interpretation will be explored in more detail here, addressing also the question how the characteristics of the instability (such as its period and amplitude) change with the model parameters.

When accretion is cyclic, the torque between disc and magnetosphere varies over a cycle; its average over a cycle is what determines the net spindown or spinup torque on the star. In sec. 4.4.4 we address the question how this net torque differs from the steadily accreting case.

In Sec. 4.5 we discuss the results in the context of the various observations mentioned above (persistent X-ray pulsars, the short recurrent outbursts in X-ray pulsars, and the episodic accretion bursts seen in both X-ray pulsars and young stars). We will find there that trapped discs may be related to a number of currently unexplained phenomena seen in magnetospherically accreting sources.

## 4.2 THE MODEL FOR MAGNETOSPHERIC ACCRETION

We briefly summarize the characteristics of our model for magnetospheric accretion, reviewing our description of the disc-field interaction and how this alters the structure of the disc when  $r_{\text{in}} > r_c$ . For a compact description see DS10b; for more detail and our numerical implementation, see DS10a.

As mentioned above, the interaction between an accretion disc and magnetic field is likely confined to the innermost regions of the disc, so that most of the disc is shielded from the field. The coupling between the disc and the field distorts the field lines by differential rotation, which generates a toroidal field component, and exerts a magnetic torque on the disc. In a very short time, the field lines become sufficiently distorted that they inflate and open, which can temporarily sever the connection between the field and disc, before reconnection events reestablish connection with the star. As a result, the variations in the magnetic field associated with the magnetosphere interaction will take place on timescales of order the rotation period of the star,  $P_*$  (Aly 1985; Hayashi et al. 1996; Miller & Stone 1997; Goodson et al. 1997) much shorter than the cycle times, which take place on a variety of viscous time scales in the disc.

It is sufficient to adopt a time-averaged value for the strength of the generated toroidal

field component,  $\eta \equiv B_\phi/B_z$  and the width of the interaction region  $\Delta r/r_{\text{in}}$ . The size of the interaction region is unknown, so it is a free parameter in our model; we assume only that  $\Delta r/r < 1$ , and explore values in the range suggested by numerical simulations.

When the inner edge of the disc  $r_{\text{in}}$  is outside corotation  $r_c$ , a magnetic torque  $T_B$  acts at the inner edge. The condition that this torque is transmitted outward by the viscous stress yields:

$$3\pi\nu\Sigma(r_{\text{in}})r^2\Omega_K(r_{\text{in}}) = T_B. \quad (4.1)$$

This yields a boundary condition on the surface density at  $r_{\text{in}}$ . When  $r_{\text{in}}$  is inside  $r_c$  however, the viscous torque and the surface density at  $r_{\text{in}}$  vanish: the standard case of a viscous disc accreting on a slowly rotating object applies. The viscous torque at  $r_{\text{in}}$  thus varies rapidly over the transition width  $\Delta r$  around  $r_c$ . This can be taken into account in (4.1) by making  $T_B$  a function of  $r_{\text{in}}$ ,

$$T_B = y_\Sigma(r_{\text{in}})T_0, \quad (4.2)$$

where  $y_\Sigma$  is a suitably steep function with the property that it varies from 0 to 1 over the width  $\Delta r$ :  $y_\Sigma \rightarrow 0$  for  $r_c - r_{\text{in}} \gg \Delta r$ ,  $y_\Sigma \rightarrow 1$  for  $r_{\text{in}} - r_c \gg \Delta r$ . For  $T_0$  we approximate the field strength at  $r_{\text{in}}$  as that of the star's dipole component, so the magnetic torque exerted by the field is

$$T_0 = \eta\mu^2\Delta r/r^4, \quad (4.3)$$

where  $\mu$  is the star's dipole moment and  $\eta$  a coefficient of order unity. For numerical reasons, it is important that  $y_\Sigma$  be a smooth function, we use a  $1 + \tanh$  -profile of width  $\Delta r$ .

For the viscosity we use a fixed radial dependence,  $\nu = k_\nu r^{1/2}$ , corresponding to an  $\alpha$ -disc of constant  $\alpha$  and aspect ratio  $H/r$ .

When  $r_{\text{in}} < r_c$  the disc can accrete onto the star. The position of the inner edge of the disc is then related to the accretion rate. We use a standard estimate (e.g. Spruit & Taam (1993)), which equates the magnetic torque with the torque needed to keep the accreting mass corotating with the star. It can be written as

$$\dot{m}_a = \frac{\eta\mu^2}{4\Omega_* r_{\text{in}}^5} \quad (4.4)$$

(the subscript <sub>a</sub> standing for 'only in the case of accretion'). It holds only for  $r_{\text{in}} < r_c$ . For  $r_{\text{in}} > r_c$ , the accretion rate drops to zero due to the centrifugal barrier. The relation between  $r_{\text{in}}$  and  $\dot{m}$  thus also changes steeply around  $r_c$ . This is another critical element that needs to be taken into account. We incorporate it by writing:

$$\dot{m}_{\text{co}}(r_{\text{in}}) = y_m(r_{\text{in}})\dot{m}_a(r_{\text{in}}) \quad (4.5)$$

where  $y_m(r_{\text{in}})$  describes the steep variation in the transition zone, and  $\dot{m}_{\text{co}}$  is the mass flux measured in frame comoving with the inner edge of the disc:

$$\dot{m}_{\text{co}} = \dot{m} + 2\pi r_{\text{in}}\Sigma(r_{\text{in}})\dot{r}_{\text{in}}, \quad (4.6)$$

where  $\dot{r}_{\text{in}}$  is the rate of change of the inner edge radius (the distinction between  $\dot{m}$  and  $\dot{m}_{\text{co}}$  was a crucial point missing in the formulation of ST93). For the ‘connecting function’  $y_m$ , with limiting values 1 inside corotation and 0 outside, we again use a smooth tanh- function. The width of this transition must be of the same order as the transition width  $\Delta r$  introduced above, but the physics determining it is rather different, so we keep it as a separate parameter  $\Delta r_2$ , and explore it independently.

Eq. (4.4) and (4.6) define an equation for  $r_{\text{in}}(t)$ . Together with the standard thin disc diffusion equation, we have a set of equations, second order in time and space, for  $\Sigma$  and  $r_{\text{in}}$ . The equations are stiff inside corotation since one of the time derivatives (for  $r_{\text{in}}$ ) disappears. A numerical method appropriate for this circumstance has to be used.

The steady-state case,  $\partial_t = 0$ , is illustrative. The solution of the thin disc diffusion equation can be written as

$$3\pi\nu\Sigma = \frac{T_B}{\Omega(r_{\text{in}})r_{\text{in}}^2} \left(\frac{r_{\text{in}}}{r}\right)^{1/2} + \dot{m} \left[1 - \left(\frac{r_{\text{in}}}{r}\right)^{1/2}\right], \quad (4.7)$$

where  $T_B$  is given by (4.2) and  $\dot{m}$  by (4.4, 4.6).

For  $r_{\text{in}}$  well outside corotation ( $r_{\text{in}} - r_c \gg \Delta r$ ),  $\dot{m}$  vanishes and we have a dead disc. The surface density is then determined by the first term on the RHS. The steady outward flux of angular momentum in this case has to be taken up by a sink at some larger distance, otherwise the disc could not be stationary as assumed. This sink can be the orbital angular momentum of a companion star, or the disc can be approximated as infinite. The latter is a good approximation for changes in the inner regions of the disc, if time scales short compared with the viscous evolution of the outer disc are considered.

#### 4.2.1 Characteristic numbers

We choose  $r_c$  (the star’s initial co-rotation radius) for our length scale, and define  $t_c \equiv \nu/r_c^2$ , the viscous accretion timescale at  $r_c$  as our characteristic timescale. We adopt  $\nu_0 \equiv \alpha(H/r)^2 = 10^{-3}$  for the dimensionless viscosity parameter, and  $\eta = 0.1$  as the relative size of the  $B_\phi$  component. We also define a characteristic accretion rate  $\dot{m}_c$ :

$$\dot{m}_c \equiv \frac{\eta\mu^2}{4\Omega_*r_c^5}, \quad (4.8)$$

This is the accretion rate in (4.4) that would put the magnetospheric radius at  $r_c$ . For a typical ms-pulsar:

$$\dot{m}_c = 10^{-14} M_\odot \text{yr}^{-1} \left(\frac{M_*}{1.4M_\odot}\right)^{-5/3} \left(\frac{B_s}{10^8 \text{G}}\right)^2 \left(\frac{R_*}{10^6 \text{cm}}\right)^6 \left(\frac{P_*}{100 \text{ms}}\right)^{-7/3}, \quad (4.9)$$

while for the case of a T Tauri star disc,

$$\dot{m}_c = 1.4 \times 10^{-9} M_\odot \text{yr}^{-1} \left( \frac{M_*}{0.5 M_\odot} \right)^{-5/3} \left( \frac{B_s}{1500 \text{G}} \right)^2 \left( \frac{R_*}{2 R_\odot} \right)^6 \left( \frac{P_*}{7 \text{d}} \right)^{-7/3}. \quad (4.10)$$

To characterize the spin change of the star, we adopt a characteristic torque based on the definition for  $\dot{m}_c$ :

$$\dot{J}_c \equiv \dot{m}_c (GM_* r_c)^{1/2}, \quad (4.11)$$

which is the rate at which angular momentum is added by mass accreting at  $\dot{m}_c$ . This definition is somewhat arbitrary, but has the advantage of being independent of  $\Delta r/r_{\text{in}}$  and  $\Delta r_2/r_{\text{in}}$ .

### 4.3 SPIN EVOLUTION AND PHYSICAL PROPERTIES OF A TRAPPED DISC

#### 4.3.1 Observability of trapped discs

The density structure of a trapped disc deviates from the standard accreting disc. In a dead disc (the limiting case of a trapped disc), the accretion rate is zero and the surface density profile is determined by the rate of angular momentum transport from the star to the disc.

Provided that the thin disc approximation remains a good description for the disc, so that the energy generated by viscous turbulence is dissipated locally the temperature of the dead disc can be estimated (Sunyaev & Shakura 1977) from the viscous dissipation.

The local energy dissipation rate in a viscous disc is:

$$Q^+ = v\Sigma(r\Omega'_K)^2 = \frac{9}{4}v\Sigma\Omega_K^2. \quad (4.12)$$

Near the inner edge of the disc where most of the energy is dissipated, the disc can be approximated as steady, so eq. (4.7) applies. For a dead disc ( $\dot{m} = 0$  and  $r_{\text{in}}$  well outside corotation),  $T_B = T_0$ , and the surface density as a function of  $r$  is given by

$$v\Sigma = \frac{1}{3\pi} \left( \frac{T_0}{\Omega r^2} \right)_{r=r_i} \left( \frac{r_i}{r} \right)^{1/2}. \quad (4.13)$$

If this energy is radiated locally as a blackbody, then

$$Q^+ = Q^- = 2\sigma T_s^4, \quad (4.14)$$

where  $T_s$  is the surface temperature of the disc as a function of radius (the factor 2 arising because the energy is lost from the two surfaces of the disc), and  $\sigma_B$  the Stefan-Boltzmann constant. With (4.3,4.13) this yields

$$\sigma_B T_s^4 = \frac{3}{8\pi} \eta \mu^2 \left( \frac{\Delta r}{\Omega r^6} \right)_{r=r_1} \frac{GM}{r^3} \left( \frac{r_1}{r} \right)^{1/2}, \quad (4.15)$$

which varies with  $r$  as  $r^{-7/2}$ , showing that most of the energy is radiated away near the inner edge by the mass piled up at the ‘centrifugal barrier’. If  $v \sim r^{1/2}$  as we assume in the calculations to follow, (4.15) implies  $T_s \sim r^{-1}$ .

With the nominal object parameters used in 4.2.1, a dead disc with its inner edge near corotation will have a maximum temperature, at  $r_{\text{in}}$ , of  $T_s \approx 300\text{K}$  in the case of a T Tauri star and  $T_s \approx 20000\text{K}$  for a ms X-ray pulsar. This estimate, however, only includes the internal energy dissipation in the disc. Both in protostars and X-ray binaries, reprocessing of radiation from the central object by the disc usually dominates over internal dissipation, especially at larger distances from the centre. It might be possible to identify a disc as belonging to the dead class with more detailed information on the spectral energy distribution

### 4.3.2 Accretion rate and angular momentum exchange with the star

The interaction between the magnetic field and the disc outside  $r_c$  removes angular momentum from the star, while the gas accreting onto the star spins it up. The net torque on the star is thus a function of both the average accretion rate through the disc and the location of  $r_{\text{in}}$ . It is given by:

$$J = \dot{m}(GM_* r_{\text{in}})^{1/2} - \frac{\eta \mu^2 \Delta r}{r_{\text{in}}^3 r_{\text{in}}} y_\Sigma, \quad (4.16)$$

where the first term gives the spin-up from accretion and the second term is the spin-down from the disc-field interaction. (The spin-down torque vanishes for  $r_{\text{in}} < r_c$ , which we impose with the  $y_\Sigma$  smoothing function.) In sec. 4.2 we defined the relationship between  $\dot{m}$  and  $r_{\text{in}}$ , so that  $J$  will just be a function of  $\dot{m}$ ,  $\Delta r$  and  $\Delta r_2/r_{\text{in}}$ . In the rest of the section we illustrate the implications of this relationship for the spin-evolution of the star.

Fig. 4.1 shows the relationship between  $r_{\text{in}}$  and  $\dot{m}$  as  $\Delta r_2/r_{\text{in}}$  changes, to demonstrate how the disc can become trapped. The three bottom curves show  $r_{\text{in}}$  as a function of  $\dot{m}$  for  $\Delta r_2/r_{\text{in}} = 0.05$  (solid blue), 0.1 (dashed green) and 0.5 (triple-dot dashed red). At high accretion rates ( $r_{\text{in}} < r_c$ ), all three curves scale as  $r_{\text{in}} \propto \dot{m}^{-1/5}$ . However as  $\dot{m}$  decreases the solutions quickly diverge. For small  $\Delta r_2/r_{\text{in}}$  ( $\Delta r_2/r_{\text{in}} = [0.05, 0.1]$ ), there is a knee in the solution around  $r_{\text{in}} = r_c$ , and  $r_{\text{in}}$  increases much more slowly as  $\dot{m}$  decreases, so that  $r_{\text{in}}$  remains close to  $r_c$  even when  $\dot{m}$  has decreases by several orders of magnitude. For  $\Delta r_2/r_{\text{in}} = 0.5$ , the knee straightens out since the transition from accreting to non-accreting solutions is much more gradual.

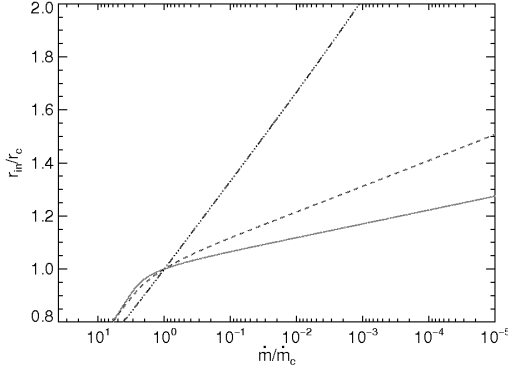


**Figure 4.1:** Change in  $r_{\text{in}}$  as a function of  $\dot{m}$  for different  $\Delta r_2/r_{\text{in}}$ . Blue solid curve:  $\Delta r_2/r_{\text{in}} = 0.05$ , green dashed curve:  $\Delta r_2/r_{\text{in}} = 0.1$ , red triple-dot-dashed curve:  $\Delta r_2/r_{\text{in}} = 0.5$

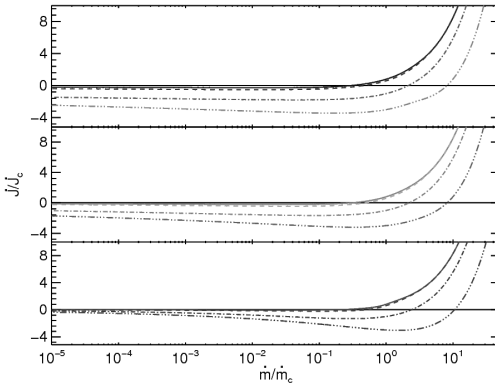


**Figure 4.2:** Change in net torque on the star as a function of  $\dot{m}$  for different values of  $\Delta r/r_{\text{in}}$  and  $\Delta r_2/r_{\text{in}}$ . From top to bottom, the individual panels correspond to  $\Delta r_2/r_{\text{in}} = [0.05, 0.1, 0.5]$ . The different patterned lines correspond to different values of  $\Delta r/r_{\text{in}}$ : 0.05 (solid), 0.1 (dashed), 0.5 (dot-dashed), and 1.0 (triple-dot dashed). The vertical dashed line shows the accretion rate for which  $r_{\text{in}} = 1.3r_*$ .

Fig. 4.2 shows the dependence of the net torque  $J$  on the star on accretion rate  $\dot{m}$ , for different values of  $[\Delta r, \Delta r_2]$ . At high accretion rates, the disc is strongly accreting, star spins up with the torque  $J \propto \dot{m}^{9/10}$ . At lower accretion rates, the interaction region moves outside  $r_c$ , causing the net angular momentum exchange to change sign, and spinning the star down. As the accretion rate decreases further and  $r_{\text{in}}$  moves increasingly far outside  $r_c$  into the effectively ‘dead’ state, the spindown torque decreases because of the decline of the star’s field strength with distance.

The detailed shape of the curves in figs 4.1,4.2 reflects the (tanh-) shape of the transition functions  $y_\Sigma$  and  $y_m$  we have used.

## 4.4 CYCLIC ACCRETION

In DS10b we studied parameter combinations ( $\dot{m}$ ,  $\Delta r$ ,  $\Delta r_2$ ) that avoided the cyclic behavior, since these complicate the study of the long-term evolution of the disc-star system. The possibility of identifying cycles like those seen in DS10a in the observations is an interesting prospect, however. Cycles would provide a direct observational connection with the trapped disc state phenomenon identified here as a likely consequence of the disc-magnetosphere interaction. The shape of the cycles and circumstances of their occurrence would provide important clues about the details of the interaction region, which we have simply parametrized with the two transition widths  $\Delta r$  (for the torque) and  $\Delta r_2$  (for the mass flux).

In this section we expand the analysis in DS10a to investigate the properties of the instability more quantitatively. In Sec. 4.4.1, we investigate the presence of the instability as a function of the system parameters. In sec. 4.4.2 we show how the period and amplitude vary with  $\dot{m}$ ,  $\Delta r/r_{\text{in}}$  and  $\Delta r_2/r_{\text{in}}$ . In sec. 4.4.4 we investigate how the presence of cycles will change the spin evolution of the star in comparison to a steadily accreting disc. Finally, in sec. 4.4.5 we investigate the appearance of cycles for non-steady accretion in systems in which the star's spin is evolving.

### 4.4.1 Parameter map of the instability

In DS10a we showed that the disc instability depends on  $\Delta r/r_{\text{in}}$ ,  $\Delta r_2/r_{\text{in}}$  and  $\dot{m}$ , and ran simulations in the parameter spaces  $[\Delta r, \dot{m}]$  and  $[\Delta r_2, \dot{m}]$  to determine when the instability occurred. Additional simulations of trapped discs at very low accretion rates show the instability is present for a larger parameter space than we investigated in DS10a, so here we have repeated our analysis on a larger parameter space.

As in DS10a, we keep the rotation rate of the star fixed, since the time scale of the cycles is much shorter than the time scale of spin changes of the star. The corotation radius is then a fixed distance, and defines a unit of mass flux,  $\dot{m}_c$  given in sec. 4.2.1. As unit of length we can use  $r_c$ , and as unit of time the viscous time scale  $r_c^2/\nu(r_c)$ . Apart from a parameter specifying the radial dependence of  $\nu$ , which we keep fixed throughout, the problem is then defined by the three dimensionless parameters  $\Delta r/r_{\text{in}}$ ,  $\Delta r_2/r_{\text{in}}$ , and  $\dot{m}/\dot{m}_c$ .

It turns out (discussed below) that this 3-dimensional parameter space contains 2 nearly separate regions of instability, which can be characterized using a few two 2-dimensional slices instead of having to scan the entire space.

In comparison to DS10a, the present results survey a larger parameter range at higher resolution for all three variables. The individual simulations at higher spatial and time resolution. In total we ran 1545 simulations: 855 in a 2-dimensional slice  $[\Delta r, \dot{m}]$ , and 690 in a  $[\Delta r_2, \dot{m}]$  slice. To be determined are the regions in parameter space where cyclic behavior occurs, as well as how the characteristics of the cycles (such as period, amplitude and appearance) change as a function of the parameters.

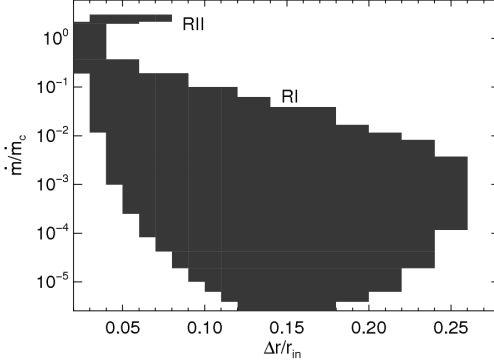


**Figure 4.3:** Instability map in  $[\dot{m}, \Delta r/r_{in}]$ , keeping  $\Delta r_2/r_{in} = 0.014$  fixed. The shaded regions denote unstable simulations. The instability occurs in two nearly disconnected regions of the parameter space. In this slice, one (RI) is present over a large range in  $\Delta r/r_{in}$  and  $\dot{m}$ , the other in a small region in  $\Delta r/r_{in}$  at  $\dot{m} \simeq \dot{m}_c$  (RII).

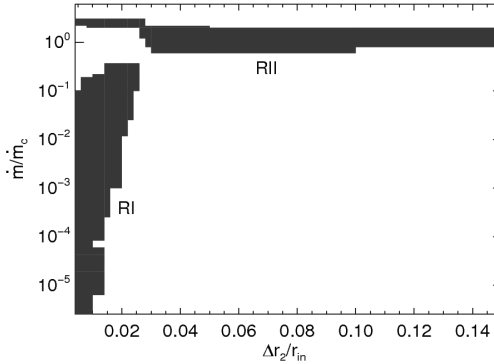


**Figure 4.4:** Instability map in  $[\dot{m}, \Delta r_2/r_{in}]$ , keeping  $\Delta r/r_{in}$  fixed at 0.05, with shaded areas denoting unstable cases. The two regions of the instability are more clearly separated than in the slice of fig. 4.3. RI only occurs for very small values of  $\Delta r_2/r_{in}$  while RII occurs around  $\dot{m} \simeq \dot{m}_c$ , over a large range in  $\Delta r_2/r_{in}$ , extending beyond the region of the graph.

Figures 4.3 and 4.4 show the unstable regions across  $[\Delta r, \dot{m}]$  and  $[\Delta r_2, \dot{m}]$ . In fig. 4.3, we kept  $\Delta r_2/r_{in}$  fixed at 0.014 and surveyed the range  $\Delta r/r_{in} = [0.02, 0.28]$  and  $\dot{m}/\dot{m}_c = [10^{-6}, 6]$ . Figure 4.4 surveys the same range in  $\dot{m}$  and the range  $\Delta r_2/r_{in} = [0.004, 0.14]$ , keeping  $\Delta r/r_{in}$  fixed at 0.05. The figures (especially figure 4.4) show that there are two distinct regions in which the instability is active, which we call RI and RII.

The instability has different properties in the two regions: the period, shape and amplitude of the outburst are all qualitatively different, as we demonstrate further below.

The first instability region (RI) appears in a small range of  $\Delta r_2/r_{in} = [0.002, 0.03]$ , but over a considerable range in  $\Delta r/r_{in}$  (up to 0.25) and five orders of magnitude in accretion rate:  $\dot{m}/\dot{m}_c \simeq [10^{-6}, 10^{-1}]$ . This instability region was the focus of our study in DS10a, where we discussed in detail the appearance of the instability. (The phenomena summarized below can

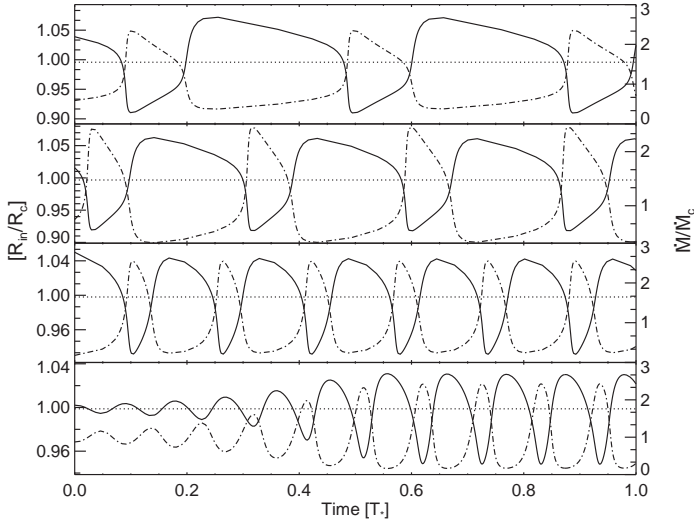


**Figure 4.5:** The accretion instability in RII, the second instability region for  $\Delta r/r_{\text{in}} = 0.05$  and  $\dot{m} = 1.05\dot{m}_c$ . The instability only manifests around  $\dot{m} \simeq \dot{m}_c$ , but occurs over a large range in  $\Delta r_2/r_{\text{in}}$ , the transition length between accreting and non-accreting states. Unlike the RI instability, the accretion rate never drops to zero during the quiescent phase of the instability.

be seen in figs. 4,5 and 6 of that paper.) The instability is characterized by large amplitude outbursts followed by long periods of quiescence in which the accretion rate drops to zero. The duty cycle for the instability depends on all three parameters, decreasing significantly as the mean accretion rate drops (and mass takes longer to accumulate to power another cycle). The outburst profile generally takes the shape of a relaxation oscillator, with an initial accretion peak followed by a tail of much lower amplitude accretion. Additionally, during the long phase of the outburst suboscillations sometimes appear in the accretion profile. These suboscillations have a much higher frequency than the overall burst, and appear to be the second instability (RII) superimposed on the outburst while the mean accretion rate onto the star is temporarily higher. As the mean accretion rate is decreased, the outburst becomes shorter and shorter, until finally it simply appears as a single spike of accretion followed by a long period of quiescence.

The second instability region (RII) occurs only around  $\dot{m}/\dot{m}_c \simeq 1$ , in a relatively small range of  $\Delta r/r_{\text{in}} = [0.01, 0.07]$ , but over a large range in  $\Delta r_2/r_{\text{in}}$ . (We have truncated the figure off at  $\Delta r_2/r_{\text{in}}$  to make RI more prominent, but additional simulations show that the instability continues to larger values of  $\Delta r_2/r_{\text{in}}$ , up to at least 0.4). Fig 4.5 shows four sample simulations for RII taken from the output of our  $[\Delta r_2, \dot{m}]$  set of simulations. The

simulations all have  $\dot{m} = 1.05\dot{m}_c$  and  $\Delta r/r_{\text{in}} = 0.05$ , with increasing  $\Delta r_2/r_{\text{in}}$  from bottom to top:  $\Delta r_2/r_{\text{in}} = [0.028, 0.05, 0.1, 0.15]$ . The instability has a different character from the RI instability. The quiescent phase is absent and there is always some accretion onto the star, even during the low phase of the cycle. The shape of the instability is also significantly different from the RI instability: there is no additional higher frequency oscillation, and the outburst profile is smoother. In particular, the initial spike of accretion seen in RI is completely absent. The profile is nearly sinusoidal for small values of  $\Delta r_2/r_{\text{in}}$  (although the duty-cycle is always less than 0.5). For larger values of  $\Delta r_2/r_{\text{in}}$ , the outburst is characterized by a rapid rise, followed by a decaying plateau and then rapid decline to the low phase of the cycle.

#### 4.4.2 Period and Amplitude of Instability

We can use our high resolution survey of the instability parameter space to study quantitatively how the properties of the instability change as a function of the different parameters. This allows us to see the differences between the RI and RII instability regions more clearly, and better understand how the instability operates. It also allows us to make more general predictions for the appearance of the instability that can be tested against observations.

To measure the period of the instability we autocorrelate the output of each simulation, and take the first peak in the autocorrelation. All our simulations take as initial conditions the stable solution given by (4.7) that then becomes unstable. However, the instability generally takes some time to reach a stable period and amplitude, which varies significantly between simulations. This introduces some error in the estimate of the period (particularly in RII, where the instability takes longer to emerge), which is reflected in the figures below.

Figs. 4.6 and 4.7 show the instability period [top] and amplitude [bottom] as a function of accretion rate for each unstable simulation in figs. 4.3 and 4.4 respectively. Each individual curve represents a different value for  $\Delta r/r_{\text{in}}$  or  $\Delta r_2/r_{\text{in}}$ , with the colours evolving from purple (smallest parameter value) to red (largest). In the top panels, the gaps in the curves denote stable cases. In the bottom panels, dashed  $y = x$  line shows the mean accretion rate for each simulation.

Some general properties of the period and amplitude of the outburst are valid for both for RI (low  $\dot{m}$ ; cf. sec. 4.4.1) and RII (high  $\dot{m}$ ). The period of the instability shows an approximately power-law dependence on accretion rate, with an index independent of  $\Delta r/r_{\text{in}}$  and  $\Delta r_2/r_{\text{in}}$ . It also varies strongly with both  $\Delta r/r_{\text{in}}$  and  $\Delta r_2/r_{\text{in}}$ . The period scales directly with  $\Delta r/r_{\text{in}}$ . It shows the opposite trend for  $\Delta r_2/r_{\text{in}}$ , decreasing as  $\Delta r_2/r_{\text{in}}$  increases. On the other hand, the amplitude of the outburst is nearly independent of the mean accretion rate onto the star for a given  $\Delta r/r_{\text{in}}$  or  $\Delta r_2/r_{\text{in}}$ , as is seen in the bottom panel of figs. 4.6 and 4.7. Rather than producing a weaker outburst, at low  $\dot{m}$  the duration of the low phase of the outburst increases as mass accumulates in the disc.

This result demonstrates that the details of the outburst, apart from the period of the cycle, are largely independent of  $\dot{m}$ , and depend almost only on  $\Delta r/r_{\text{in}}$  and  $\Delta r_2/r_{\text{in}}$ . For large

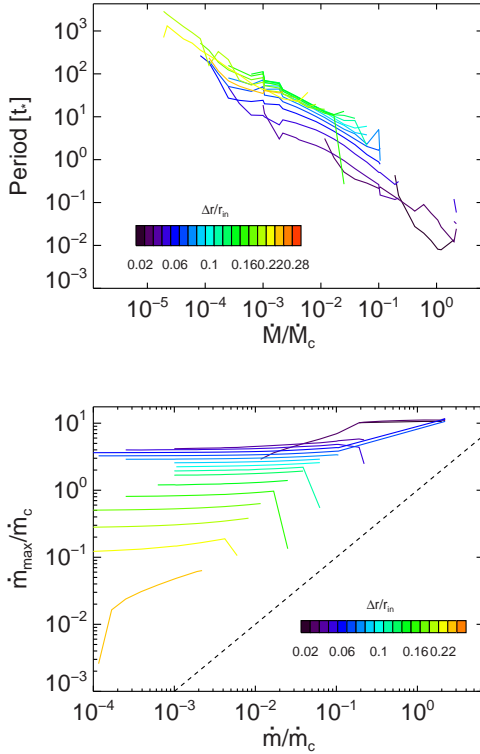


**Figure 4.6:** Period [top] and amplitude [bottom] of the instability as a function of  $\dot{m}/\dot{m}_c$  for the unstable simulations shown in fig. 4.3. The accretion rate spans the range  $\dot{m}[10^{-6}, 6]$  and  $\Delta r/r_{\text{in}} = [0.02, 0.28]$ . The individual curves show different values of  $\Delta r/r_{\text{in}}$ , increasing from black (smallest) to red (largest). In the top panel, the gaps in the curves indicate regions of stable accretion. In the bottom panel, the mean accretion rate is indicated by the dashed  $y = x$  line.

$\Delta r/r_{\text{in}}$  a larger reservoir of mass is available for outburst, so that the duration of each burst increases. Smaller  $\Delta r_2/r_{\text{in}}$  means a more abrupt transition around  $r_c$  from accreting to non-accreting states, so that for the same  $\dot{m}$ , a simulation with small  $\Delta r_2/r_{\text{in}}$  can build up more mass in quiescence than a simulation with larger  $\Delta r_2/r_{\text{in}}$ , leading to a longer outburst phase and longer period.

Although the trends described above apply to both RI and RII, figs. 4.6 and 4.7 clearly demonstrate significant differences between the two regions. In RI the accretion amplitude scales inversely with both  $\Delta r/r_{\text{in}}$  and  $\Delta r_2/r_{\text{in}}$ , so that a large  $\Delta r/r_{\text{in}}$  (or  $\Delta r_2/r_{\text{in}}$ ) corresponds to an outburst with an amplitude up to  $100\times$  smaller than for the same  $\dot{m}$  and smaller  $\Delta r/r_{\text{in}}$  ( $\Delta r_2/r_{\text{in}}$ ). The transition between accreting and non-accreting states becomes more gradual as  $\Delta r/r_{\text{in}}$  ( $\Delta r_2/r_{\text{in}}$ ) increase, so it makes sense that the initial peak of the outburst will be lower for larger  $\Delta r/r_{\text{in}}$  ( $\Delta r_2/r_{\text{in}}$ ). Interestingly, the cycle amplitude scales inversely with  $\Delta r/r_{\text{in}}$ , while the period scales directly. The opposite behaviour is true of  $\Delta r_2/r_{\text{in}}$ . Insta-

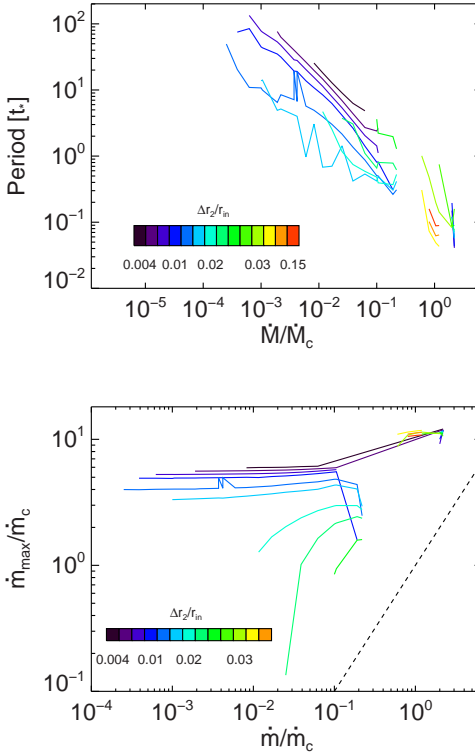


**Figure 4.7:** Period [top] and amplitude [bottom] of the instability as a function of  $\dot{m}/\dot{m}_c$  for the simulations shown in fig. 4.4. The plot is the same as fig. 4.6, replacing  $\Delta r/r_{\text{in}}$  with  $\Delta r_2$ . Each curve shows a different  $\Delta r_2/r_{\text{in}}$  spanning the range  $\Delta r_2/r_{\text{in}} = [0.004, 0.14]$ .

bilities with large  $\Delta r/r_{\text{in}}$  thus have weaker outbursts with a longer duty cycle (compared to an instability with smaller  $\Delta r/r_{\text{in}}$ ), while those with a large  $\Delta r_2/r_{\text{in}}$  instead have weaker outbursts with a shorter period, and less variation between outburst and quiescence.

The RII instability is presently not as well-sampled as RI, but some general characteristics are evident. Most significantly, the amplitude is much larger ( $\sim 40\%$ ) than the largest amplitude RI instability, and the period of oscillation is up to  $\sim 60\%$  shorter. As well, our present results suggest that the outburst amplitude for RII is *independent* of  $\Delta r/r_{\text{in}}$ ,  $\Delta r_2/r_{\text{in}}$ , and  $\dot{m}$ , staying fixed at about  $10\dot{m}/\dot{m}_c$ . Instead of changing in amplitude, as  $\langle \dot{m} \rangle$  decreases (or  $\Delta r_2/r_{\text{in}}$  increases), the period increases as well and the source spends more time in the low phase of the cycle (as is seen in fig. 4.5).

In summary, the instability is very different in RI and RII. In RI, the period of the instability is 1-1000 times longer than the viscous accretion timescale in the inner parts of the disc, and is a strong function of  $\Delta r/r_{\text{in}}$ ,  $\Delta r_2/r_{\text{in}}$  and  $\dot{m}$ . The amplitude and duty cycle

of outburst is a strong function of the detailed disc-field interaction around  $r_c$ , but appears nearly independent of  $\dot{m}$ . The instability occurs over a wide range in  $\dot{m}$  and  $\Delta r/r_{\text{in}}$ , but is confined to small values of  $\Delta r_2/r_{\text{in}}$ , the parameter describing the transition from accretion to ‘centrifugal barrier’. RII is confined to a small range in  $\dot{m}$ , but extends to much larger values of  $\Delta r_2/r_{\text{in}}$ . The cycle period is typically shorter than the viscous timescales in the inner disc ( $P_{\text{cyc}} \sim 10^{-2} - 1t_c$ ), and the amplitude of the outburst is higher than RII. The amplitude of the outburst appears to be independent of  $\dot{m}$ ,  $\Delta r$  and  $\Delta r_2$ , with a typical value of  $\sim 10\dot{m}_c$ .

#### 4.4.3 Interpretation of the instability regions

The instability in region I is easiest to understand; it corresponds to the cyclic accretion predicted by SS73, and studied in ST93. Mass piling up at the centrifugal barrier eventually becomes large enough to ‘open the gate’, and the resulting accretion rate is large enough to push the inner edge of the disc inside corotation for a while, until the reservoir outside corotation has been drained. Unlike a fixed reservoir, the mass in it is not a fixed number, since it depends on the extent of the disc participating in the cycle. This explains the large range in cycle period over which it operates (ST93).

This view of the RI cycle implicitly assumes a sharp transition from accretion to pile-up outside  $r_c$ . If the transition is not sharp, the centrifugal barrier ‘leaky’, the cyclic behavior can be avoided. Mass still piles up outside  $r_c$ , but accretion can be matched by mass leaking through the barrier. This explains why the cycles are limited to low values of  $\Delta r_2/r_{\text{in}}$ . As in ST93, the cycles can start from a steady accreting state in the form a linear instability, which sets in only if the transition is steep enough.

Region II is restricted to accretion rates close to transition to steady accretion. Its restricted range of oscillation periods, a fraction the viscous time scale at  $r_c$  shows that it operates on a region of finite extent, of the order of the width of the transitions  $\Delta r/r_{\text{in}}$ ,  $\Delta r_2/r_{\text{in}}$ . This makes it likely that it is sensitive to the details of the physics in the transition region.

#### 4.4.4 The effect of cycles on angular momentum exchange

The accretion instability can have a significant effect on the spin change with the star. When accretion is stable, the rate of angular momentum exchange between the star and the disc is given by (4.16), and illustrated in fig. 4.2. When accretion proceeds via cycles, the amplitude of the outburst is generally much higher, and the disc spends a significant amount of time in the low phase of the cycle, in which little or no accretion takes place (sec. 4.4.2). This will affect the net angular momentum exchange between the star and the disc: since the low phase of the instability almost always lasts longer than the outburst phase, the star will spin down faster than if accretion proceeded steadily.

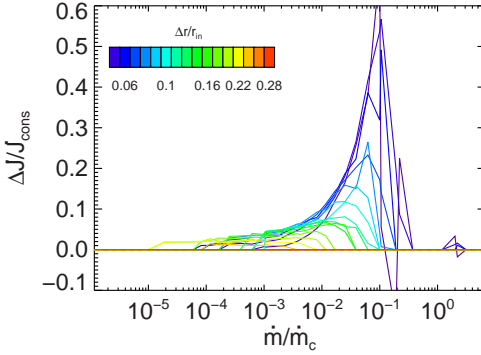


**Figure 4.8:** Effect of cycles on the average torque, as a function of accretion rate. Figure shows the difference between the torque in the unstable initial state before the cycle develops, and the value measured in the fully developed limit cycle. The different curves represent different  $\Delta r/r_{\text{in}}$ , increasing from purple ( $\Delta r = 0.05$ ) to red ( $\Delta r = 0.22$ ).  $\Delta r_2 = 0.014$  is held constant. Cases that do not become cyclic lie on the red line along the x-axis.

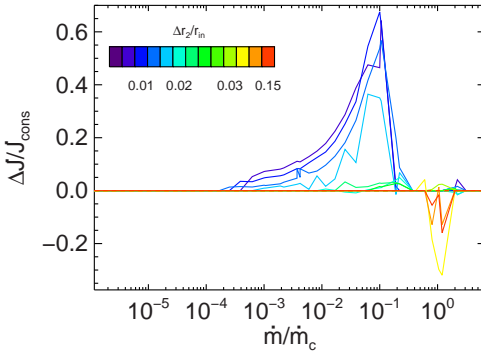


**Figure 4.9:** Difference between the torque in the unstable initial state before the cycle develops, and the value measured in the fully developed limit cycle. The different curves represent different  $\Delta r_2/r_{\text{in}}$ , increasing from purple ( $\Delta r_2 = 0.004$ ) to red ( $\Delta r_2 = 0.028$ ).  $\Delta r = 0.05$  is held constant. Solutions that lie along the x-axis do not show cyclic variations.

Using the results of the simulations presented in sec. 4.4.1 and 4.4.2, we can compare the torque exerted on the star for stable and unstable accretion:

$$\frac{\Delta \dot{J}}{\dot{J}_{\text{cons}}} \equiv \frac{\langle \dot{J}_{\text{sim}} \rangle - \dot{J}_{\text{cons}}}{\dot{J}_{\text{cons}}}. \quad (4.17)$$

Here  $\dot{J}_{\text{cons}}$  is the torque exerted on the star in the initial state (calculated using 4.16), and  $\langle \dot{J}_{\text{sim}} \rangle$  is the average torque exerted over one full cycle once a stable limit cycle is reached.

Figs. 4.8 and 4.9 show  $\Delta \dot{J}/\dot{J}_{\text{cons}}$  as a function of accretion rate for the simulations in figs. 4.3 (varying  $\Delta r/r_{\text{in}}$ ) and 4.4 (varying  $\Delta r_2/r_{\text{in}}$ ), respectively. The individual curves show  $\Delta r/r_{\text{in}}$  (or  $\Delta r_2/r_{\text{in}}$ ), with the colours from purple to red showing increasing values of the parameter. Lines along the x-axis indicate stable solutions.

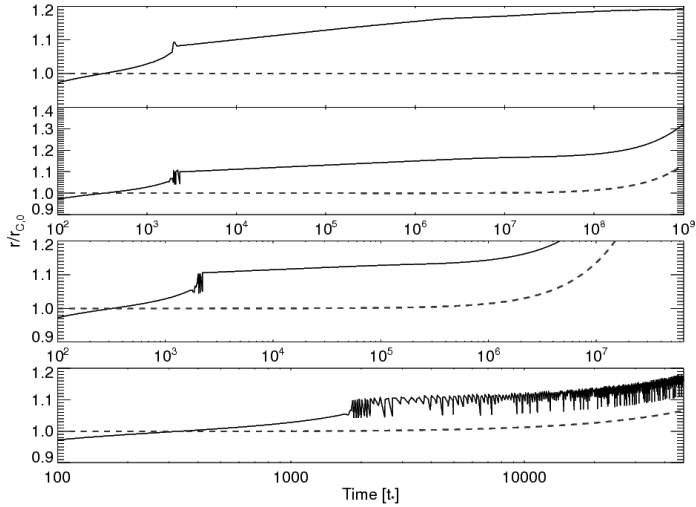


**Figure 4.10:** Evolution from an accreting to a non-accreting disc, for increasing (top to bottom) ratios of  $T_{\text{visc}}/T_{\text{SD}}$  for stable discs ( $\Delta r/r_{\text{in}} = 0.1$ ,  $\Delta r_2/r_{\text{in}} = 0.04$ ). From top to bottom, the ratio  $T_{\text{visc}}/T_{\text{SD}}$  is  $2.5 \times [10^{-9}, 10^{-7}, 10^{-5}, 10^{-4}]$ . The instability appears in all four panels, for varying lengths of time. As the ratio between the two timescales decreases, the disc is not able to move outwards as quickly before the star begins to spin down, so that  $r_{\text{in}}$  will always remain close to  $r_c$  and the instability persists for longer.

The results are easily separated into the RI (low  $\dot{m}$ ) and RII (high  $\dot{m}$ ) instability regions. In RI, both  $\dot{J}_{\text{cons}}$  and  $\dot{J}_{\text{sim}}$  are negative (cf. 4.2) over the entire unstable region, and the star spins down. As expected, the presence of the instability increases the efficiency of the spin-down torque considerably: by up to 60% for  $[\Delta r/r_{\text{in}}, \Delta r_2/r_{\text{in}}] = [0.05, 0.01]$ . For a given value of  $\Delta r/r_{\text{in}}$  or  $\Delta r_2/r_{\text{in}}$ ,  $\Delta \dot{J}/\dot{J}_{\text{cons}}$  is largest at the highest  $\dot{m}$  and decreases for smaller  $\dot{m}$ . When  $\dot{m}$  stays fixed,  $\Delta \dot{J}/\dot{J}_{\text{cons}}$  is largest for the smallest values of  $\Delta r/r_{\text{in}}$  and  $\Delta r_2/r_{\text{in}}$  (where the outburst amplitude is largest, cf. sec. 4.4.2). This behaviour is readily understandable: the added angular momentum from accretion is most relevant at high  $\dot{m}$ , and the rate at which this material is accreted (i.e. the duty cycle of the outburst) will determine how much the star will spin up or down. The larger the amplitude of the outburst, the faster the reservoir of mass will be accreted, and so the shorter the duty cycle.

In RII the situation is quite different. In the parameter range for  $\Delta r/r_{\text{in}}$  and  $\Delta r_2/r_{\text{in}}$  where the solution is unstable,  $\langle \dot{J}_{\text{sim}} \rangle$  and  $\dot{J}_{\text{cons}} > 0$  when  $\dot{m} = \dot{m}_c$  (fig. 4.2). The presence of the instability decreases the rate of spin-up by a maximum by up to about 20%.

#### 4.4.5 Transient instability cycles

In DS10b we studied how discs in our model evolved as the spin of the star changed. To do this we introduced the star's moment of inertia,  $I_*$  as an additional parameter of the problem, which introduced a new characteristic timescale for the problem, the spindown timescale  $T_{\text{SD}}$ :

$$T_{\text{SD}} \equiv P_*/\dot{P}_* \sim \frac{I_* \Omega_* r_{\text{in}}^4}{\eta \mu^2 \Delta r}. \quad (4.18)$$

We found that the ratio of  $T_{\text{visc}}$ , the viscous accretion timescale at  $r_c$ , and  $T_{\text{SD}}$  plays an important role in determining whether a disc will become trapped with  $r_{\text{in}}$  close to  $r_c$  when  $\dot{m}$ , the mean accretion rate through the disc drops to zero.

The spin change of the star can also determine whether or not the accretion instability occurs. For a given set of  $[\Delta r, \Delta r_2]$  the instability frequently appears over a narrow range in  $\dot{m}/\dot{m}_c$ , so that changing  $r_c$  (and hence  $\dot{m}_c$ ) will cause the instability to appear or disappear. This effect is difficult to observe in our simulations, since the timescale of the instability ( $\sim 10^{-2} - 10^3 T_{\text{visc}}$ ) is in general much shorter than the spin-down timescale of the star ( $T_{\text{SD}} \sim 10^3 - 10^{17} T_{\text{visc}}$ ; DS10b), so once the instability occurs the simulation typically proceeds on the instability timescale. Despite this, we do find some solutions that show transient oscillations (typically with the long periods,  $P \sim 10^3 T_{\text{visc}}$ ) for a constant  $\dot{m}$ , which appear and disappear as  $r_c$  changes.

This transient instability is illustrated in figs. 4.11 and 4.10. For these simulations we have adopted the same scaling parameters as we used in DS10b. We take  $r_*$ , the star's radius, as our characteristic lengthscale, and define  $t_* \equiv \nu/r_*^2$ , the nominal viscous timescale at the star's radius, as the characteristic timescale. We set  $T_{\text{SD}} \equiv 380 T_{\text{visc}}$  (where  $T_{\text{visc}}$  is the viscous timescale for  $r_c(t=0)$ ), which is appropriate for a protostellar system. We set  $r_c(t=0) = 1.8 r_*$ .

In fig. 4.11 we show the evolution of an initially dead disc ( $\dot{m} = 0$ ) with  $[\Delta r/r_{\text{in}}, \Delta r_2/r_{\text{in}}] = [0.2, 0.02]$ . The disc is initially in the steady-state solution given by (4.7) with  $r_{\text{in}} = 1.3 r_c$ . The top panel shows the evolution of  $r_{\text{in}}$  (black) and  $r_c$  (red) in time, while the bottom panel shows the accretion rate onto the star, scaled to  $\dot{m}_c$  at  $t = 0$ . At early times [not shown] there is no accretion onto the star and  $r_{\text{in}}$  remains fixed while  $r_c$  moves steadily outwards. Once  $r_c$  moves close enough to  $r_{\text{in}}$  (at  $\sim 10^4 t_*$ ) to begin accreting matter, gradients in the surface density cause  $r_{\text{in}}$  to move quickly closer to  $r_c$ . At  $r_{\text{in}}/r_c \sim 1.1$ , however, the disc suddenly becomes unstable and accretion proceeds via a series of large amplitude bursts, which increase the maximum accretion rate onto the star enormously.  $r_c$  continues to move outwards as the source oscillates, which causes  $\dot{m}_c(r_c)$  to decrease as well. Eventually  $\dot{m}/\dot{m}_c$  moves out of the unstable range, and the disc settles back into a steadily accreting solution with a gradually decreasing accretion rate. This result emphasizes the fact the instability can depend sensitively on  $\dot{m}/\dot{m}_c$ , so that as  $r_c$  evolves, cycles can appear and then disappear.

For constant  $\Delta r/r_{\text{in}}$  and  $\Delta r_2/r_{\text{in}}$ , the appearance of cycles depends on  $\dot{m}$  and  $\dot{m}_c$ . As we showed in DS10b, when the mean accretion rate through the disc drops so low that the disc

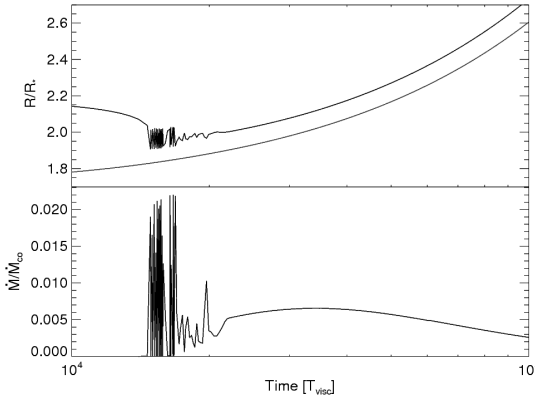


**Figure 4.11:** Unstable disc solution for  $[\Delta r, \Delta r_2] = [0.2, 0.02]r_{\text{in}}$ . At  $t = 0$ ,  $r_{\text{in}}/r_c = 1.3$ , so that  $\dot{m} \simeq 0$ . Initially  $r_{\text{in}}$  remains constant, before decreasing sharply as  $r_c$  increases. This prompts the onset of the accretion instability, which continues even while the star spins down. At later times, the amplitude and frequency of the instability decrease and the disc reverts back to accreting steadily. Top: Evolution in  $r_{\text{in}}$  (black curve) and  $r_c$  (red curve), before, during, and after the instability appears. Bottom: Corresponding accretion rate onto the star. The accretion rate is given in terms of  $\dot{m}_c$  corresponding to  $r_c$  at ( $t = 0$ ).

becomes trapped, the accretion rate at  $r_{\text{in}}$  depends strongly on  $T_{\text{visc}}/T_{\text{SD}}$ . This ratio also plays an important role in determining the presence and duration of unstable accretion phases.

We illustrate this in fig. 4.10, which shows a disc evolving from an accreting disc to a trapped disc for different  $T_{\text{visc}}/T_{\text{SD}}$ , adopting parameters appropriate for a neutron star. We take the field strength  $10^{12}$  G, initial spin period 5s, and initial inner edge radius  $0.95r_c$ . The disc is thus initially in an accreting state. The outer boundary is located at  $100r_{\text{in}}$ . The initial spindown timescale of the star is  $T_{\text{SD}} = 10^5$  years. We adopt the same system parameters as for fig. 4.11, with  $[\Delta r/r_{\text{in}}, \Delta r_2/r_{\text{in}}] = [0.2, 0.02]$ . At  $t = 0$  we set  $\dot{m} = 0$  at the outer boundary of the disc, so that the accretion rate through the disc gradually drops.

The figure shows the evolution of  $r_c$  (dashed curve) and  $r_{\text{in}}$  (solid curve) as a function of time for increasing  $T_{\text{visc}}$ , with  $T_{\text{visc}}/T_{\text{SD}} = 2.5 \times [10^{-9}, 10^{-7}, 10^{-5}, 10^{-4}]$  from top to bottom. In all four simulations, the disc initially move outwards as  $\dot{m}$  decreases to about  $1.05r_c$ , where the accretion rate triggers the onset of the instability.

The appearance of the disc changes dramatically with changing viscosity. Discs with a high viscosity are able to diffuse outwards at a faster rate as  $\dot{m}$  declines, so that  $r_{\text{in}}$  in the top panel (with the highest viscosity) moves far from  $r_c$  before the star can begin to spin down, and the disc never becomes trapped close to  $r_c$ . The instability (which only occurs between  $\dot{m}/\dot{m}_c \simeq [10^{-3}, 0.1]$ ) will only appear briefly before  $r_{\text{in}}$  moves too far from  $r_c$  and the accretion rate drops. In the middle two panels the instability also appears briefly, but the star does begin to spin down quickly enough that  $r_c$  begins to move outwards at the same rate as  $r_{\text{in}}$  and the disc remains trapped. In the bottom panel (with the lowest viscosity), the disc diffuses outwards slowly, and the star spins down more rapidly. Once the instability is

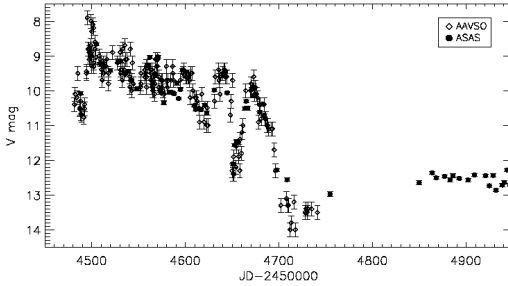


**Figure 4.12:** The 2008 outburst of EX Lupi. From January to August, the source was up to 4 magnitudes larger than its quiescent value. *figure courtesy A. Juhasz.*

triggered,  $r_{\text{in}}$  remains close enough to  $r_c$  that the instability persists as the star continues to spin down.

## 4.5 RELEVANCE FOR ASTROPHYSICAL SOURCES

### 4.5.1 Trapped discs and the disc instability in EXors

We have previously suggested that the disc instability discussed in this paper is operating in a class of T Tauri stars known as ‘EXors’. EXors, like their prototype, EX Lupi are characterized by repeated large outbursts: changes by up to four magnitudes in luminosity lasting several months, with a characteristic total period of several years (Herbig 2007, 2008). Observations of these sources in both outburst and quiescence can produce valuable constraints on both the disc instability and the trapped disc itself.

Figure 4.12 shows the  $m_V$  brightness of EX Lupi over 500 days, taken from the AAVSO and ASAS archives (from Attila Juhasz, *private communication*). In January 2008, EX Lupi underwent a large outburst, increasing by 3 magnitudes, from  $m_V = 11$  to  $m_V = 7.9$  (Aspin et al. 2010) in about 20 days. In July 2008 EX Lupi was at  $m_V = 12.4$  Sipos et al. (2009), so the total change in luminosity was probably more than 4 magnitudes. EX Lupi remained in outburst for eight months, decaying from maximum to about  $m_V = 10$  before abruptly dropping to  $m_V = 14$  over about 40 days. The data show evidence of an additional higher-frequency modulation with a period of about 30 days and amplitude of 1-2 magnitudes.

The outburst profile looks similar to some of the profiles seen in our simulations, with a rapid rise and a gradual decreasing plateau phase, followed by a rapid decay as the source returns to quiescence. The higher frequency modulation is also suggestive of the higher frequency oscillations seen in the RI instability discussed above and in DS10a, although its short timescale  $\sim 30$  days, or  $\sim 4 - 10\times$  longer than  $P_*$  (Sipos et al. 2009) might also indicate

direct modulation between the disc and magnetic field (e.g. Goodson et al. 1997; Romanova et al. 2008).

Spectral observations taken both during the outburst and quiescence allow additional constraints on the disc model. Aspin et al. (2010) analysed a series of spectra of EX Lupi from the 2008 outburst to constrain the parameters of the disc. They calculated an accretion rate of  $2 \times 10^{-7} M_{\odot} \text{yr}^{-1}$  in outburst, and modelled the  $2.2935 \mu\text{m}$  CO overtone emission to suggest an inner gap of about  $10 r_*$  in the disc. They also used previously published results to calculate  $6 \times 10^{-9} M_{\odot} \text{yr}^{-1}$  for the quiescent emission. Sipos et al. (2009) analysed a series of spectra for EX Lupi in quiescence (with  $m_V \sim 12$ ), and did a detailed fit for the spectrum. They estimated an accretion rate of  $4 \times 10^{-10} M_{\odot} \text{yr}^{-1}$ , and fit the spectrum with a dust-dominated disc truncated at about 0.2 AU. These observations thus suggest that the accretion rate increased by  $\sim 30 - 500 \times$  during the outburst, and that close to the star, gas is either absent or optically thin.

To see whether these observations are compatible with our model of a trapped disc, we adopt the best-fit parameters of Sipos et al. (2009), with  $M_* = 0.6 M_{\odot}$ ,  $r_* = 1.6 R_{\odot}$ , and  $P_* = 6.3 d$  (based on  $v \sin i = 4.4 \text{ km/s}$  and an inclination of 20 degrees). The magnetic field is unknown, so we assume a strong dipolar field with  $B_* = 1500 G$ , which is comparable to field strengths observed in T Tauri stars such as BP Tau (Donati et al. 2008). The rest of the parameters we adopt are the same as for our representative model (sec. 4.2.1). This puts the co-rotation radius at  $7.6 r_*$ , and sets  $r_{\text{in}} \simeq r_c$  for the quiescent disc. The viscous timescale at  $r_c$  is thus  $\sim 30$  yrs. If we assume that the period of the instability is  $\sim 60$  yrs (the time between the 2008 outburst and the similar amplitude outburst in 1955), or  $\sim T_{\text{visc}}$ . The instability would then fall in the RII region.

Additional information could come from directly detecting the accretion disc itself in quiescence. A trapped disc will have both a higher surface density and temperature than a purely accreting disc with the same  $r_{\text{in}}$ . For EX Lupi in quiescence (using the parameters given above), our model predicts a surface temperature from internal viscous dissipation of 530-650K (depending on  $\dot{m}$ ), compared with 290-570K for a Shakura-Sunyaev disc. This modest temperature increase is likely insignificant compared to heating from the central star, which will thus still determine the gas behaviour at these low accretion rates (e.g. Muzerolle et al. 2004). The surface density in the disc will also increase modestly, from a maximum of between  $3-40 \text{ g cm}^{-2}$  ( $\rho \simeq 4 \times 10^{-11} - 6 \times 10^{-10} \text{ g cm}^{-3}$  to  $40-80 \text{ g cm}^{-2}$  ( $\rho \simeq 4 \times 10^{-10} - 10^{-9}$ ). At these low densities the disc is probably optically thin (e.g. Dullemond & Monnier 2010), so that it is likely not possible to directly distinguish between a trapped disc and normal accreting one except through detailed modelling of spectral features in the disc.

Unlike the accretion instability (which only occurs under certain conditions in the disc-field interaction), the build-up of mass just outside the co-rotation radius should be generic in stars with strong magnetic fields and relatively low accretion rates. The best opportunity to detect a trapped disc directly would come from a star with a strong dipolar magnetic field, high spin rate and low accretion rate, so that the disc would be optically thick rather than thin

(as would be expected for the given accretion rate), and could be directly detected through modelling of its spectral features.

#### 4.5.2 NS transients w/ weak recurrent outbursts

In DS10b we suggested that the large ratio between the spin-down and viscous timescales in accreting millisecond pulsars makes it unlikely that the disc will become trapped, since as  $\dot{m}$  drops  $r_{\text{in}}$  moves outwards much faster than  $r_c$ . This agrees with the typical outbursts seen in transient X-ray pulsars, which show outbursts of variable duration followed by long periods of quiescence and are believed to be triggered by ionization instabilities in the disc (e.g. Lasota (2001)).

However at least two accreting X-ray pulsars, NGC 6440 X-2 (Heinke et al. 2010) and IGR J00291+5934 (Hartman et al. 2010) have been observed to undergo weak, recurrent outbursts on much shorter timescales (around 30 days) than would be predicted from an ionization-instability model (Lasota (2001)). The weakness of the outburst has been interpreted to mean that the disc is never completely ionized during the outburst Hartman et al. (2010), which suggests the ratio of  $T_{\text{SD}}/T_{\text{visc}}$  becomes small enough to trap the disc as when the accretion rate drops. This large reservoir of matter would then be present when the accretion rate again increases, and so could allow more frequent outbursts. These sources thus offer an excellent opportunity for comparison with our model of a trapped disc.

IGR J00291+5934 is a 599Hz X-ray pulsar in a 147 minute orbit, which historically has shown standard single outbursts (in 1998, 2001, and 2004) followed by long periods of quiescence. However, in 2008 it underwent a substantially different outburst, with two weaker outbursts (respectively lasting nine and 13 days) separated by 27 days of quiescence (Hartman et al. 2010). The authors estimated that the total mass flux of weaker outbursts together was approximately equal to the single 2004 outburst. Similar outbursts have been seen in NGC 6440 X-2, a recently discovered X-ray binary with a frequency of 442Hz in a 57 minute orbit (Altamirano et al. 2010). Since discovery on July 28, 2009, five distinct outbursts have been observed, each typically lasting around four days at a luminosity of around  $L_X \sim 10^{35} \text{erg s}^{-1}$ , with a minimum recurrence time of around 31 days.

The short recurrence timescales suggest that a considerable amount of mass is stored in the disc when the accretion rate drops, which can then fuel another outburst when  $\dot{m}$  increases again. In both sources the quiescent X-ray luminosity is at least 4 orders of magnitude lower than the outburst luminosity, indicating a large change in accretion rate (although the X-ray luminosity may not be a good indicator of bolometric luminosity at such low accretion rates, so there is some uncertainty in the change in  $\dot{m}$ ). However, if we assume that  $\dot{m}$  falls by at least 2-3 orders of magnitude, this requires  $\Delta r_2/r_{\text{in}} < 0.1$  to prevent the disc from moving into the propeller regime.

During two outbursts, the power spectrum of NGC 6440 X-2 was dominated by a strong low-frequency QPO ( $\sim 1$  Hz) (Patruno et al. 2010; Hartman et al. 2010). A similar QPO was previously detected in the tail an outburst in X-ray pulsar SAX J1808.4-3658 (Patruno et al.

2009) which was attributed to the disc instability presented in DS10a and Spruit & Taam (1993). A much weaker QPO at  $0.5\text{Hz}$  was observed in the outbursts IGR J00291+5934 and might also be attributed to the disc instability Hartman et al. (2010).

The fact that all of these QPOs were observed at a similar frequency presents a challenge to our interpretation. The outbursts seen in SAX J1808.8-3658 follow the more conventional pattern of a large outburst followed by a long quiescence, which would suggest that a dead disc does not form. However, the similarity of the QPO frequency (which is roughly correlated with the viscous timescale near  $r_{\text{in}}$  in our model) suggests that the viscous timescale is similar in all these sources. This contrasts with our suggestion that the viscosity in these weak outbursts is substantially smaller than in larger outbursts. The number of uncertain parameters in our model (in particular this assumes that  $\Delta r_2/r_{\text{in}}$  is similar in all sources) means that the picture we have presented could still be valid, but then the similarity in QPO frequency in both (or all three) of these sources is coincidental. On the other hand, a strong low-frequency QPO has currently been observed in only two sources, while as Altamirano et al. (2010) have noted, weakly outbursting sources like NGC 6440 X-2 will generally be missed in current surveys.

In our present model, the disc-field interaction is not responsible for directly regulating the accretion rate onto the star to control the outbursts, as was suggested by Hartman et al. (2010). The field can temporarily halt accretion onto the star, but only on the much shorter timescale on which the 1Hz QPO is seen. Thus the mechanism that directly triggers an accretion outburst remains underdetermined.

### 4.5.3 Persistent X-ray pulsars

A small subset of accreting pulsars with low-mass companions have sufficiently persistent X-ray emission to measure the spin change directly and study the connection between spin change and luminosity. Three well-studied persistent sources (Her X-1, 4U 1626-67, and GX 1+4) all show episodes of spin-up and spin-down, although the pattern of spin-up and spin-down is different in all three (Bildsten et al. 1997). A fourth, (GRO J1744-28) shows clear spin-up when in outburst, allowing the relationship between  $\dot{\nu}$  and  $\dot{m}$  to be constrained.

The binary properties of all these sources varies considerably, both in their companions and orbital periods. However, it is still possible to make some general observations that apply to all sources. First, there is a clear correlation between luminosity and spin change, with higher luminosity corresponding to spin up, and vice versa. Second, when the star is spinning up, the spin-up rate is substantially lower than would be predicted from the X-ray luminosity. Third, where the relationship between  $\dot{\nu}$  and  $\dot{m}$  can be measured,  $\dot{\nu} \propto \dot{m}^\gamma$ , where  $\gamma > 6/7$ , i.e. the scaling expected for  $r_{\text{in}} \propto \dot{m}^{-2/7}$ . Finally, the spin-up torque is often comparable (within a factor 2) to the spin-down torque, with only a change in sign.

The first observation is universally expected in magnetospheric accretion, since in order to spin up the star the matter must be able to overcome the centrifugal barrier imposed at  $r_c$ . The second point is also readily understandable in our model, which assumes that there is

a transition region for  $r_{\text{in}} \sim r_{\text{c}}$  in which there is both accretion and spin-down torque. This behaviour is also seen in MHD simulations of the disc-star interaction (e.g. Romanova et al. 2004). For high accretion rates, our model predicts  $\dot{v} \propto \dot{m}^{9/10}$ , which is close to the dependence measured in some X-ray pulsars in outburst. For example, the 1995/1996 outburst of GRO J1744-28 (a disc-fed binary), was measured to follow  $\dot{v} \propto \dot{m}^{0.96}$  (Bildsten et al. 1997). This is closer to observation than the standard model, which predicts an index of 6/7.

The final point is most puzzling in a model in which  $r_{\text{in}} \propto \dot{m}^{-2/7}$ , because it requires that the change in accretion rate is finely tuned to preserve this symmetry. It is more plausible for our model, however, which shows a steep decrease in  $\dot{v}$  around  $\dot{m}/\dot{m}_{\text{c}} = 1$ , and then a flattening around the minimum in  $\dot{v}$ . Thus, a small decrease in  $\dot{m}$  will cause an initial steep transition to spin-down before settling around the minimum in  $\dot{v}$ . There is no comparable turnover at high  $\dot{m}$ , but in order to switch between spin-up and spin-down, the star must have an average accretion rate such that  $r_{\text{in}} \sim r_{\text{c}}$ , while in order to be a persistent source, the accretion rate at large distances cannot be very variable. If we assume that the average accretion rate has been steady enough on long timescales to affect the star's rotation rate, then there will be a natural spin-down torque, set by the minimum in 4.2, and we would expect that on average the accretion rate would fluctuate around the level that keeps  $r_{\text{in}}$  close to  $r_{\text{c}}$ . This still does not account for the observations (for example of 4U 1626-27) in which the magnitude of the torque is very nearly symmetric.

Our present model is too simple to make quantitative comparisons to data. For one thing, the relation between  $\dot{v}$  and  $\dot{m}$  depends on the least certain parts of our model: both the transition widths  $\Delta r/r_{\text{in}}$  and  $\Delta r_2/r_{\text{in}}$  and the connecting functions  $y_m$  and  $y_{\Sigma}$ . There is also much more variation in the luminosity at which the system moves from spin-up to spin-down than is generically predicted in any simple magnetospheric accretion model. This variability could indicate fluctuations in  $\langle \eta \rangle$ , and  $\Delta r/r_{\text{in}}$ , which would both affect the magnitude of spin-down torque. Agapitou & Papaloizou (2000) demonstrated that the value of  $B_{\phi}$  changes if field lines are able to diffuse radially through the disc. The diffusion of field lines is expected to happen on viscous timescales (Fromang & Stone 2009), so that the details of the disc-field interaction could in fact rely on the complicated interplay between the accretion rate and the field strength and geometry. Such questions require detailed MHD modelling which are beyond the scope of the present work.

## 4.6 DISCUSSION

At low accretion rates, the strong magnetic field of a star can strongly alter the structure of an accretion disc, preventing it from either accreting or expelling material outward, and preventing the inner edge of the disc from moving considerably away from  $r_{\text{c}}$ . As we have discussed in this paper, this disc state can lead to substantially different behaviour from what is conventionally assumed, and could explain a variety of observed phenomena in magnetically accreting stars. However, in order to construct our model we used a parameterized descrip-

tion for the interaction between the magnetic field, introducing the free parameters  $\Delta r/r_{\text{in}}$ , and  $\Delta r_2/r_{\text{in}}$ . Here we discuss what sets the value of these parameters, and whether these parameters could vary in time, which could account for some of the additional behaviour not described by our current model.

The first parameter,  $\Delta r/r_{\text{in}}$  is the width of the direct interaction between the field and the disc in the disc's innermost region. We have assumed in all cases that  $\Delta r/r_{\text{in}} < 1$ , so that the interaction region (where the field lines remain closed long enough to exert a significant stress on the disc) remains fixed. MHD simulations suggest that this region will fluctuate in time as field lines open and reconnect, but we have assumed that this will occur on timescales of  $\sim P_*$ , which are much shorter than the viscous timescale of the instability ( $T_{\text{visc}} > 10^3 P_*$ ). Numerical MHD simulations do sometimes show variability on longer timescales (e.g. Romanova et al. (2009)), which could lead to changes in  $\Delta r/r_{\text{in}}$  between individual outbursts. Given that even small changes in  $\Delta r/r_{\text{in}}$  can significantly change the appearance and amplitude of the outburst (seen in figure 4.6), variability in the disc-field interaction could produce variability in the appearance of the instability, especially if the instability occurs in RII.

A second possible source of variability could come from the radial evolution of the magnetic field itself. This was studied by (Agapitou & Papaloizou 2000), who found that radial field-line diffusion through the disc can reduce the effective torque at  $r_{\text{in}}$ , and increase the extent of the closed-field line region. The timescale for magnetic diffusion is typically assumed to be about the same as for viscous diffusion (which is supported by recent MRI calculations; Fromang & Stone 2009), so that the radial diffusion of closed field-lines outward could compete with accretion of matter (and field lines) inward, creating an additional, longer timescale source of variability in  $\Delta r/r_{\text{in}}$ . This could allow the instability to appear and disappear at the same  $\dot{m}$  (as has been seen in Patruno et al. (2009), where the 1-Hz QPO was seen in portions of the outburst but not others at the same flux).

The physics that sets  $\Delta r_2/r_{\text{in}}$  (the transition length between the accreting and non-accreting solutions) is considerably less clear, although presumably the same variations in the disc-field interaction that change  $\Delta r/r_{\text{in}}$  could also change  $\Delta r_2/r_{\text{in}}$ . In DS10b we discussed the model proposed by Perna et al. (2006), which considers a strongly inclined dipole, so that the disc truncation radius lies both inside and outside  $r_c$ , allowing for simultaneous accretion and confinement of material. If this is the case then  $\Delta r_2/r_{\text{in}}$  should remain constant for a given system, and the variability must come from fluctuations in  $\Delta r/r_{\text{in}}$ .

Another open question remains what regulates the mean accretion rate onto the star. In all our simulations we have treated the accretion rate,  $\dot{m}$  as a free parameter, and shown how the instability and spin-evolution of the star change as a result. However, observations of neutron star binaries suggest that the accretion rate from the donor star remains roughly constant Bildsten et al. (1997), and variations in  $\dot{m}$  are often assumed to arise from ionization instabilities Lasota (2001). Hartman et al. (2010) suggested that the disc-field interaction could regulate the accretion rate onto the star by storing it up, in a similar way to what we have discussed here. However, our model does not agree with this conclusion: the disc-field interaction can only halt accretion long enough to build up mass to drive the disc instability

and only substantially alters the inner regions of the disc. Our trapped disc solutions evolve *as a response* to the decreased accretion rate in the disc, and only become relevant once the average accretion rate has decreased below a threshold,  $\dot{m}_{\text{crit}}/\dot{m}_c \sim 4\Delta r/r_{\text{in}}$  (sec. 4.3.1).

On the other hand, if radiation feedback from accretion onto the star plays an important role in regulating the viscosity (and so accretion rate) in the disc, then temporarily suppressing accretion onto the star might cause the level of ionization to drop and drive the source back into quiescence.

A final question remains: why do some sources show the accretion instability and trapped disc behaviour and not others? The vast majority of outbursting neutron stars show long periods of quiescence, consistent with being driven by the ionization instability with  $r_{\text{in}}$  far from  $r_c$ , rather than remaining trapped near  $r_c$ . Of the two sources we have considered, IGR J00291+5934 has previously shown a normal outburst pattern (a much stronger outburst followed by a long quiescence; Hartman et al. 2010).

In their discovery paper for NGC 6440 X-2, Altamirano et al. (2010) remark that the short recurrence time and weak outburst likely cause similar NS sources to be missed by current surveys, so it is possible that such sources are common but remain undiscovered. As well, in DS10b we showed that the very small ratio  $T_{\text{visc}}/T_{\text{SD}} \sim 10^{-17}$  for rapidly spinning pulsars made it more likely that the disc would become untrapped (with  $r_{\text{in}}$  moving rapidly away from  $r_c$ ) as  $\dot{m} \rightarrow 0$ . Hartman et al. (2010) suggested that the disc might remain weakly ionized during the entire outburst, which would then decrease the viscosity and increase  $T_{\text{visc}}$ , perhaps enough to prevent the disc from becoming untrapped. If the RI instability is responsible for the 1Hz QPO seen in NGC 6440 X-2 and SAX J1808.4-3658, then the fact that only sometimes manifests is consistent with the idea that  $\Delta r/r_{\text{in}}$  is variable (since the instability only occurs over a small range in  $\Delta r/r_{\text{in}}$ ).

For T Tauri stars, the main constraint on the instability is the presence of a strong ( $\sim 1$  kG) dipolar magnetic field. Although most T Tauri stars show a strong surface field component, the dipolar component can vary considerably, to the point that it is not clear whether the disc-field interaction considered here is primarily responsible for the low spin-rate of the star. The inclination between the rotation axis of the star and the magnetic field could also affect the instability by changing  $\Delta r_2/r_{\text{in}}$  (as above). This would suggest that, as a class, EXors are T Tauri stars with moderate accretion rates and strong, aligned dipolar magnetic fields compared with normal T Tauri stars.

## 4.7 CONCLUSIONS

As found in DS10, accretion from a disc onto a magnetosphere tends to take place in what in a companion paper (DS10b) we have called ‘trapped’ states. The inner edge of the disc hovers around the corotation radius in this state, even at very low accretion rates. The accretion in this state can be steady or cyclic. We have investigated here the conditions under which the cyclic form takes place, the kinds of cycles, their amplitudes, cycle periods and their effect

on the average torque on the accreting star.

Two forms of cycle are found; the first form (labeled RI here) is the accretion/dead disc cycle already surmised by Sunyaev & Shakura (1977). A pile-up of mass at the ‘centrifugal barrier’ outside corotation is followed by an episode of accretion emptying the pile and the beginning of a new cycle. Mass loss or ‘propellering’, whether it takes place or not, is a separate piece of physics not needed for understanding the effect of a centrifugal barrier on a viscous disc accreting on a magnetosphere.

Whether accretion is cyclic or continuous is found to depend on the width of the transition from an accreting state (inner edge inside corotation) to a suspended accretion state (edge outside corotation). A narrow width leads to RI cycles, a broader transition to continuous accretion. The effect of these cycles is to increase the average spindown torque on the star. A second form of cycle takes places when the average accretion rate is close to the standard accreting case (edge inside corotation). It decreases the average torque on the star.

A review of the available literature shows forms of variability that may be related the the cyclic forms of accretion found here, the most promising ones may be the ‘EX Ori’ outbursts, and a new form of cyclic accretion found in X-ray binaries NGC 6440 X-2 and SAX J1808.4-3658.

## 4.8 ACKNOWLEDGMENTS

CD’A acknowledges financial support from the National Science and Engineering Research Council of Canada, and thanks Attila Juhasz for interesting dicussions and the use of figure 4.12.

### REFERENCES

- Agapitou V., Papaloizou J. C. B., 2000, MNRAS, 317, 273
- Altamirano D., Patruno A., Heinke C. O., Markwardt C., Strohmayer T. E., Linares M., Wijnands R., van der Klis M., Swank J. H., 2010, ApJ, 712, L58
- Aly J. J., 1985, A&A, 143, 19
- Aly J. J., Kuijpers J., 1990, A&A, 227, 473
- Aspin C., Reipurth B., Herczeg G. J., Capak P., 2010, ApJ, 719, L50
- Bildsten L., Chakrabarty D., Chiu J., Finger M. H., Koh D. T., Nelson R. W., Prince T. A., Rubin B. C., Scott D. M., Stollberg M., Vaughan B. A., Wilson C. A., Wilson R. B., 1997, ApJS, 113, 367
- Camero-Arranz A., Finger M. H., Ikhsanov N. R., Wilson-Hodge C. A., Bekken E., 2010, ApJ, 708, 1500
- Chakrabarty D., Bildsten L., Finger M. H., Grunsfeld J. M., Koh D. T., Nelson R. W., Prince T. A., Vaughan B. A., Wilson R. B., 1997, ApJ, 481, L101+

- D'Angelo C. R., Spruit H. C., 2010a, MNRAS, 406, 1208
- D'Angelo C. R., Spruit H. C., 2010b, in prep.
- Davidson K., Ostriker J. P., 1973, ApJ, 179, 585
- Donati J., Jardine M. M., Gregory S. G., Petit P., Paletou F., Bouvier J., Dougados C., Ménard F., Cameron A. C., Harries T. J., Hussain G. A. J., Unruh Y., Morin J., Marsden S. C., Manset N., Aurière M., Catala C., Alecian E., 2008, MNRAS, 386, 1234
- Dullemond C. P., Monnier J. D., 2010, ARA&A, 48, 205
- Fromang S., Stone J. M., 2009, A&A, 507, 19
- Getman K. V., Feigelson E. D., Micela G., Jardine M. M., Gregory S. G., Garmire G. P., 2008, ApJ, 688, 437
- Goodson A. P., Winglee R. M., Boehm K., 1997, ApJ, 489, 199
- Hartman J. M., Galloway D. K., Chakrabarty D., 2010, ArXiv e-prints
- Hayashi M. R., Shibata K., Matsumoto R., 1996, ApJ, 468, L37+
- Heinke C. O., Altamirano D., Cohn H. N., Lugger P. M., Budac S. A., Servillat M., Linares M., Strohmayer T. E., Markwardt C. B., Wijnands R., Swank J. H., Knigge C., Bailyn C., Grindlay J. E., 2010, ApJ, 714, 894
- Herbig G. H., 2007, AJ, 133, 2679
- Herbig G. H., 2008, AJ, 135, 637
- Illarionov A. F., Sunyaev R. A., 1975, A&A, 39, 185
- Lasota J., 2001, New Astron. Rev., 45, 449
- Lovelace R. V. E., Romanova M. M., Bisnovaty-Kogan G. S., 1995, MNRAS, 275, 244
- Matt S., Pudritz R. E., 2005, ApJ, 632, L135
- Matt S. P., Pinzón G., de la Reza R., Greene T. P., 2010, ApJ, 714, 989
- Miller K. A., Stone J. M., 1997, ApJ, 489, 890
- Muzerolle J., D'Alessio P., Calvet N., Hartmann L., 2004, ApJ, 617, 406
- Patruno A., Watts A., Klein Wolt M., Wijnands R., van der Klis M., 2009, ApJ, 707, 1296
- Patruno A., Yang Y., Altamirano D., Armas-Padilla M., Cavecchi Y., Degenaar N., Kalamkar M., Kaur R., Klis M. V. D., Watts A., Wijnands R., Linares M., Casella P., Rea N., Soleri P., Markwardt C., Strohmayer T., Heinke C., 2010, The Astronomer's Telegram, 2672, 1
- Perna R., Bozzo E., Stella L., 2006, ApJ, 639, 363
- Pringle J. E., Rees M. J., 1972, A&A, 21, 1
- Romanova M. M., Kulkarni A. K., Lovelace R. V. E., 2008, ApJ, 673, L171
- Romanova M. M., Ustyugova G. V., Koldoba A. V., Lovelace R. V. E., 2004, ApJ, 616, L151
- Romanova M. M., Ustyugova G. V., Koldoba A. V., Lovelace R. V. E., 2009, ArXiv e-prints

- 
- Sipos N., Ábrahám P., Acosta-Pulido J., Juhász A., Kóspál Á., Kun M., Moór A., Setiawan J., 2009, A&A, 507, 881
- Spruit H. C., Taam R. E., 1993, ApJ, 402, 593
- Sunyaev R. A., Shakura N. I., 1977, Pis ma Astronomicheskii Zhurnal, 3, 262



---

## Chapter 5

---

# Soft X-ray Components in the Hard State of Accreting Black Holes

Caroline D'Angelo, Dimitrios Giannios, Cornelis Dullemond Hendrik Spruit

A&A, 488, 441, 2008

Recent observations of two black hole candidates (GX 339-4 and **R**J1753.5-0127) in the low-hard state ( $L_X/L_{\text{Edd}} \simeq 0.003 - 0.05$ ) suggest the presence of a cool accretion disk very close to the innermost stable orbit of the black hole. This runs counter to models of the low-hard state in which the cool disk is truncated at a much larger radius. We study the interaction between a moderately truncated disk and a hot inner flow. Ion-bombardment heats the surface of the disk in the overlap region between a two-temperature advection-dominated accretion flow and a standard accretion disk, producing a hot ( $kT_e \simeq 70\text{keV}$ ) layer on the surface of the cool disk. The hard X-ray flux from this layer heats the inner parts of the underlying cool disk, producing a soft X-ray excess. Together with interstellar absorption these effects mimic the thermal spectrum from a disk extending to the last stable orbit. The results show that soft excesses in the low-hard state are a natural feature of truncated disk models.

## 5.1 INTRODUCTION

The geometry of the low-luminosity (“low-hard”) state of Galactic Black Hole Candidates (GBHC), in which the spectrum is dominated by a power law X-ray flux extending to high energies, has been an open question for several decades. While it is generally believed that the power law spectrum is formed by inverse Compton scattering, there is no consensus about the geometry of the flow, source of seed photons or energy distribution for the Comptonizing electrons.

Broadly speaking, there are two classes of model to explain the spectrum in the low-hard state. The first is the “corona” model, in which the disk remains untruncated or nearly untruncated at luminosities  $L_X \simeq 10^{-3} L_{\text{Edd}}$ . The hard power law spectrum comes from a hot and patchy corona (perhaps powered by magnetic flares (di Matteo 1998; Beloborodov 1999; Merloni & Fabian 2001)) on top of the disk, while the surrounding region is bombarded with high energy photons, producing the observed reflection and Fe-K fluorescence components. In the alternate, “truncated disk” model the thin disk is truncated at some distance from the black hole and the inner region is filled with a hot, radiatively-inefficient flow, which produces the hard spectrum. The reflection spectrum and Fe-K fluorescence is then produced by the interaction of the hard X-rays with the inner part of the truncated disk, or in some cool outflow moving away from the disk. For a recent discussion of the low-hard state see sect. 4 of Done et al. (2007).

In theory, the presence or absence of a cool disk should be confirmable through direct detection of a soft X-ray blackbody component at low energies. In practice however, this is made difficult by the fact that at low accretion rates the temperature of even an untruncated disk will drop from about 1-2keV in the high soft state to  $\sim 0.1$ -0.3keV, which puts it out of the range of most X-ray detectors. Additionally, the effects of interstellar absorption become very strong at around 0.1keV, so that detecting a soft excess and accurately measuring its parameters will depend somewhat on how accurately the interstellar absorption can be determined.

Even with these challenges, a soft excess in the low-hard state has previously been reported in several sources. The first was Cyg X-1 (Balucinska-Church et al. 1995; Di Salvo et al. 2001), although its association with an accretion disk is complicated by the fact that Cyg X-1 is a high mass X-ray binary accreting from a wind. This question was also the focus of two recent papers, Miller et al. (2006a,b), in which the authors studied long-exposure *XMM-Newton* spectra of two different GBHCs, SWIFT J1753.5-0127 and GX 339-4, at low luminosities ( $L_X/L_{\text{Edd}} \sim 0.003 - 0.05$ ). Soft excesses at similar luminosities in these two sources have also been reported in Ramadevi & Seetha (2007) (J1753.5-0127) and Tomsick et al. (2008) (GX 339-4). Since these two observations, there have also been observations of soft excesses in several other sources. Rykoff et al. (2007) made several observations of the soft component of XTE J1817-330 with *Swift* during the outburst decline of that source down to a luminosity of  $L_X/L_{\text{Edd}} \sim 0.001$ , while a soft component in GRO J1655-40 has been reported by both Brocksopp et al. (2006) and Takahashi et al. (2008) using different

telescopes.

To interpret the soft excesses in SWIFT J1753.5-0127 and GX 339-4, Miller et al. (2006a,b) fit the data with a several *XSPEC* models, trying various black-body disk models and simple hard X-ray components (both a power law and various Comptonization models). In GX 339-4 a broad Fe-K line was also observed and fit with a relativistically broadened reflection model. Using blackbody models for a standard accreting disk, the authors found disks with maximum temperatures of  $kT \sim 0.2\text{-}0.4$  keV, and inner radii consistent with the innermost stable circular orbit of a black hole.

At the inferred low accretion rates in the hard state, a disk extending to the last stable orbit would produce a soft X-ray component with peak close to the cutoff due to interstellar absorption. Unless an accurate independent measure of the interstellar absorption column is available, spectral fitting procedures cannot reliably distinguish between a thermal peak at  $kT = 0.3$  keV with one interstellar absorption column and a cooler component with a lower energy component cutoff by a slightly higher interstellar absorption column.

For energetic reasons the hard X-ray component which dominates the luminosity in the hard state must originate near the black hole, the same region as the proposed cool disk. Some form of interaction of hard X-rays with the cool disk must take place, and this implies that the isolated cool disk models used as ‘components’ in fits to observed spectra are unrealistic. In fact, most models for the hard X-ray component include some prescription for the reprocessing of hard into soft radiation, whether these be truncated disks or extended disk models. As shown by Haardt and Maraschi (1991), such models generically produce a similar energy flux in soft and hard X-rays. A strong soft component is thus a natural consequence in truncated as well as extended disk models for the hard state.

The main difference in a truncated disk model is that the soft flux originates from a larger surface area and consequently has a lower temperature, putting its spectral peak below 0.5 keV. After interstellar absorption the soft component has a peak around 0.5 keV that can be mistaken for an apparent thermal peak with the temperature of a disk near the last stable orbit.

In this paper we examine this with a more quantitative model for truncated disks. At the inner edge of a truncated disk the accretion flow must change in nature from a relatively cool, thin disk into a much hotter, vertically-extended inner flow. There will thus necessarily be some interaction between the two, either through radiation (e.g. Haardt & Maraschi (1991)) or matter exchange (Spruit 1997), or both. Our goal is to determine whether such a model could reproduce the soft spectral components reported by Miller et al. (2006a,b). We will find that disks truncated at 15–20 Schwarzschild radii can in fact produce soft components of the observed strength and shape. An alternative model investigating re-condensation from an ADAF is considered by Taam et al. (2008).

## 5.2 PHYSICS OF INTERACTION REGION

### 5.2.1 Origin of soft excesses

Determining the inner radius of an accretion disk from its spectrum relies on (among other things) an accurate understanding of how luminosity in the disk is produced. In the higher luminosity “high-soft” state, (approximately) blackbody flux from the disk dominates the spectrum. The disk’s inner radius can be inferred, provided the distance and inclination of the source are known, from the assumption that the radiation is produced by internal viscous dissipation in the disk as it accretes, and an assumed ‘color correction’ to the blackbody spectrum.

However, when the spectrum becomes dominated by very hard X-ray and  $\gamma$ -ray radiation, the radial temperature and luminosity profile of the disk will depend on the interaction between the hard radiation and the disk. This is because most of the accretion power is now in the hot gas producing the hard radiation, some of which will interact with the cool disk (as is seen in the reflection spectrum and Fe fluorescence), and may provide a substantial source of heating. This heating of the disk surface converts the hard radiation into a soft component. In the simplest version of this model, Haardt & Maraschi (1991) calculated the energy balance for a hot corona covering a cool disk and found that the flux in the soft and hard components will be roughly equal. This predicts that a substantial soft X-ray component is a universal feature of the hard-state spectrum, whether the disk is truncated or not. Its detectability depends on the sensitivity of detectors in the 0.1-1 keV range, and the interstellar absorption column.

For models in which a cool, truncated accretion disk encircles a very hot inner flow (which cools through inverse Compton scattering), there will necessarily be a region of interaction near the truncation radius, which will heat the inner edge of the disk. This will come either from hard photons bombarding the disk as in the Haardt-Maraschi model, or through matter interaction, with hot protons from the inner flow directly colliding with the cool disk. In both cases previous work has shown that a soft component is produced, but a more detailed model is needed to predict the radiation spectrum. The first case, examining the structure of a thin accretion disk bombarded by hard photons has been studied by for AGN disks Ballantyne et al. (2001) and Nayakshin & Kallman (2001), and more recently for GBHC disks by Ross & Fabian (2007). In this paper we focus on the second case, in which a moderately truncated disk is embedded in a hot, two-temperature advection-dominated accretion flow (ADAF).

### 5.2.2 Definition of the model

We begin with the results from a prototype model for ion bombardment on cool disks, initially proposed by Spruit (1997), and extended in Spruit & Deufel (2002), Deufel et al. (2002) and Dullemond & Spruit (2005) (hereafter DS05). In this model a cool disk is em-

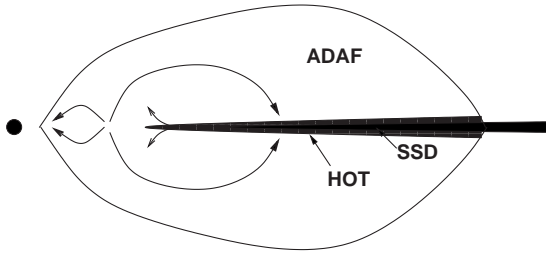


**Figure 5.1:** Schematic structure of a cool disk embedded in an ADAF. Here the ADAF (the transparent outer region) extends over the inner edge of the cool Shakura-Sunyaev disk (SSD), shown by the solid thin disk, bombarding it with high energy protons ( $kT_p \sim 20$  MeV). This evaporates the surface of the disk into a ( $kT_e \sim 70$  keV) corona, called here the hot layer (HOT LAYER, hatched). The higher viscosity of the hot layer causes it to spill over the inner edge of the SSD where cooling through inverse Compton scattering is no longer efficient (HOT RING), and thermal instability causes the layer to evaporate into the ADAF. The mass transfer is represented by the small arrows.

bedded in a two-temperature ADAF in which the protons are close to their virial temperature ( $\sim 20$  MeV). The protons bombard the disk, and are stopped via Coulomb collisions with the disk's electrons, thus transferring their energy to the disk. The energy from the protons is sufficient to evaporate the upper layers of the disk into a hot corona with  $kT_e \sim 60 - 80$  keV (called the "hot layer" in our nomenclature, although the temperature in this layer is still much cooler than the virial temperature), whose temperature is set by a balance between heating from the ions and cooling, predominantly through inverse Compton scattering of disk photons. Deufel & Spruit (2000) found that the optical depth of the hot layer is around unity, varying only weakly with irradiating flux and distance from the hole.

The higher viscosity of the hot layer also allows it to spill over inside the inner edge of the cool disk (see fig. 5.1). Using 1-D simulations, Deufel et al. (2002) suggested that the lack of seed photons in this layer will cause the temperature to rise to about  $kT_e \sim 200 - 300$  keV, since cooling from inverse Compton scattering will be much less efficient. Spruit & Deufel (2002) found that this region will become unstable and evaporate into the ADAF. This shows how an ADAF can be maintained inside a truncated cool disk. The key for the whole process is the presence of a component of intermediate temperature (the hot layer). On one hand this component produces a hard, Comptonized spectrum, while on the other its evaporation feeds the ADAF.

DS05 extended this work to examine the radial dependence of the three components of the flow. They set up a model in which the truncation radius of the cool disk is a free pa-

parameter, and the three layers are assumed to interact only via the mass transfer processes outlined above. They assumed the cool disk was a standard Shakura-Sunyaev disk (Shakura & Sunyaev 1973), and that the ADAF flow temperature followed the model of Narayan & Yi (1994). They approximated the temperature in the hot layer to be constant, and also assumed a constant temperature for its extension inside the inner edge of the cool disk (which we will call here the “hot ring”)<sup>1</sup>. With these assumptions, the radial profiles of the three components can then be determined by solving the equations for mass and angular momentum conservation for a thin disk.

This simplified analysis yields for each component estimates of the mass accretion rate  $\dot{M}_i$ , heating rate  $Q_i$  (from internal viscous dissipation and ion heating), and surface density  $\Sigma_i$  as a function of radius. For further discussion of the model, see sect. 2 of DS05.<sup>2</sup> The input parameters for the model are the black hole mass  $M_{BH}$ , the magnitude of the  $\alpha$  viscosity parameter (Shakura & Sunyaev 1973), and the truncation radius  $R_{SSD}$  for the disk. A sketch of the model with its various components is seen in fig. 5.1. Assuming we know the dominant radiation mechanisms, we can determine the spectrum from the resulting energy distribution for each layer. This is the primary goal of the current work.

### 5.2.3 Energy and mass balance

The three components of the model exchange mass and energy. In the steady state assumed here, the sources and sinks balance in each. The topmost layer, the ADAF, loses mass and energy to the hot layer, at rates per unit area of the order  $c_{s,i}\rho_i$  and  $c_{s,i}w_i$ , respectively. Here  $c_{s,i}$ ,  $\rho_i$ , and  $w_i$  are respectively the thermal speed in the ADAF (i.e. near the virial speed or orbital velocity), the density, and enthalpy. Depending on its radiative efficiency the ADAF could make a substantial contribution to the hard X-ray flux in addition to the flux from the ion-heated hot layers. For our prototype model we ignore this contribution, since Esin et al. (1997) estimate the efficiency of an ADAF to be about  $\epsilon \sim \dot{m}\alpha^2 \simeq 1.5 \times 10^{-4}$  (where  $\dot{m}$  is the accretion rate scaled in terms of Eddington). If this is the case, the luminosity of the ADAF will scale with  $\dot{m}^2$ , while the energy influx into the cool disk scales as  $\rho_i \sim \dot{m}$ , (since  $T \sim T_{vir}$  in the ADAF), meaning that the ADAF’s indirect contribution to radiation through heating the cool disk will dominate at low luminosities. However, the radiative efficiency of hot inner ring is strongly model dependent, and may be much higher, which would make the spectral contribution of the ADAF important. We discuss this question further in sect. 5.4.

There is a mass flux by evaporation from the hot layer into the ADAF, as derived in Spruit & Deufel (2002). The energy flux into the ADAF associated with this evaporation can be neglected, since the temperature of the hot layer is low compared with the temper-

<sup>1</sup>The nomenclature we adopt in this paper is slightly different from DS05. They referred to the ADAF as an “ISAF”, or Ion-Supported Accretion Flow, while what we have called the “hot inner ring” they term the “hot layer”, and our “hot surface layer” is in that paper referred to as the “warm layer”.

<sup>2</sup>We note that in that work the numerical factor of equation (2) is incorrect, it should be  $2.64 \times 10^8$ , and equation (3) should be the same as equation (16) in Spruit & Deufel (2002).

ature of the ion flow. The hot layer is heated in similar measure by viscous dissipation and the hot ions it absorbs from the ion flow above ( $Q_{visc,w} = 2 \times 10^{16}$  ergs $^{-1}$ cm $^{-2}$ , and  $Q_{i,w} = 7 \times 10^{15}$  ergs $^{-1}$ cm $^{-2}$ , respectively for the reference model). It is cooled by Compton upscattering of disk photons passing through it, which will produce a hard X-ray spectrum.

There is also a mass flux feeding mass into the hot layer from the cool disk underneath; it is parametrized as in sect. 2.2 of DS05. The cool disk is heated in three ways: by internal viscous dissipation, by reprocessing of hard (Comptonized) X-rays from the hot layer above, and by the (small) number of hot ions from the ADAF that pass through the hot layer.

The reprocessing of the hard X-rays is further divided into a fraction  $a$  that is *reflected*, and a fraction  $(1 - a)$  that is absorbed and assumed to thermalize completely. The reflection process and the spectrum resulting from it are based on results from the literature; this is described in sect. 5.2.4. The spectrum of the cool disk feeding photons to the Comptonization process in the hot layer thus consists of a blackbody component plus a reflection spectrum.

The surface temperature of the cool disk, assumed to be close to its effective temperature, is given by

$$\sigma_B T_{eff}^4 = Q_{c,visc} + (1 - a)F_h^- + f_c Q_i, \quad (5.1)$$

where  $Q_{c,visc}$  is the viscous heating rate of the cool disk  $c$ ,  $a$  its X-ray reflection albedo,  $F_h^-$  the flux of downward directed X-ray photons from the hot layer  $h$ , and  $f_c Q_i$  the fraction  $f_c$  of the energy flux  $Q_i$  in hot ions that make it through the hot layer and are absorbed instead in the cool disk. The albedo  $a$  of the disk depends on how ionized the disk is, which we discuss more in sec. 5.2.4.

Compton upscattering of the soft flux from the cool disk determines the detailed shape of the spectrum emerging from the hot layer. In addition there is an X-ray component from the ‘hot ring’ interior to the inner edge of the cool disk. Since it receives fewer of the soft photons and hence is hotter, it adds a harder component to the spectrum.

These ingredients are the same as in DS05, except that the reflection process is included more realistically, and the Comptonization of soft photons is treated in detail with the Monte Carlo code of Giannios (see sec. 5.3) so a realistic X-ray spectrum is obtained.

## 5.2.4 Reference model

We illustrate the model first with representative parameter values for a black hole binary. In sects 5.3.1 and 5.3.2 the parameters are adjusted for application to observations of specific objects.

We take  $M_{BH} = 10M_\odot$  for the mass,  $R_{in} = 20R_S$  for the truncation radius (where  $R_S = 2GM/c^2$  is the Schwarzschild radius). A typical if somewhat large viscosity parameter  $\alpha = 0.2$  is used for all accretion components. The flow model of DS05 yields an accretion rate of  $\dot{M} = 3.1 \times 10^{16}$  g/s for these parameter values. In terms of the Eddington accretion rate (defined here with an assumed bolometric efficiency of 10%) this translates to  $\dot{M} = 2.2 \times$

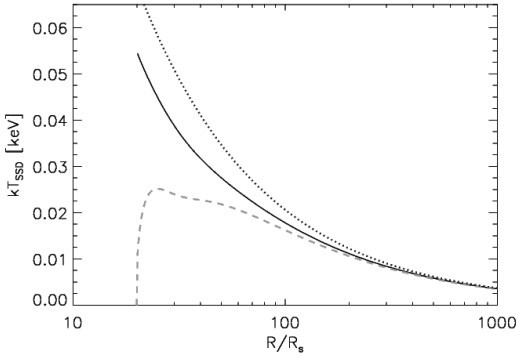


**Figure 5.2:** Effect of ion-bombardment on the surface temperature of a cool (SSD) disk with inner edge at  $20R_S$  (for the other model parameters see text). Black solid line: radial temperature profile when disk heating is considered. Green dashed line: radial temperature profile in disk without considering heating from hot layer. Blue dotted line: radial temperature profile for an untruncated disk at the same accretion rate.

$10^{-3}\dot{M}_{\text{Edd}}^3$ , and bolometric luminosity is  $L_X = 4.2 \times 10^{-4}L_{\text{Edd}}$ , which is significantly lower than observed luminosities for the low/hard state. We discuss this discrepancy and possible solution further in sects 5.3 and 5.4.

In fig. 5.2 we show the temperature profile of the cool disk component of this reference model. The dashed line shows the temperature profile that would result if only the viscous dissipation in the cool disk were included. The cool disk is completely evaporated into the hot layer before the inner edge of the accretion disk, hence its surface density drops to zero at the inner edge of the disk in the same way as for a standard cool disk accreting on a slowly rotating object (the standard “zero-torque inner boundary condition”). If there were viscous coupling between the inner edge of the disk and the hot ring, however, the resulting temperatures near the inner edge would be higher than in our current model. This would result in a stronger soft component, whose contribution would remain observable for larger truncation radii than we have considered here. The solid line shows the effect when heating from the hot layer is included. As can be seen in the figure, the effect of heating extends to large radii. The dotted line shows the temperature profile for an standard untruncated disk for the same accretion rate.

We can also compute the bolometric radiative efficiency for the model, assuming that the hot layer and inner ring radiate efficiently. For our reference model with a disk truncated at  $20R_S$ , we find a radiative efficiency (the ratio of the total luminosity to the accreting rest-mass energy flux) of about 4%. In comparison, the radiative efficiency of a disk truncated at  $20R_S$  alone is about 1%, which demonstrates that the ion-bombardment process can significantly increase the radiative efficiency.

<sup>3</sup>In DS05 a plotting error resulted in the mass accretion rates in all figures being overstated by a factor of 100 with respect to the Eddington rate.

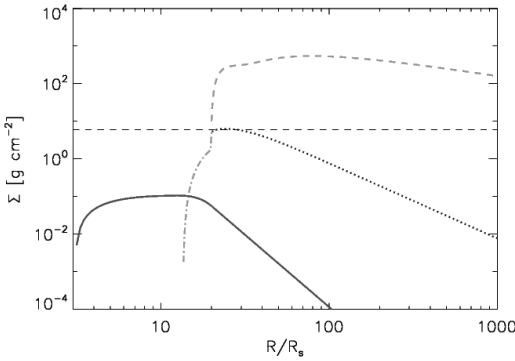


**Figure 5.3:** Surface density ( $\Sigma$ ) profile for reference model, where  $M_{BH} = 10M_{\odot}$ ,  $\alpha = 0.2$  and  $R_{ssd} = 20R_s$ . Green dashed line: Shakura-Sunyaev disk. Blue dotted line: Hot layer. Orange dash-dotted line: Hot ring. Red solid line: ADAF.

### Cool disk emission

We begin by estimating the spectrum of the radiation produced by the thin disk, i.e. the seed photons of the Comptonization in the hot layer. At large effective optical depths in the disk the radiation field is a blackbody. The flux emerging from the photosphere of the disk is reduced, however, by Thomson scattering, resulting in a ‘modified blackbody’, a spectrum with same temperature but reduced flux. In the literature, it is often described equivalently by a ‘color correction’ factor  $f_{col}$ , measuring the effect instead as the ratio of color temperature to effective temperature,  $T_{col} = f_{col}T_{eff}$ . Several papers have done extensive calculations of this spectral hardening in the outer layers of a disk dominated by electron scattering, including Shimura & Takahara (1995), Merloni et al. (2000), and Davis et al. (2005), and concluded that the the color-correction is of the order  $f_{col} \simeq 1.4 - 2$ , with the magnitude of correction increasing gradually as the luminosity increases. The approximation of a single parameter across the entire spectrum become less good as the flux decreases.

In a cool disk the (vertically integrated) viscous dissipation  $Q_{visc}$  is balanced by radiative loss at its surface,

$$Q_{visc} = \sigma_B T_{eff}^4 = \sigma_B (T_{col}/f_{col})^4. \quad (5.2)$$

The value for  $f_{col}$  will change the determination of the inner disk radius, since the luminosity will be depressed by a factor of  $f_{col}^{-4}$  relative to the temperature, so that when color correction is considered, the inner radius of the accretion disk will be increased by a factor  $f_{col}^2$ .

In this work we have the additional complication of the hot surface layer, which will heat the upper layers of the disk substantially and may change the spectral hardening. Ross & Fabian (2007) have estimated the effects of incident hard X-ray radiation on galactic black hole disks, although they focus on systems in which the disk is hotter ( $kT \sim 0.35$  keV)

than ours and dominates the overall spectrum. However, they do find substantial spectral hardening, and disk temperatures which increase with increasing X-ray flux (fig. 4 of that paper). They also find that the incident radiation can change the ionization structure of the upper layers of the cool disk, so that the shape of the disk spectrum is significantly altered by absorption lines (see their fig. 6).

Since it is beyond the scope of this work to do a similar radiation transfer calculation, we instead choose a single color correction factor,  $f_{col} = 1.7$  as a typical value for all our models.

### Reflection spectrum

The hard flux incident on the cool disk undergoes reprocessing by electron scattering and atomic processes, giving rise to a series of emission lines (especially the Fe-K fluorescence line) and a Compton reflection hump. In the course of these processes, part of the incident energy flux ends up heating the plasma. Detailed calculations of these processes is beyond the scope here. Instead, we simplify the physics by separating the incident flux into a reflected part and a part that is treated as being absorbed. We treat the absorbed part in the same way as the energy input by viscous dissipation in the disk, i.e. a fraction  $(1 - a)$  is added to the left hand side in (5.2).

The remaining part is treated by a modified version of the XSPEC model “REFLION” described in (Ross & Fabian 2005). This model calculates the reflection spectrum of a power law flux between 0.1-300 keV hitting a constant density AGN disk. We set the lower cutoff of this power law at 0.2 keV, since we expect disk temperatures around 0.1 – 0.2 keV. REFLION calculates the reflection spectrum for a fixed ionization parameter,  $\xi \equiv 4\pi F_X n_H^{-1}$ , the ratio of the incident flux on the disk to the hydrogen number density. The disk, however, is stratified, so an estimate has to be made of the depth in the disk atmosphere where most of the reprocessing takes place. We assume here that this depth is just the electron scattering photosphere of the cool disk,  $\tau_{es} = 1$ . By hydrostatic balance, the pressure at this depth is approximately

$$P \simeq \frac{g}{\kappa_{es}}, \quad (5.3)$$

where  $g$  is the vertical component of the acceleration of gravity at the height of  $\tau_{es} = 1$  above the midplane. Assuming this height is about twice the nominal disk thickness  $H = c_s/\Omega_K$ , the pressure is  $P \simeq 2c_s\Omega_K$ . Here  $c_s$  is the sound speed at the midplane of the disk, which is determined from the heating rate  $Q_{visc}$  by a standard thin disk model. To fix the density corresponding to this pressure the temperature has to be determined. We assume for this the effective surface temperature  $T_{eff}$  that follows from the viscous heating rate. If  $F_h^-$  is the incident X-ray flux from the hot layer, the ionization parameter is then

$$\xi \simeq \frac{2\pi F_h^- k T_{eff} \kappa_{es}}{\Omega_K c_s}. \quad (5.4)$$

The value of  $\xi$  varies with distance  $r$  from the black hole; an energy-weighted mean is  $\xi \simeq 10 \text{ erg cm s}^{-1}$  for the reference model. We use this as a representative value for the reflection calculation instead of an integration over the disk. For this value of  $\xi$ , the resulting albedo is low ( $\simeq 0.2$ ), so that most of the hard flux is absorbed and thermalized in the disk. The total reflection and disk spectrum (before being passed through the hot layer), is seen in the red long-dashed line in fig. 5.4. This is the input spectrum for the Comptonization by the hot layer. Since the optical depth of the hot layer is only around unity, it will also make a significant direct contribution to the output spectrum.

### Uncertainties in the reflection spectrum

Through its effect on the gas density, the temperature assumed in the reprocessing region has a direct effect on the ionization parameter and the resulting reflection spectrum. Unfortunately, there is a significant uncertainty in this temperature, since it depends itself on the ionization parameter. At low densities higher in the atmosphere, the ionization parameter is high and the temperature will be close to the Compton temperature of the incident X-ray spectrum. For our reference model, this would be around 3 keV. Deeper in the atmosphere, the ionization parameter would be lower and the temperature closer to equilibrium with the energy density of the radiation field, of the order of the effective temperature of the cool disk. Since the transition between these regimes takes place around the reprocessing layer itself, all depends on details of the radiation physics.

Several groups (Ballantyne et al. 2001; Nayakshin et al. 2000) have calculated the change in the vertical structure of AGN disks as a result of incident hard radiation, and found the upper layers become stratified, with the top being heated to close to the Compton temperature and a sharp transition to the inner layer which radiates at the disk's effective temperature. They find that this stratification will change the disk's reflection properties substantially. Although Ross & Fabian (2007) study a similar situation in galactic black holes, and find no similar stratification, they focus on cases in which the disk dominates the luminosity. For lower disk temperatures stratification could presumably still occur. However, Nayakshin & Kallman (2001) studied the case where a disk was overlaid with a surface corona, and included the effect of its weight on the gas pressure. They found that this was sufficient to prevent stratification.

An additional caveat in using the constant density models of Ross & Fabian (2005) is that they consider AGN disks, which are much cooler and less dense than those in GBHCs. As a result, the reflection spectra do not consider the flux in the disk itself (which can change the ionization state significantly), and the effects from things like three-body recombination, which will become important as the disk densities become higher. Recent work by Ross & Fabian (2007) has examined reflection spectra in GBHCs, although they focus on systems in which the disk dominates the spectrum and is hotter ( $kT_e = 0.35 \text{ keV}$ ) than the disks considered in this work.

### Comptonization

To calculate the spectrum from inverse Compton scattering through the hot layers of the disk we use a one-dimensional Monte Carlo simulation. The radial variation of quantities in the disk and hot layer is replaced by representative values, for which we use energy-weighted means. The simulation assumes a slab geometry, with the cool optically thick disk below a much hotter surface layer with moderate optical depth. For the seed photons, we use the disk+reflection spectrum found in the previous two sections. To capture the emission lines in this spectrum, we set the resolution of the simulation to  $\Delta E/E = 0.046$ . The number of seed photons followed through the hot layer is of the order  $10^7$ , sufficient to represent the result to a noise level comparable with typical observations. The output spectrum is angle dependent (because of the increasing optical depth with inclination), so a value has to be assumed for the inclination angle  $\theta$  to the line of sight (measured from the normal of the disk). For our reference model we use  $\mu = \cos \theta = 0.5$  as a representative value.

The input parameters of the Comptonization calculation are the input spectrum, the optical depth and the temperature of the hot layer. The resulting total energy flux in Comptonized photons (integrated over the spectrum and summed over both sides of the hot layer) has to match the energy input into the hot layer: the sum of ion heating and viscous dissipation. We can estimate the optical depth for the hot layer from the surface density of the hot layer, where  $\langle \tau \rangle = \kappa_{es} \langle \Sigma_{\text{Hot}} \rangle$ . The temperature of the hot layer is adjusted iteratively in the calculations to meet this condition to an accuracy of 10%. For the reference model, we find  $kT_e = 70\text{keV}$ , and  $\tau = 0.87$ . The resulting emergent spectrum of the hot layer is shown in the blue dotted line in fig. 5.4, for an inclination angle of  $\mu = 0.5$ . The photon index of this spectrum in the range 2-10 keV is about  $\Gamma = 1.96$ .

### Treatment of the hot ring

In the hot ring (where the hot layer has spilled over inside inner edge of the cool disk) there is no underlying cool disk any more and it receives its soft photons only by scattering from larger distances: it is ‘photon starved’ compared with the hot layer itself. Since the energy input by ion heating and viscous dissipation are still similar, the temperature is higher and Comptonization correspondingly stronger. The hot ring therefore makes its contribution mostly at the high energy end of the spectrum, and is less important for the ‘soft component’ of the spectrum that is the focus of our study. We include it, however, since we also want to achieve a reasonable fit to the overall spectral energy distribution in the observations discussed in the next sections.

The calculation of DS05 relied on the earlier one-dimensional work of Deufel et al. (2002) in order to set the temperature and energetic contribution from the hot inner ring, which predicts a very small contribution from the hot ring. With a sufficiently detailed geometrical model for the hot ring, the soft photon input by scattering could in principle be modelled more accurately, but the level of detail needed is probably beyond the limits of the present model. We therefore treat the soft input flux in this component of the model as

an adjustable unknown when fitting to spectra. For this, we introduce a parameter  $\zeta$ , which represents the fraction of seed photons from the cool disk that cool the hot layer, so that  $1 - \zeta$  goes to cool the hot ring. For the reference model,  $\zeta$  is set by the contribution predicted from the DS05 model for the hot inner ring.

Also treated as adjustable is the temperature reached by equilibrium between heating and Comptonization. We assume that cooling in this region is still moderately efficient, choosing temperatures in the range  $kT_e = 180 - 200$  keV. For simplicity (since the angular distribution of seed photons is also uncertain) we model the hot ring with a plane-parallel Monte Carlo simulation with the same resolution as in the hot layer. We discuss the limitations of this approach in sect. 5.4.

As in the hot layer, the X-ray energy flux produced by Comptonization has to match the energy input by viscous dissipation and ion heating. Together with the now assumed value for the temperature, this determines  $\zeta$ , and the optical depth of the ring. For the reference parameters of this section, we find  $\zeta = 0.99$  and an optical depth of  $\sim 0.7$ . At a temperature of 200 keV we find that the ring contributes only 11% of the overall hard flux ( $F_X = 2 - 200$  keV) for the reference values  $\alpha = 0.2$  of the viscosity and  $R_{in} = 20R_S$ .

This is because the radial width of the hot ring has a rather limited extent, since the evaporation process is very efficient. The hot layer evaporates very quickly after it has flowed over inner edge of the cool disk. The hot Comptonized component from the hot ring is shown in the orange dash-dotted line in fig. 5.4.

### 5.2.5 Results for the reference model

The final spectrum and its various components is shown in the top panel of fig 5.4. The accretion rate for the reference model is  $\dot{M}/\dot{M}_{\text{Edd}} = 0.002$  assuming an efficiency of 10%, while the luminosity in the 0.5-10 keV range is  $L_X/L_{\text{Edd}} = 10^{-4}$ . The total spectrum is shown in black. The individual components run as follows. The green thermal component (dash-double dotted line) shows the spectral contribution from the outer part of the disk where the hot layer is no longer significant (outside  $R/R_S = 100$ ), while the red long-dashed component shows the rest of the disk and reflection spectrum. For the reference model the reflection ionization parameter is small enough that the reflection and iron line are not apparent in the final spectrum, although we again stress that we are using a reflection model developed for AGN, so in reality the reflection could be stronger. The blue dotted line shows the Comptonized spectrum from the hot layer, while the orange dash-dotted line shows the Comptonized spectrum from the hot ring. Fitting the overall spectrum with a photon index  $\Gamma = 1.91$  in the 1-10 keV range, we see a small soft excess below 0.5keV, even though the maximum disk temperature is only 0.05keV. The bottom panel of fig 5.4 shows the total spectrum divided by a power law with  $\Gamma = 1.91$ . The observed deviation from a single power law in the hard part of the spectrum (which leads to a deficit around 1 keV and a harder power law index above 10 keV) is caused by anisotropic Comptonization resulting from considering a plane-parallel configuration (see e.g. Haardt (1993) and sect. 5.4 of this

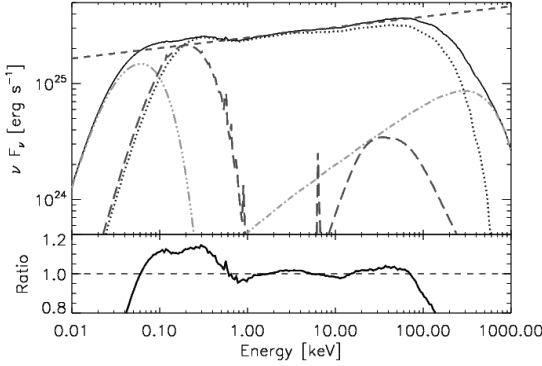


**Figure 5.4:** Top: Relative contribution from each component for reference model,  $\alpha = 0.2$ ,  $R_{in} = 20R_s$ ,  $M = 10M_\odot$ . Red long-dashed line: Spectrum from the disk (modified blackbody plus reflection spectrum). Green dash-double dotted line: Spectrum from outer disk. Blue dotted line: Comptonized spectrum from hot layer. Orange dash-dotted line: Comptonized spectrum from hot ring. Black: total spectrum. Red short-dashed: power law with  $\Gamma = 1.9$ . Bottom: Total spectrum divided by power law with  $\Gamma = 1.9$ .

paper), and also by the contribution from the hot ring. Except for the very low accretion rate, we see a spectrum that is qualitatively similar to those of Miller et al. (2006a) and Miller et al. (2006b).

### 5.3 COMPARISON TO OBSERVATIONS

The luminosity of our reference model described above, of the order  $10^{-4}L_{\text{Edd}}$  is substantially lower than the luminosities (of the order  $3 \times 10^{-2}$ - $10^{-3}L_{\text{Edd}}$ ) inferred for the observed sources to which we want to apply the model. This is a consequence of the flow model in DS05 that is the basis of our analysis. In it, the surface density of the hot layer is governed by the physics of the Coulomb interaction of the hot ions penetrating through it, and its temperature by the energy balance between it and the underlying disk. With temperature and surface density constrained in this way, the mass flux then depends only on the radial drift speed, i.e. the viscosity parameter,  $\alpha$ . The actual mass flux is low because the temperature of the layer is only about 80keV. This suggests that the current model is incomplete, and we discuss a possible solution in sect. 5.4. In this paper, however, we solve this problem by introducing a parameter,  $C$ , by which the accretion rate (or equivalently the energy output of each component of the flow) is increased. This makes the implicit assumption that increasing the accretion rate causes the energy output in each component to increase, but the relative contribution of each component to the overall energy budget and geometric configuration of the flow to stay constant. Scaling the accretion rate in this way increases the luminosity in all components, which thus causes an increase in temperature for the cool disk at a fixed truncation radius.

With the introduction of the parameters  $C$  and  $\zeta$  our model loses its predictive power, but

the goal of this paper is to present a model that is plausible rather than precise in its details. In the next section we compare our spectra to the best fits from observations, and show that for reasonable values of the hot layer and inner ring and accretion rate, we can reproduce the observed soft excesses using a significantly truncated accretion disk.

To illustrate how our model can be made consistent with observed soft excesses, we perform a qualitative comparison between the soft excesses observed in SWIFT J1753.5-0127 (Miller et al. 2006a) and GX 339-4 (Miller et al. 2006b) and our model. For each object we use the estimates for black hole mass, inclination and distance to source presented in those two papers and take  $\alpha = 0.2$  as a standard value for the viscosity parameter. We then assume a moderate truncation radius and find a solution for energy and surface density as was discussed in sect. 5.2, and calculate the spectrum. We change  $C$  (the accretion rate) and  $\zeta$  (the ratio between seed photons in the hot layer and inner ring) in order to match the luminosity and spectral index of the best fit to the observed spectrum, and compare our soft excess to the observed one. If necessary we also change the amount of interstellar absorption, although for both the cases we consider we do not need to change it very much. Given the systematic uncertainties in our model, a more statistical comparison to the data is not possible; our goal is instead to demonstrate that we are able to reproduce the observed spectra with physically reasonable parameters.

### 5.3.1 SWIFT J1753.5-0127

We begin with the spectrum from the source SWIFT J1753.5-0127. Miller et al. (2006a) took a 42 ksec *XMM-Newton* observation and estimated an X-ray luminosity (0.5-10 keV) of  $L_X/L_{\text{Edd}} = 2.6 \times 10^{-3} (d/8.5\text{kpc})^2 (M/10 M_\odot)$ . They fit the spectrum to a power law with a photon index  $\Gamma = 1.67$  (2-10 keV), and interstellar absorption of  $N_{\text{H}} = 2.3 \times 10^{21} \text{ cm}^{-2}$ . Fitting the spectrum with an absorbed power law component alone reveals a small soft excess below 2 keV, which they fit to a disk with  $kT_{\text{in}} \simeq 0.22 \text{ keV}$  and  $R_{\text{in}} \simeq R_{\text{S}} (M/10M_\odot) (d/8.5\text{kpc})/\cos^{1/2} i$ .

A very truncated disk will be too cool to be observable in X-rays, while an untruncated disk will have a higher temperature than is observed (because of the effects of heating from the corona). To compare with the observed spectra we assume a moderate truncation radius of  $15R_{\text{S}}$ , which is qualitatively very different from an untruncated disk (which will have an inner radius between  $0.5 - 3R_{\text{S}}$  depending on the spin of the black hole). We make the same assumptions for mass ( $M = 10M_\odot$ ) and distance ( $d = 8.5\text{kpc}$ ) as in Miller et al. (2006a) and assume an inclination of  $\mu = 0.5$ . The simulation then predicts an accretion rate of  $\dot{M}/\dot{M}_{\text{Edd}} = 1.5 \times 10^{-3}$  for an efficiency of 10%. In order to match the measured flux in the power law component, we increase the flux in each component by a factor  $C = 12$ , to give an accretion rate  $\dot{M}/\dot{M}_{\text{Edd}} = 1.7 \times 10^{-2}$ .

In the hot layer, the predicted surface density profile gives the optical depth  $\langle\tau\rangle = 0.87$ , and the energy balance between the cool disk and hot layer (see sect. 5.2.3) determines a

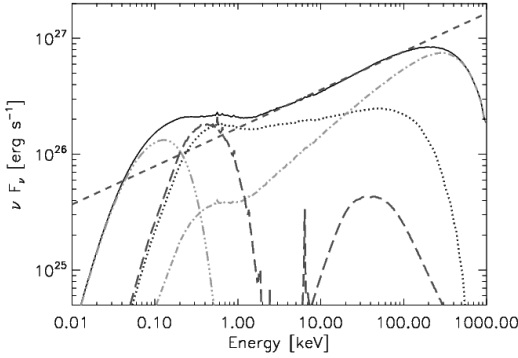


**Figure 5.5:** Model spectrum for SWIFT J1753.5-0127, for a truncated disk with inner radius of  $15 R_S$  with  $\alpha = 0.2$  and  $M = 10M_\odot$ . Red long-dashed line: Spectrum from the disk (modified blackbody plus reflection spectrum). Green dash-double dotted line: Spectrum from outer disk. Blue dotted line: Comptonized spectrum from hot layer. Orange dash-dotted line: Comptonized spectrum from hot ring. Black: total spectrum. Red short-dashed: power law with  $\Gamma = 1.66$ .

temperature of  $kT_e = 75$  keV, which gives a photon index of  $\Gamma = 1.87$  (3-10 keV).<sup>4</sup> The density of the disk and flux in the hot layer also allows us to estimate the ionization parameter,  $\xi = 50$  erg cm s<sup>-1</sup>, from which we get an albedo and find that the Comptonized flux incident on the disk heats it to  $kT_e = 0.11$  keV, which looks like  $kT_e = 0.19$  keV when spectral hardening is taken into account.

The predicted surface density in the hot inner ring also allows us to calculate the optical depth of this layer, which we find to be  $\langle\tau\rangle = 0.7$ . Since we do not have a detailed model for the radiative transfer in this component, we take a plausible value of  $kT = 200$  keV, which gives a photon index of  $\Gamma = 1.39$  between 2 and 10 keV. The resulting spectrum is still too soft, so we set  $\zeta = 0.89$ , meaning that 89% of the disk and reflection photons are used to seed the hot layer, while the rest seed the hot inner ring. Figure 5.5 shows the resulting spectral energy distribution for SWIFT J1753.5-0127. The different components shown in the figure are the same as in fig. 5.4.

Figure 5.6 (taken from Miller et al. (2006a)) shows the spectrum divided by an absorbed power law with an absorption column density of  $N_H = 2.3 \times 10^{21}$  cm<sup>-2</sup>. Overlaid we show their best fit using the XSPEC “diskbb+pow” model (in red) and the soft excess predicted by our model (in green). To obtain a better fit we change the absorption column density to  $N_H = 2.35 \times 10^{21}$  cm<sup>-2</sup> to render the two excesses effectively indistinguishable, even though the temperature and peak fluxes of both disks are very different. We discuss the reasons for this at the beginning of sect. 5.4.3. Figure 5.6 also shows that the deviation from a simple power law in the range 2-100 keV is less than 10%, which is consistent with observation.

<sup>4</sup>The spectral index of a Comptonizing corona will change depending on viewing angle, since the mean optical depth will change depending on whether the disk is face-on or tilted, which will harden the spectrum. To calculate the energy in the hot layer and thus its temperature we take the spectral index for the spectrum integrated from 0°-180°.

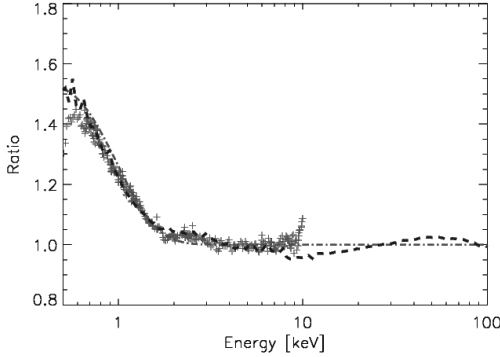


**Figure 5.6:** The soft excess in SWIFT J1753.5-0127. The crosses show the observed spectrum divided by a simple power law fit above 3 keV with a best-fit column density of  $N_{\text{H}} = 2.3 \times 10^{21} \text{cm}^{-2}$ , taken from fig. 2 of Miller et al. (2006a). The dashed-dotted red line shows the best fit two-component XSPEC “diskbb+pow” (as reported in Miller et al. (2006a)). The dashed blue line shows the ratio between our best fit model (see fig. 5.5) and the same power law, with an increase of  $0.05 \times 10^{21} \text{cm}^{-2}$  in interstellar absorption.

### 5.3.2 GX 339-4

Our second source for comparison is the relatively better constrained X-ray source GX 339-4. This source has an estimated mass of  $6M_{\odot}$ , distance of around 8 kpc and inclination  $\mu = 0.9$ . Miller et al. (2006b) took a 280ks *XMM-Newton* observation of this source, which they observed at a flux of about  $L_{\text{X}}/L_{\text{Edd}} \simeq 0.05(M/10M_{\odot})(D/8\text{kpc})$ . They fit the data with a moderate absorption column density ( $N_{\text{H}} = 3.72 \times 10^{21} \text{cm}^{-2}$ ) and very hard power law ( $\Gamma = 1.44$ ) and find a soft excess below 3 keV which they fit to a disk with  $R_{\text{in}} = 0.6R_{\text{S}}$  and  $kT_{\text{in}} = 0.38$  keV. Additionally, they observe a broad asymmetric Fe-K line with a maximum at 6.9 keV, from which they measure a reflection fraction of about 0.2-0.3 and ionization parameter  $\xi \sim 10^3 \text{erg cm s}^{-1}$ . Fitting the Fe-K line using relativistic broadening suggests an inner radius of  $0.7R_{\text{S}}$ .

For an assumed radius of the inner edge of the disk  $R_{\text{in}} = 19R_{\text{S}}$ , a good fit for this source is obtained with the following set of parameter values:  $C=77$  (or  $\dot{M}/\dot{M}_{\text{Edd}} = 0.15$ ),  $\zeta=0.63$ , and the temperature of the hot layer and hot ring 75 keV, and 200 keV respectively. The resulting spectral energy distribution is shown in fig. 5.7. Figure 5.8 shows the soft excess observed in Miller et al. (2006b). The luminosity enhancement factor is higher than for the SWIFT source because of the higher luminosity inferred from the observations. The ionization parameter in the reflection region is also higher, with  $\xi = 550 \text{erg cm s}^{-1}$ .

Note the structure in the data around 1 keV, which is suggestive of the structure of the interstellar absorption in this region of the spectrum. In fact, we can best reproduce the observation for a column  $N_{\text{H}} = 4.9 \times 10^{21} \text{cm}^{-2}$ , some 30% higher than found by Miller et al. (2006b).

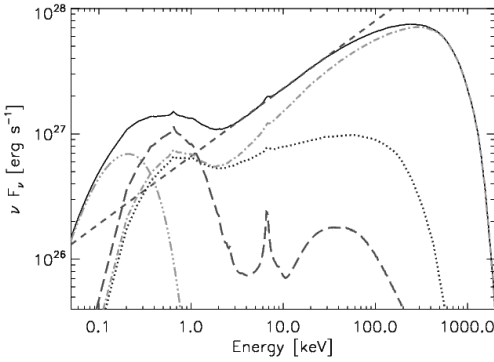


**Figure 5.7:** Model spectrum for GX339-4, for a truncated disk with an inner radius of  $19R_S$ ,  $\alpha = 0.2$  and  $M = 6M_\odot$ . Red long-dashed line: Spectrum from the disk (modified blackbody plus reflection spectrum). Green dash-double dotted line: Spectrum from outer disk. Blue dotted line: Comptonized spectrum from hot layer. Orange dash-dotted line: Comptonized spectrum from hot ring. Black: total spectrum. Red short-dashed: power law with  $\Gamma = 1.47$ .

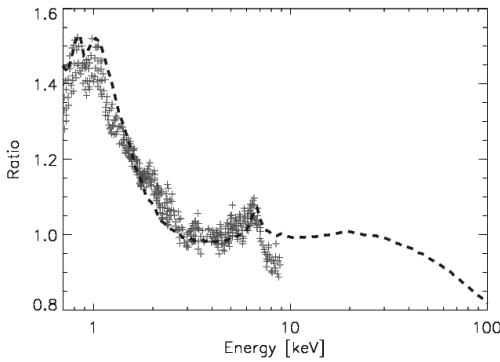


**Figure 5.8:** The soft excess in GX 339-4, taken from fig. 3 of Miller et al. (2006b). The crosses show the spectrum divided by a simple power law fit to the *XMM-Newton* and *RXTE* spectra with an absorption column density of  $N_H = 3.72 \times 10^{21} \text{ cm}^{-2}$ . The 4-7 keV range, where a broad Fe-K line is clearly visible, was omitted from the fit. The dashed blue line shows the ratio between our best fit model (see fig. 5.7) and the same power law fit with interstellar absorption  $N_H = 4.9 \times 10^{21} \text{ cm}^{-2}$ .

As is seen in fig. 5.8, we also find an Fe-K emission line in our fit, with a strength comparable to the observations. The combination of parameters that fits the overall spectral shape in our model therefore also fits the reflection component of the spectrum. Since this component depends on details of the interaction between the hot layer and the cool disk under it, this adds some confidence in this part of the physics of our model.

## 5.4 DISCUSSION

In the paper thus far we have produced spectra of an ion-bombardment model with a truncated disk for Low-Hard state accretion, incorporating a spectrally-hardened blackbody com-

ponent, physical reflection models from the literature and a Monte Carlo Comptonization calculation.

Detailed fits to observations have shown that the model can reproduce the observed soft excess, high-energy spectral index and the approximate strength of the Fe-K line in GX 339-4. We have also shown that the structure observed in the soft excess in GX 339-4 is consistent with interstellar absorption features, suggesting that the absorption column density for this source might be underestimated.

However, we have also found that further work is necessary to develop the flow model outlined in Deufel et al. (2002) and DS05. Most significantly, a large viscosity in the hot regions of the flow (the hot layer and ADAF) is required to increase the accretion rate sufficiently to match observations. This may suggest the presence of strong ordered magnetic fields in the inner regions of the accretion flow, which are also believed to be associated with observed jets.

#### 5.4.1 Mass flux in the hot layer

As was discussed in sect. 5.3, the global accretion rate in the present model is limited by the rate at which the hot layer can flow over the cool disk. The surface density and temperature of the hot layer are in turn narrowly constrained by the physics of the Coulomb interaction which allow the layer to form and the energy balance between it and the underlying disk. There are thus two ways to increase the flow rate in the hot layer: by increasing the effective viscosity or providing another mechanism besides viscous dissipation to transport angular momentum.

The interaction between the ion supported ADAF and the hot layer provides such a mechanism. The ion supported flow is partially supported against gravity by gas pressure and rotates slower than Keplerian. The mass condensing from the ADAF on the hot layer thus acts as a sink of angular momentum, which increases the mass flux in the hot layer. This effect was not included in DS05 and the calculations above. An estimate of its importance can be made by evaluating the angular momentum exchange *a posteriori* from the solutions in sect. 3. We find that, for the viscosity parameter  $\alpha = 0.2$  assumed for the hot layer, the effect increases the mass flux by a factor 2–3. The effect is thus significant, but not sufficient to increase the mass flux by the factors indicated by the comparison with observations in sect. 3.

The missing ingredient most likely to lead to the higher mass fluxes inferred from the observations may well be a strong magnetic field. Strong ordered magnetic fields in the inner regions of the flow are implied by the presence of jets, especially in the hard X-ray states discussed here. A bundle of strong ordered magnetic field held together by a disk (Bisnovaty-Kogan & Ruzmaikin 1974) can have field strengths well above those produced by magnetorotational turbulence. The angular momentum exchange by interaction of such a bundle with the disk (Stehle & Spruit 2001; Igumenshchev et al. 2003; Narayan et al. 2003; De Villiers et al. 2005) can be much more effective than turbulence parametrized with a

viscosity parameter  $\alpha \sim 1$ . This aspect is beyond the present study, and is a promising field for further study.

#### 5.4.2 Spectrum of the hot ring

The spectrum from the hot ring in our model is hard to predict without a more detailed model. The uncertainty lies chiefly in the distribution and number of seed photons available for cooling. The more photon-starved the hot ring is, the higher its temperature will be, and (since the evaporation rate into an ADAF scales with  $T_e^2$ ) the smaller its contribution to the overall spectrum. The temperature we assumed for the hot ring in practice could be much lower, which would bring it more in line with observations of the high energy cutoff observed in some spectra (which suggest a maximum temperature of about  $kT_e \sim 150$  keV). Additionally, the geometric distribution of seed photons will change the structure of the Compton spectrum. This is because photons that scatter once preferentially scatter back in the direction they were originally travelling, and there is a deficit of photons in the first scattering hump in the spectrum. This effect is most pronounced in the plane-parallel case (e.g. Haardt & Maraschi (1991)), but there will also be some anisotropy in the hot ring's spectrum if the seed photons are primarily from the disk. We have considered only seed photons from the disk, but there may also be photons produced from other processes (such as synchrotron emission) which would allow the hot ring to cool more efficiently and make the effects of anisotropy less pronounced (since the seed photons would be travelling through the hot ring in essentially random directions). Finally, in this paper we have neglected the spectral contribution from the ADAF. Depending on its radiative efficiency, its contribution could also harden the observed high-energy Comptonized spectrum considerably.

#### 5.4.3 Comparison with other work

Our model of a disk truncated at 15-20  $R_S$  and surrounding corona is qualitatively very different from the untruncated disk (with  $R_{in} \sim 1R_S$ ) models fit by Miller et al. (2006a) and Miller et al. (2006b), and it is natural to ask how the observed soft excess can be so small when the radiating area is so much larger. The answer lies in several points. The most important of these is that the temperature in our disks is about a factor 2 smaller than is found by Miller et al. (2006a), so that the flux is intrinsically much smaller and (even after the colour-correction is applied) most of the flux is cut off by interstellar absorption. There is a further reduction from the hot surface layer, which upscatters about two-thirds of the photons. Finally, the shape of the upscattered photons deviates from a power law at low energies, so that measuring the temperature of the soft excess depends very sensitively on modelling the Comptonized spectrum correctly.

The effects of irradiation on the measured truncation radius have also been studied using a more phenomenological approach in Gierliński et al. (2008), who re-analyzed the data from

J1817-330 (Rykoff et al. 2007) to demonstrate that irradiation can increase the measured truncation radius in this source (although they assume continual stress at the inner boundary of the truncated disk, which we have not done here). In particular, they note future plans to test the effects of incomplete thermalization from incident radiation (cf. sect. 5.2.4), which can further increase the truncation radius.

Several well-studied sources show some evidence of deviations from a single power law. Done et al. (2007) notes that spectra from Cyg X-1 have additional structure in their spectra that can be fit with an additional very soft Comptonizing component, while both the source GX 339-4 and Cyg X-1 sometimes show an excess of very high energy photons compared to a fit with a single power law, which suggests a second site for Comptonization that is naturally explained with this model.

For GX 339-4, Miller et al. (2006b) detected a broad Fe-K line, which they fitted with a relativistically broadened profile, implying an untruncated disk and a spinning black hole. However, the observation of a broadened Fe-K line may also be consistent with a truncated disk if the broadening instead comes from an outflow, as has been suggested in Done & Gierliński (2006) and Laurent & Titarchuk (2007).

The truncated disk picture of hard states in X-ray binaries has received support from analyses of the noise spectrum of the X-ray variability. In the model by Churazov et al. (2001), for example, the characteristic frequency at  $\sim 0.01$  Hz in Cyg X-1 corresponds to the viscous frequency ( $\sim v_r/r$ ) of a geometrically thin accretion flow at a truncation radius of about  $25R_S$ . X-ray timing data typically contain several characteristic frequencies, while theoretical models allow for different mechanisms of variability (eg. Giannios & Spruit (2004)). The model presented here does not contain enough physics to make predictions about the source and nature of X-ray variability. For reference we note that, for a truncation radius at  $20R_S$ , the viscous frequencies for our model are  $\sim 0.8$  Hz for the hot layer,  $\sim 2$  Hz for the hot ring, and  $\sim 50$  Hz for the ADAF. 1 Hz is a characteristic frequency often observed in Cyg X-1.

The physics of interaction of an ion-supported flow with a cool disk is very well defined. The process produces a hot layer of tightly constrained thickness and temperature. The physics is detailed enough, for example, to be implemented in a numerical hydrodynamic simulations of the accretion flow. The present model falls short of achieving this: the inner hot ring where the evaporation into the ADAF takes place, in particular, contains parametrizations that would need to be improved with a more detailed (2-D) treatment of radiative transfer. Thus the model used here has adjustable parameters but compared with other hot corona models there is a straightforward path to more rigorous calculations.

Note, however, that the likely presence of a strong ordered magnetic field in the inner regions of the accretion (see 4.1 and 4.2 above) adds additional physics that is not included either in existing hot corona models or the present ion illumination model.

## 5.5 CONCLUSIONS

From energetic considerations, the hard spectra observed in the low-hard state of LMXBs must be produced by hot ( $kT_e \sim 100$  keV) matter in the inner regions surrounding the black hole. If there is also a much cooler disk present, there will necessarily be some degree of interaction between the two components, and the disk will be somewhat heated by irradiation from the hot Comptonizing component. The fits reported in Miller et al. (2006a) and Miller et al. (2006b) neglect this interaction by fitting the disk and hard component separately. In this paper we have shown that incorporating the effects of this interaction heats the inner regions of a moderately truncated disk so that, when coupled with the effects of interstellar absorption, the size of the soft excess matches observations. Our work also highlights the potential pitfalls of using simple power law or analytic Comptonization fits at low energies, which can provide significant deviations in the soft X-rays, thus changing the shape and intensity of the observed soft excess.

In the case of GX 339-4, our model predicts an Fe-K component of comparable strength to that observed, although we did not do a detailed comparison. However, work by others has suggested that part of the broadening in the Fe-K line that was observed for GX 339-4 can be attributed to a large outflow, and detailed models of Fe-K fluorescence in galactic black holes show lines that are much broader than is found in AGN models (and which are normally used to fit spectra).

The model we have envisioned presents several opportunities for further improvement, in order to better constrain the introduced fitting parameters,  $C$  and  $\eta$ . The spectrum from the hot ring and ADAF are particularly uncertain, and dependent on a more detailed model for the radiative transfer through this region, as well as the source and number of seed photons (which will set the electron temperature in both regions). The model's global accretion rate (which is limited by the rate at which the hot layer spills over into the hot ring and then evaporates into the ADAF) is also very low, although this can be increased if the viscosity in the warm layer can be increased, perhaps as a result of accretion through an ordered magnetic field.

CD'A acknowledges financial support from the National Sciences and Engineering Research Council of Canada.

## REFERENCES

- Ballantyne, D. R., Ross, R. R., & Fabian, A. C. 2001, MNRAS, 327, 10  
Balucinska-Church, M., Belloni, T., Church, M. J., & Hasinger, G. 1995, A&A, 302, L5+  
Beloborodov, A. M. 1999, ApJ, 510, L123  
Bisnovatyi-Kogan, G. S. & Ruzmaikin, A. A. 1974, Ap&SS, 28, 45  
Brocksopp, C., McGowan, K. E., Krimm, H., et al. 2006, MNRAS, 365, 1203

- Churazov, E., Gilfanov, M., & Revnivtsev, M. 2001, MNRAS, 321, 759
- Davis, S. W., Blaes, O. M., Hubeny, I., & Turner, N. J. 2005, ApJ, 621, 372
- De Villiers, J.-P., Hawley, J. F., Krolik, J. H., & Hirose, S. 2005, ApJ, 620, 878
- Deufel, B., Dullemond, C. P., & Spruit, H. C. 2002, A&A, 387, 907
- Deufel, B. & Spruit, H. C. 2000, A&A, 362, 1
- di Matteo, T. 1998, MNRAS, 299, L15+
- Di Salvo, T., Done, C., Życki, P. T., Burderi, L., & Robba, N. R. 2001, ApJ, 547, 1024
- Done, C. & Gierliński, M. 2006, MNRAS, 367, 659
- Done, C., Gierliński, M., & Kubota, A. 2007, A&A Rev., 15, 1
- Dullemond, C. P. & Spruit, H. C. 2005, A&A, 434, 415
- Esin, A. A., McClintock, J. E., & Narayan, R. 1997, ApJ, 489, 865
- Giannios, D. & Spruit, H. C. 2004, A&A, 427, 251
- Gierliński, M., Done, C., & Page, K. 2008, MNRAS, 717
- Haardt, F. 1993, ApJ, 413, 680
- Haardt, F. & Maraschi, L. 1991, ApJ, 380, L51
- Igumenshchev, I. V., Narayan, R., & Abramowicz, M. A. 2003, ApJ, 592, 1042
- Laurent, P. & Titarchuk, L. 2007, ApJ, 656, 1056
- Merloni, A. & Fabian, A. C. 2001, MNRAS, 321, 549
- Merloni, A., Fabian, A. C., & Ross, R. R. 2000, MNRAS, 313, 193
- Miller, J. M., Homan, J., & Miniutti, G. 2006a, ApJ, 652, L113
- Miller, J. M., Homan, J., Steeghs, D., et al. 2006b, ApJ, 653, 525
- Narayan, R., Igumenshchev, I. V., & Abramowicz, M. A. 2003, PASJ, 55, L69
- Narayan, R. & Yi, I. 1994, ApJ, 428, L13
- Nayakshin, S. & Kallman, T. R. 2001, ApJ, 546, 406
- Nayakshin, S., Kazanas, D., & Kallman, T. R. 2000, ApJ, 537, 833
- Ramadevi, M. C. & Seetha, S. 2007, MNRAS, 378, 182
- Ross, R. R. & Fabian, A. C. 2005, MNRAS, 358, 211
- Ross, R. R. & Fabian, A. C. 2007, MNRAS, 381, 1697
- Rykoff, E. S., Miller, J. M., Steeghs, D., & Torres, M. A. P. 2007, ApJ, 666, 1129
- Shakura, N. I. & Sunyaev, R. A. 1973, A&A, 24, 337
- Shimura, T. & Takahara, F. 1995, ApJ, 445, 780
- Spruit, H. C. 1997, in LNP Vol. 487: Accretion Disks - New Aspects, ed. E. Meyer-Hofmeister & H. Spruit, 67–76
- Spruit, H. C. & Deufel, B. 2002, A&A, 387, 918

Stehle, R. & Spruit, H. C. 2001, MNRAS, 323, 587

Taam, R. E., Liu, B. F., Meyer, F., & Meyer-Hofmeister, E. 2008, ArXiv e-prints, 807

Takahashi, H., Fukazawa, Y., Mizuno, T., et al. 2008, PASJ, 60, 69

Tomsick, J. A., Kalemci, E., Kaaret, P., et al. 2008, ArXiv e-prints, 802

---

## Hoofdstuk 6

---

# Samenvatting

In dit proefschrift gaat het over accretieschijven waarvan de binnenste gebieden, rond het accreterende object, gestoord zijn. Er worden twee verschillende oorzaken van storing behandeld. In het eerste geval gaat het om dunne schijven ('Shakura-Sunyaev-schijven') rond zwarte gaten of neutronensterren, en wel in gevallen waar de waarnemingen erop lijken te wijzen dat er een 'gat' in zit: alsof de binnengebieden ontbreken. In het tweede geval wordt het binnengebied onderbroken door een in het accreterende object verankerd sterk magnetisch veld. De fysica in de twee gevallen is verschillend.

### 6.1 RÖNTGENDUBBELSTERREN

De Röntgenspectra van accreterende neutronensterren en zwarte gaten komen vaak aardig overeen met de voorspellingen van het dunne schijfmodel van Shakura en Sunyaev. In ieder geval als de bronnen in hun 'zachte Röntgentoestand' zijn, die optreedt als de helderheid het hoogst is. De fotonen hebben dan een gemiddelde energie van de orde van een keV. Bij lagere helderheden, in de 'harde toestand' zien de spectra er heel anders uit, ze zijn dan gedomineerd door fotonen rond de 100 keV.

Het 'truncated disk' model stelt voor dat die hardere fotonen ontstaan in een binnengebied rond het zwarte gat, waar de accretie anders verloopt dan in de koele Shakura-Sunyaev schijf. De temperatuur is er veel hoger, het plasma is optisch dun. De waargenomen harde fotonen ontstaan door inverse Comptonstrooiing van zachte fotonen uit de koele schijf in dit hete plasma. Op zijn weg naar het zwarte gat maakt het accreterende gas dus om een of andere reden een overgang van koel ( $\sim 1$  keV) naar een heet ( $\sim 100$  keV) plasma. In het 'truncated disk' model heeft de koele schijf een binnenrand op een zekere afstand van het centrale object.

Dit model is niet het enige, een alternatief is het 'corona' model. Dit gaat ervan uit dat de koele schijf wél tot aan het oppervlak van het accreterende object blijft bestaan. Aangenomen wordt dat de harde fotonen geproduceerd worden in een heet plasma boven het oppervlak van de koele schijf (in analogie met hete corona van de zon). Een kleine controverse tussen deze twee modellen ontstond door waarneming van een 'koele component' in het harde spectrum: in de harde spectra zit vaak nog een zeker overschot aan fotonen met energie  $\sim 0.1 - 1$  keV. Dit werd geïnterpreteerd als bewijs dat er een koele schijf is die zich tot aan de rand van het

accreterende object uitstrekt.

In dit proefschrift (hoofdstuk 5) wordt aangetoond dat deze conclusie voorbarig is. In het truncated disk model is er noodzakelijkerwijs een overgangsgebied waar de hete plasma in het binnengebied interageert met de binnenrand van de koele schijf. Met een gedetailleerd model voor het overgangsgebied kon aangetoond worden dat deze wisselwerking de binnenrand van de schijf verhit tot de temperatuur die nodig is om de koele component te verklaren. De 'koele component' is dus niet een waarneming waarmee tussen de twee modellen kan worden onderscheiden. Overigens laat de analyse in hoofdstuk 5 ook zien dat een belangrijk deel van de zachte component eigenlijk een artefact is van de manier waarop modellen van de spectra aan de waarnemingen aangepast worden.

## 6.2 'MAGNETOSFERISCHE' ACCRETIE

De binnenkant van een koele schijf kan ook gestoord worden door het magneetveld van de accretor. In veel neutronensterren, witte dwergen en protosterren worden veldsterkten waargenomen die sterk genoeg zijn om in de buurt van de ster het accretieproces te domineren. De energiedichtheid in het magneetveld hoger is dan de kinetische energie van de roterende schijf. De veldsterkte valt snel af met de afstand van de ster, zodat de invloed ervan zich slechts tot een eindig gebied rond de ster uitstrekt, de magnetosfeer. Binnen de magnetosfeer volgt het accreterende gas de veldlijnen en roteert met de ster mee, erbuiten heerst een volgens Kepler roterende schijf. Ertussen is een overgangsgebied dat zich niet zo eenvoudig laat beschrijven.

Het kan gebeuren dat het gas van de schijf accreteert op een ster die sneller roteert dan de Keplerrotatie aan de binnenrand van de schijf; de binnenrand ligt dan binnen de zgn. corotatie radius. Dit leidt tot een conceptueel probleem. Zodra het gas de magnetosfeer binnen dringt, roteert het sneller dan de schijf, en wordt weer naar buiten geslingerd. Wat gebeurt er nu als er tegelijk continu gas door de schijf wordt aangevoerd?

Een antwoord hierop werd gegeven door Sunyaev en Shakura in 1976 (SS76): het gas hoopt zich op in de schijf. De massa die aangevoerd wordt accreteert niet op de ster (voorlopig niet in elk geval). Zij noemden dit 'dead disks'. Wanneer zich een kritische hoeveelheid massa verzameld heeft kan een overgang plaatsvinden naar een accreterende toestand, waarin de binnenrand van de schijf zover de magnetosfeer indringt dat de Keplersnelheid hoger wordt dan de rotatie van de ster. De massaflux op de ster is dan hoog, het reservoir in de schijf loopt leeg, en er volgt weer een 'dead disk' fase: het is een proces van cyclische accretie.

Dit aantrekkelijke beeld heeft tot nu toe weinig invloed gehad in de literatuur. In plaats daarvan overheerst het beeld van de zgn. 'propellering': het idee dat het gas, dat niet kan accreteren weggeslingerd wordt, dwz. het systeem moet verlaten. Hoofdstukken 2-4 volgen het inzicht van Sunyaev en Shakura, dat propellering in deze zin niet nodig is. Daarbij valt nog op te merken dat het als verklaring van het conceptuele probleem niet eens voldoende is.

Als het 'wegslingeren' namelijk minder dan exact 100% effectief is zou er toch nog massa door de magnetosfeer moeten accreteren, en blijft het oorspronkelijke conceptuele probleem net zo onopgelost. Wegslingeren kan in de praktijk best ook gebeuren, maar staat als proces nogal los van het eigenlijke magnetosferische accretieprobleem.

In hoofdstukken 2-4 van het proefschrift wordt de logica van SS76 verder ontwikkeld met tijdsafhankelijke berekeningen van het magnetosferische accretieprobleem. Daarvoor is een model nodig voor de overgang van de accreterende naar de 'dode' toestand. Aangenomen wordt dat de accretiesnelheid door de magnetosfeer geleidelijk afneemt tot nul als de binnenrand van de schijf door de corotatie radius naar buiten beweegt. Verder is er een aanname nodig voor het door het magneetveld van de ster op de schijf uitgeoefende koppel. Hiervoor is een soortgelijke overgang geconstrueerd.

Met dit eenvoudige model is het overgangsgebied rond de corotatie radius voldoende gespecificeerd om de evolutie te berekenen van een schijf die op een magnetosfeer accreteert. Het stelsel vergelijkingen blijkt mathematisch van het 'stijve' type te zijn. Een daarvoor aangepast numeriek schema is in staat de evolutie de schijf zowel op korte als zeer lange tijdschalen te vervolgen.

De resultaten laten zien hoe accretie op een magnetosfeer verloopt als wegslingeren van materie verwaarloosd wordt. De door SS76 vermoede cyclische accretie vindt inderdaad plaats, de berekeningen laten mooi zien hoe de periode van de cyclus langer wordt naarmate de gemiddelde accretiesnelheid afneemt. Het blijkt echter dat er naast dit cyclische gedrag nog een andere mogelijkheid is, die hier 'trapped disks' wordt genoemd. In deze toestand blijft ook bij zeer lage accretiesnelheid de binnenrand van de schijf dicht bij de corotatie radius hangen. Dit is mogelijk omdat de accretiesnelheid door het overgangsgebied een sterke functie is van de afstand tussen corotatie radius en binnenrand van de schijf. Welk van de twee in een bepaald systeem plaats vindt is niet uit deze berekeningen te voorspellen, het hangt af van de details van de fysica van het overgangsgebied.

Met de resultaten worden nieuwe interpretaties van waarnemingen van magnetosferische systemen mogelijk, zowel van protostellaire schijven als Röntgendubbelsterren.



# Acknowledgments

Finishing this thesis offers an excellent chance to reflect on the last four years and the large number of people who have assisted, in one way or another, in its production. I will do my best to acknowledge everyone, but apologize in advance for omissions. (I promise I'll make it up to you).

First and foremost I would like to thank my supervisor, Henk Spruit, for his encouragement and guidance. His frequently patient and always erudite and opinionated conversations have made the past four years extremely fun and instructive, and I am grateful to have had the opportunity to work with him. I am also deeply indebted to Stuart Sim, for countless hours of interesting scientific discussion over tea, writing and editing advice, instruction in C and radiative processes, and general assistance in pushing back the boundaries of human ignorance. I would also like to thank Cornelis Dullemond, Dimitrios Giannios, and Anna Watts for interesting scientific discussions, encouragement and advice.

In preparing the final version of my thesis, I am very grateful to Candy Girling, for allowing me to use her artwork on my cover, and to Max Davis, for help in laying it out. I am also grateful to the Max Planck Institute of Astrophysics and the National Science and Engineering Research Council of Canada for financial support.

My time in Munich would not nearly have been so fun without the large number of wonderful people around me. First I am grateful to my fellow Amochette: Silvia Bonoli, Payel Das, Mona Frommert, Shy Genel and Margarita Petkova, who have been a constant source of entertainment and support as we dragged each other through our PhDs. Thanks also to Andre Waelkens and Maria-Paola Bottino (not least for getting married in Italy and inviting me!), Klaus Dolag, Remo Collet, Kate O'Shea, and Team Supernova: Stephan Hachinger, Rüdiger Pakmor, Ulrich Noebauer, and Michael Fink. Outside the institute, I am grateful to Caroline Lindenbeck and Paulo Waelkens for many hours of entertainment, and especially to Hias Heinrich who made me very welcome in the cello section of the SOMA orchestra. Finally thanks are due to my fellow all-weather Garching-Munich cyclists, who made the

ride fun in the summer and bearable in the winter: Roderik Overzier, Janina von Groote, Max Knötig, Stuart (again), Ivo Seitzzahl and Ashley Rüter.

I have also derived huge encouragement from friends and family in Canada and abroad. I am particularly grateful to my sister, Laura D'Angelo, and friend Zuzana Betkova, for many long, late-night telephone calls. Thanks too to the rest of Team D'Angelo, my brother Justin and sister Beatrice, whose Munich visit was a highlight of my time there. I am also grateful to Ken Shen, Michael Jeavons and Marc Goodman, for his enthusiastic descriptions of Munich. Thanks to my supervisors at the University of Toronto, Marten van Kerkwijk and Roman Rafikov, for their encouragement to continue with graduate studies, and endorsement of Garching as a good place to study.

Finally I acknowledge my very enthusiastic supporters and parents, Lucy Girling and Joseph D'Angelo, who have both sat patiently through long and often convoluted explanations in response to the question, "What are you working on?", but who still persist in asking. Thanks.

Caroline D'Angelo  
Toronto, January 2011